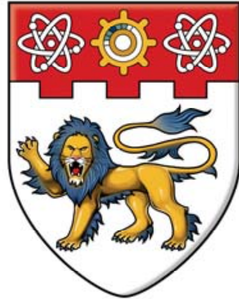

NANYANG
TECHNOLOGICAL
UNIVERSITY

THERMAL STRESS ANALYSIS AND CHARACTERIZATION OF THERMO-MECHANICAL PROPERTIES OF THIN FILMS ON AN ELASTIC SUBSTRATE

HU YINGYONG

SCHOOL OF MECHANICAL AND AEROSPACE ENGINEERING

2011

THERMAL STRESS ANALYSIS AND CHARACTERIZATION OF THERMO-MECHANICAL PROPERTIES OF THIN FILMS ON AN ELASTIC SUBSTRATE

HU YINGYONG

School of Mechanical and Aerospace Engineering

A thesis submitted to the Nanyang Technological University
in fulfillment of the requirement for the degree of
Doctor of Philosophy

2011

Acknowledgments

First, and foremost I would like to express my heartfelt and sincere gratitude to my supervisor, Dr. Huang Weimin, for his guidance, inspirations, keen insights, and encouragements.

I am also grateful to the director of the Photonics and Microsciences Lab, Dr. Xiao Zhongmin, for supplying the lab facilities. Special thanks to Dr. Wu Mingjie for his help in experiments and discussion.

The technicians in the Photonics and Microsciences Lab, the Micromachine Center, the Materials Lab, and the Strength of Materials Lab, are appreciated for their assistance and kindness in various aspects.

Last, but not least, I thank NTU for giving me the chance to study here with a research scholarship.

Contents

Acknowledgements Ⅰ

Contents Ⅱ

Abstract Ⅴ

List of Figures Ⅶ

List of Tables Ⅺ

List of Symbols Ⅻ

Chapter 1 Introduction 1

1.1 Background of thin film technology 1

1.2 Residual stress and thermo-mechanical properties of thin films 3

1.3 Objectives of this study 5

1.4 Outline of the dissertation 6

Chapter 2 Literature Review 8

2.1 Stress in deposited thin films 8

2.2 Stoney equation 11

2.3 Recent modifications of Stoney equation 13

2.4 Thermo-mechanical properties of thin films 19

2.5 Determination of thermo-mechanical properties of thin films 22

2.5.1 Bulge-testing method 23

2.5.2 Gauge technique 25

2.5.3 Nanoindentation method 26

2.5.4 Brillouin scattering technique 28

2.5.5 X-ray diffraction technique 29

2.5.6 Microtensile test 31

2.5.7 Microstructures technique 32

2.5.8 Beam bending method 33

2.5.9 Curvature measurement methods 35

2.5.10 Other techniques 36

Chapter 3 Elastic and Elastic-Plastic Analysis of Multilayer Thin Films 39
3.1 Introduction 39
3.2 Multilayer thin film on substrate (elastic analysis) 40
3.3 Bilayer structures (elastic analysis) 45
3.4 Neutral axis in bilayer structures (elastic analysis) 52
3.5 Bilayer structures (elastic-plastic analysis) 55
3.6 A case of elastic-plastic analysis 61
3.7 Numerical simulation 70
3.8 Conclusions 77

Chapter 4 Determination of Thermo-Mechanical Properties 79
4.1 Introduction 79
4.2 Five properties in a bilinear material 81
4.2.1 Simplified formula in the literature 81
4.2.2 Determine thermo-mechanical properties of a thin film 82
4.3 Determination of intrinsic stress and thermal stress 91
4.3.1 Introduction 91
4.3.2 Determination of residual stress 92
4.3.3 Determination of intrinsic and thermal stress 95
4.4 Conclusions 96

Chapter 5 Determination of Stress versus Strain Relationship and Other Thermomechanical Properties of Thin Films 98
5.1 Introduction 98
5.2 Thermally induced curvature approach 99
5.2.1 Nonlinear stress versus strain relationship of thin films by thermal tests 100
5.2.2 Closed-form solutions for very thin films 103
5.3 Four-point bending approach 108
5.3.1 Nonlinear stress versus strain relationship of thin films by bending test 108
5.3.2 Close-form solutions for very thin films 109
5.4 A case study 111

5.5 Conclusions 115

Chapter 6 Applications 117

6.1 Introduction 117

6.2 Characterization of metallic thin films 117

6.2.1 Experimental procedure 117

6.2.2 Experimental results and comparison 120

6.3 Reversible trenches atop NiTi thin films 127

6.3.1 Reversible trenches atop shape memory alloy thin films 127

6.3.2 Determination of curvature and stress in TiO_2 128

6.4 Conclusions 130

Chapter 7 Conclusions and Future Works 132

7.1 Conclusions 132

7.2 Future works 134

References 136

Appendix

A Derivation of the Stoney formula 151

B Expressions for ε_t and ε_b 155

C FEA Model for Section 3.7 Numerical Simulation 158

Publications 161

Abstract

Stress and thermomechanical behavior of thin films deposited atop a substrate upon thermal loading/unloading have been investigated extensively in the past decades, which was partially stimulated by the development of micro- and nanotechnology. However, most of the previous effort in analysis was focused on thin films in their linear elastic deformation range. On the other hand, either very dedicated equipments or complicated procedures were required for the determination of their properties.

This dissertation presents a systematic and detailed study of the thermally induced stress in multilayer thin films within both the elastic and elastic-plastic deformation ranges and several approaches to determine the thermomechanical properties of thin films. The elastic analysis based on the linear strain assumption results in the closed-form solutions and approximations (for very thin films). The condition that the film stress is of the same sign is identified for bilayer cases. Subsequently, the investigation is extended into the elastic-plastic deformed films in bilayer structures. Closed-form solutions of the maximum, average and minimum film stresses and curvatures are obtained for plastically deformed films. The difference among the maximum stress, average stress and Stoney stress in films is investigated systematically. In addition, the result of a case study reveals that the yield start point may be estimated as a linear function of temperature in the elastic-plastic deformation range.

A simple approach to determine the values of five thermomechanical properties of thin films, namely, the Young's modulus, coefficient of thermal expansion, yield start stress, strain hardening modulus and Poisson's ratio, is proposed. The approach is based on the conventional curvature test on bilayer structures upon temperature variation, which can be easily implemented using many conventional techniques.

Some simple and generic approaches for characterization of thin films with nonlinear stress versus strain relationship and/or temperature dependent material properties are proposed. In the case of very thin films, analytical solutions are obtained.

Approaches and solutions developed here are applied to investigate the moduli of metallic films. The film thickness effect on the modulus of Ag films is observed. The approach developed here is also utilized to identify the critical role of a compressive stress in thin TiO_2 layer atop NiTiCu film in the reversible trench phenomenon.

Keywords: thin film, elastic-plastic, stress, strain, multilayer, bilayer, thermomechanical properties, Young's modulus, coefficient of thermal expansion, strain hardening modulus, yield start stress, Poisson's ratio, curvature, bending test

List of Figures

1.1 Cantilever with a NiTi shape memory thin film deposited atop silicon. (a) at room temperature; and (b) upon heating. (Huang et al 2003) 2

2.1 Cracking of thin films (a) flat elliptical through-crack lying in the film plane loaded uniaxially in tension; (b) crack leading to coating fracture due to tensile stress; (c) crack leading to coating delamination due to compressive stress; (d) mechanism of metal whisker formation and cracking of overlying brittle film layer. (Adapted from Ohring 2002) 10

2.2 Four-point bending of a monolithic material. 34

2.3 Four-point bending of a bi-layer material. 34

3.1 Thin film and substrate. (a) Coordinate system; (b) illustration of strain distribution. 41

3.2 Contour of $[1-2\frac{E_f}{E_s}(\frac{t_f}{t_s})^3-3\frac{E_f}{E_s}(\frac{t_f}{t_s})^2]$ against thickness ratio (t_f/t_s) and modulus ratio (E_f/E_s). When $E_s t_s^3-2E_f t_f^3-3E_f t_f^2 t_s \geq 0$, the film stress is of the same sign. 49

3.3 Normalized stress against thickness ratio (t_f/t_s). 50

3.4 Contour of η (%) against thickness ratio (t_f/t_s) and modulus ratio (E_f/E_s). 51

3.5 Bilayer structure. (a) Coordinate system; (b) illustration of strain distribution. 52

3.6 The locations of neutral axes in film and substrate. 54

3.7 Bilinear strain vs. stress model. 55

3.8 Film stress development. (a) Pure elastic; (b) partially in plastic; (c) pure plastic 56

3.9 Contour of difference ($(\sigma_0-\sigma_f^{\max})/\sigma_f^{\max}$, in %) against H_f/E_s and thickness ratio (t_f/t_s) when the whole film is in plastic deformation. 59

3.10 Contour of difference ($(\sigma_0-\sigma_f^{mean})/\sigma_f^{mean}$, in %) against H_f/E_s and thickness ratio (t_f/t_s) when the whole film is in plastic deformation. 59

3.11 Stress distribution in the film and substrate at 25°C and 35 °C. (a) $H_f = 15GPa$ (b) $H_f = 0$; (c) $H_f = -15GPa$. 64

3.12 Film stresses as function of temperature variation. (a) $H_f = 15GPa$ (b) $H_f = 0$; (c) $H_f = -15GPa$. 65

3.13 Location of d against ΔT in the range between ΔT_1 and ΔT_2. Symbol: exact solution; line: determined by Equation (3.33). (a) $H_f = 15GPa$ (b) $H_f = 0$; (c) $H_f = -15GPa$. 67

3.14 Difference between exact solution and approximate solution (in %). (a) $H_f = 15GPa$ (b) $H_f = 0$; (c) $H_f = -15GPa$ 69

3.15 Curvature as a function of temperature variation. 69

3.16 Film stresses σ_x as function of temperature variation (H_f =15GPa) 72

3.17 Film stress σ_x versus film thickness (temperature variation is 15°C and H_f =15GPa) 73

3.18 Film stress (σ_x) at the interface at three different temperature variations (H_f =15GPa) 74

3.19 Film stress (σ_y) at the interface at three different temperature variations (H_f =15GPa) 75

3.20 Film shear stress (σ_{xy}) at the interface at three different temperature variations (H_f =15GPa) 76

3.21 Film shear stress (σ_{xy}) distribution through film thickness at different location (x=100, 110, and 120 μm, respectively) and with different strain hardening moduli (H_f =15, 5, and 0 GPa, respectively) when temperature variation is 35°C 77

4.1 Illustration of curvature as a function of temperature variation. Subscripts 1 and 2 stand for the results of two structures. ($\Delta T_1^*, K_{p,1}^*$) is any point in the full plastic range (for the film) 83

4.2 Schematic sketch of a multilayer structure (n layers atop a thick substrate) 93

5.1 Film and substrate. (a) Coordinate system; (b) illustration of strain distribution 100
5.2 Curvature variation versus temperature variation 101
5.3 Stress versus strain relationship 102
5.4 Contour of η_ε (%) against thickness ratio (t_f / t_s) and modulus ratio (E_f / E_s) 107
5.5 Comparison of stress versus strain relationships 108
5.6 Four-point bending of bilayer structure 109
5.7 Nonlinear stress vs. strain relationship 112
5.8 Curvature vs. temperature variation 113
5.9 Schematic illustration of the bow of the bilayer 114
5.10 Comparison of the stress vs. strain curves 115

6.1 Curvature variation vs. temperature relationship of Cu film deposited on Si substrate during heating 120
6.2 Curvature variation vs. temperature relationship of Al film deposited on Si substrate during cooling 120
6.3 Curvature variation vs. temperature relationship of Ag film deposited on Si substrate during second cooling (the curves obtained in the first cooling process follow almost the same curve) 121
6.4 Stress evolution and strain evolution in Cu film 122
6.5 Stress evolution and strain evolution in Al film 122
6.6 Stress evolution and strain evolution in Ag films 124
6.7 Relative stress vs. relative strain relationship of Cu film 124
6.8 Relative stress vs. relative strain relationship of Al film 124
6.9 Relative stress vs. relative strain relationship of Ag films 126
6.10 Moduli of different thickness Ag films 127
6.11 Curvature evolution upon thermal cycling in a NiTiCu film (From Wu 2009 with permission) 128
6.12 Stresses in NiTiCu thin film and TiO_2 layer upon thermal cycling (Wu MJ et al 2009) 130

A.1 Stress analysis of film/substrate composite: (a) composite structure; (b) free-body diagrams of film and substrate with indicated interfacial forces and end moments; (c) elastic bending of beam under applied end moment (Ohring 2002) 152

C.1 FEA model for the case that the thickness of film is 5 μm 159

List of Tables

3.1 Parameters used in neutral axis case study 54

3.2 Parameters used in elastic0plastic case study 62

3.3 ΔT_1 and ΔT_2 of three kind film with different H_f 62

5.1 Parameters 112

6.1 Thicknesses of metallic films 118

6.2 CTEs of materials used in calculation 119

6.3 Moduli of films obtained by stress vs. strain relationship slope. a: Zhao (2000), b: Lima et al (1999) c: Zoo et al (2006). 126

6.4 Material properties and thickness of each layer used in the analysis (Wu MJ et al 2009) 129

List of Symbols

A	Indentation contact area
$\bar{E}$	Biaxial modulus
E_f	Young's modulus of film
E_{ind}	Young's modulus of indenter
E_s	Young's modulus of substrate
H	Hardness
H_f	Strain hardening modulus of film
I	Moment of inertia
K	Curvature
K_e	Curvature of bilayer structure when film is in the elastic range
K_P	Curvature of bilayer structure when film is in fully plastic range
L	Length
M	Bending moment
P	Load
P_d	Differential pressure
$P_{\max}$	Peak indentation load
S	Contact stiffness measured by experiment in indentation test
a	Distance between support point and loading point in four-point bending test
c	Uniform strain component
d	Location of the yield start point in the film

d_l	Lattice spacing
d_{l0}	Unstressed bulk lattice spacing
h	Dome height
i	The i th layer, the i th step
l	Middle span in four-point bending
n	The number of layers, the number of steps
r	Radius of curvature
r_0	Initial radius of curvature
r_{sp}	Specimen radius
t_b	Location of the bending axis
t_f	Thickness of film
$t_{f,n}$	Location of neutral axis in the film
t_s	Thickness of substrate
$t_{s,n}$	Location of neutral axis in the substrate
w	Width
y_e	Location of moment equilibrium axis
y^n	Location of neutral axis
ΔK	Variation of curvature
ΔT	Variation of temperature
ΔT_1	The temperature at which plastic deformation starts to appear in the film
ΔT_2	The temperature at which plastic deformation starts to occupy the whole film
Ψ_e	$dK_e / dT = 1/\Psi_e$

Ψ_P $dK_p / dT = 1/\Psi_p$

α Coefficient of thermal expansion (CTE)

α_f CTE of film

α_s CTE of substrate

β A constant which depends on the indenter geometry

δ Deflection

ε Strain

ε_b Strain at the bottom of multilayer structure

ε_e Elastic strain

ε_m Mechanical strain

$\varepsilon_{\sec}$ $(\alpha_s - \alpha_f)\Delta T$

ε_T Thermal strain

ε_t Strain at the top of multilayer structure

γ Ratio of Young's moduli of film and substrate

η $(\sigma_f^{\max} - \sigma_f^{mean}) / \sigma_f^{\max}$

η_ε $(\varepsilon_{\sec} - \varepsilon_m) / \varepsilon_{\sec}$

λ Ratio of thicknesses of film and substrate

σ Stress

σ_0 Stoney stress

σ_{AT} Film stress obtained by Atkinson's equation

σ_{BS} Film stress obtained by Brenner and Senderoff's equation

σ_f Film stress

$\sigma_f^{\max}$ Maximum stress in the film

$\sigma_f^{\min}$ Minimum stress in the film

σ_f^{mean} Average stress in the film

σ_f^{top} Stress at the top surface of film

σ^{in} Intrinsic stress

σ_s Substrate stress

$\sigma_s^{\max}$ Maximum stress in the substrate

σ^{th} Thermal stress

σ_Y Yield start stress

υ_f Poisson's ratio of film

υ_{ind} Poisson's ratio of indenter

υ_s Poisson's ratio of substrate

CHAPTER 1 INTRODUCTION

1.1 Background of Thin Film Technology

Thin film technology is simultaneously one of the oldest arts and one of the newest sciences (Ohring 2000). Thin films are coated atop a substrate by various methods, such as, evaporation, sputtering or electrolytic deposition, etc, to construct multilayer structures, which have a wide range of applications.

The importance of thin films has increased dramatically over the past several decades. The micro-electro-mechanical systems (MEMS) industry is rapidly growing in quantity and diversity, which raises a range of great opportunities for micro mechanical components based on thin film technology (Tada et al 2000, Townsend et al 1987). Consequently, thin films have attracted more and more attention from many engineering/research communities.

Nowadays, multilayer structures have already been widely adopted in applied physics research and numerous industrial applications. Thin films can store energy and provide activation force and/or large displacement due to, for instance, the mismatch in coefficient of thermal expansion (CTE) or phase transformation. A number of

applications in micro actuators, such as micropumps (Benard et al 1998), microvalves (Krulevitch et al 1996), and microsensors (Muralt 2000) etc., have been achieved based on these principles.

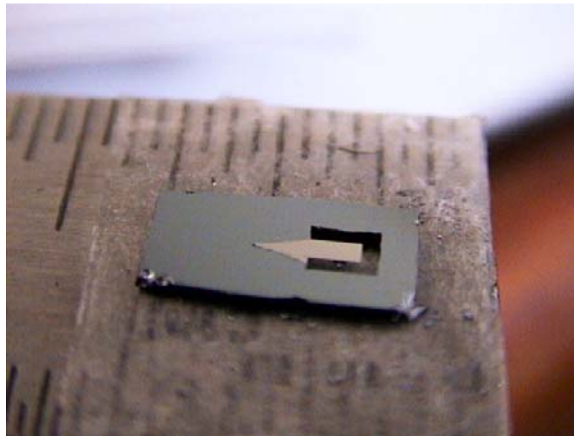

(a)

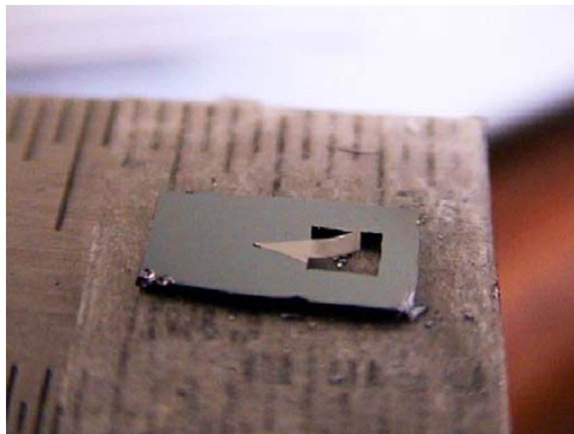

(b)

Figure 1. 1 Cantilever with a NiTi shape memory thin film deposited atop silicon. (a) at room temperature; and (b) upon heating. (Huang et al 2003)

Huang et al (2003) proposed an application of shape memory thin film for microgrippers. The microgripper was fabricated by bonding two identical micro-

cantilevers together with a silicon spacer between them. The cantilevers were made of silicon with a NiTi shape memory thin film deposited atop silicon. Figure 1. 1(a) reveals the straight shape of a cantilever beam at room temperature, while Figure 1. 1(b) is the curved shape at high temperatures.

Thin film based surface coating to protect structural materials in harsh environment is another application of commercial significance. In addition, thin film technology is also utilized extensively for magnetic data storage in hard disk drives (Freund and Suresh 2003).

1.2 Residual Stress and Thermo-mechanical Properties of Thin Films

Residual stress in thin films may be resulted due to different reasons. The most important ones in micro thin films are as follow (Lima et al 1999, Elshabini 1998, Liu and Murarka 1992),

(1) Thermal stress

Thermal stress results from the difference in CTE between thin film and substrate;

(2) Interfacial stress

Interfacial stress is largely caused by the difference in the lattice structural properties between thin film and substrate;

(3) Intrinsic stress

Intrinsic stress in thin films is normally induced during deposition or post-deposition treatment, e.g. annealing.

Residual stress inevitably has an important influence on the physical properties and performance of thin films (Maissel and Glang 1970, Roll 1976 and Jin et al 2001). Several failure mechanisms associated with the residual stress in thin films in integrated circuit (IC) industry have been identified. Consequently, it is an important issue to determine film stress for various purposes. Structural integrity and structural dynamics characteristics are two among others (Chen and Ou 2002).

The determination of thermo-mechanical properties of thin films has also attracted great interest from many communities, since the stability and reliability of thin film based devices are very much dependent on these properties (Huang et al 2004).

It is well known that the properties of thin films may be significantly different from those of bulk materials (e.g., Lima et al 1999, Zhao et al 2000 and Kalkman et al 2001). In addition, the thermo-mechanical properties of thin films may also depend upon the film geometry (e.g. thickness), fabrication techniques, and processing history (Fang and Wickert 1995, Fang et al 1999 and Jain et al 2001). It is of great importance to use the actual thermo-mechanical properties of thin films, not those of bulk materials, for a precise understanding of their response.

On the other hand, finite element analysis (FEA) is often utilized for prediction of the stress and deformation of thin film based complicated structures. For such an analysis, accurate thermo-mechanical properties of thin films as well as those of substrate, for example, the Young's modulus, CTE, Poisson's ratio and strain hardening modulus, are necessary as the original input.

1.3 Objectives of this Study

Although the residual stress in thin films has been investigated for decades and numerous publications can be found in the literature, for multilayer thin films with arbitrary thickness and properties, closed-form solutions were not available until 1983 (Feng and Liu 1983). However, in these previous methods, the number of both unknowns and boundary conditions increases dramatically with the number of layers (Townsend et al 1987, Liu and Murarka 1992). Furthermore, all previous closed-form solutions are limited to within the elastic deformation range for both thin films and substrates.

There are also well documented approaches in the literature about the characterization of thin films due to the practical importance as discussed in Section 1.2. However, most of the existing techniques require either very complicated and/or dedicated equipments or tedious procedures, and have many difficulties in dealing with a few properties by just a couple of simple experiments.

The first objective of this project is to systematically analyze thin film stress in multilayer structures in the whole elastic-plastic deformation range.

The second objective, which is more of practical interest, is to develop simple approaches to determine thermo-mechanical properties of thin films deposited atop a substrate.

1.4 Outline of the Dissertation

The outline of this dissertation is as follows,

Chapter 1 briefly introduces the background and applications of thin films and presents the objectives of this study.

Chapter 2 is an extensive literature review, which covers the formulas for determination of thermally induced stress in thin films and the major available techniques to determine the thermo-mechanical properties of thin films.

In Chapter 3, we develop closed-form solutions of elastic and elastic-plastic analysis of multilayer thin films atop a substrate.

Chapter 4 presents a simple approach to determine the thermo-mechanical properties of thin films coated atop a substrate. Apart from this, a curvature-based approach, which can determine not only the residual stress but also the intrinsic stress and thermal stress in each layer of a multilayer structure, is proposed.

In Chapter 5, we propose some simple and generic approaches for characterization of thin films with nonlinear stress versus strain relationship and/or temperature dependent material properties. Only standard testing techniques are required in these approaches.

Chapter 6 demonstrates two applications of the proposed approaches and formulas.

The dissertation is concluded by some major conclusions and future works in Chapter 7.

CHAPTER 2 LITERATURE REVIEW

2.1 Stress in Deposited Thin Films

Interfacial bonding of thin films to each other and to a substrate causes physical interaction and maybe chemical interaction as well. That is, the films and substrate can be held together under a state of compressive or tensile stress, known as interfacial stress, which appears due to differences between structural properties of the substrate and thin films (Lima et al 1999). Besides interfacial stress, there are other two sources of stress: intrinsic stress and thermal stress. Intrinsic stress is incorporated into a film during deposition or post-deposition treatment, i.e., it is intrinsic to these processes and strongly depends on the materials involved, the technique applied and the preparation conditions, such as substrate temperature during deposition, growth chamber conditions etc (Maissel and Glang 1970, Freund and Suresh 2003). Thermal stress results from the difference in the coefficients of thermal expansion (CTE) of thin films and substrate when a multilayer structure undergoes temperature fluctuation, which might be due to the variation of environmental temperature (Lima et al 1999). The sign of thermal stress depends on the relative magnitudes of the respective CTEs.

Some researchers categorized interfacial stress and intrinsic stress as one, i.e., intrinsic stress or growth stress, while treated thermal stress and others arising from external

influences, such as electrostatic or magnetic forces as extrinsic stress. In this dissertation, the focus is mainly on the thermally induced stress, while others are assumed to be ignorable or can be determined by other technologies.

Thin films' stresses as well as their effects on delamination, cracking and performance of thin films based structures were recognized as early as in the nineteenth century (Stoney 1909, Freund and Suresh 2003). A thin film stress reveals information about the behavior of the deposition process and affects the integrity of the film-substrate system as well as its performance. It may have various beneficial or detrimental effects. Whether thin film stress causes any problems in an application mainly depends on the stress level. In general, a lower level of compressive stress may effectively strengthen a thin film, because it reduces the chances of a thin film being under a high tensile stress which causes fracture in some applications, such as tool-bit coatings (Elshabini 1998). Corrosion resistance is also improved by avoiding tensile stress. A low strain of either sign can improve the properties of epitaxial structures in electronic applications (Liu and Murarka 1992). High compressive stress in a film can be beneficial to prevent the initiation of surface cracks by suppressing crack formation and propagation (Gunnars and Wiklund 2002). On the other hand, strain/stress in films may modify the electronic transport characteristics of layered semiconductor systems through modification of the band structure of the material (Singh 1993).

However, if the resultant stress is over a certain limit, which is the point of catastrophic or long-term failure, it naturally leads to many problems. Tensile stress failure is characterized by cracking, which appears as a mosaic pattern when viewed from the top (Ohring 2002). The cracked film may then peel away from the substrate at

the crack edges, where the stress is concentrated. Compressive stress failure is characterized by de-adherence and buckling, which from the top appears sometimes as domes or bubbles and some other times as an undulating meander pattern looking like a mole tunnel (Ohring 2002). Other effects may include substrate warpage and/or stress-induced phase transformations (Huang et al 2001).

As a summary, typical failure modes due to cracking in thin films are illustrated in Figure 2.1.

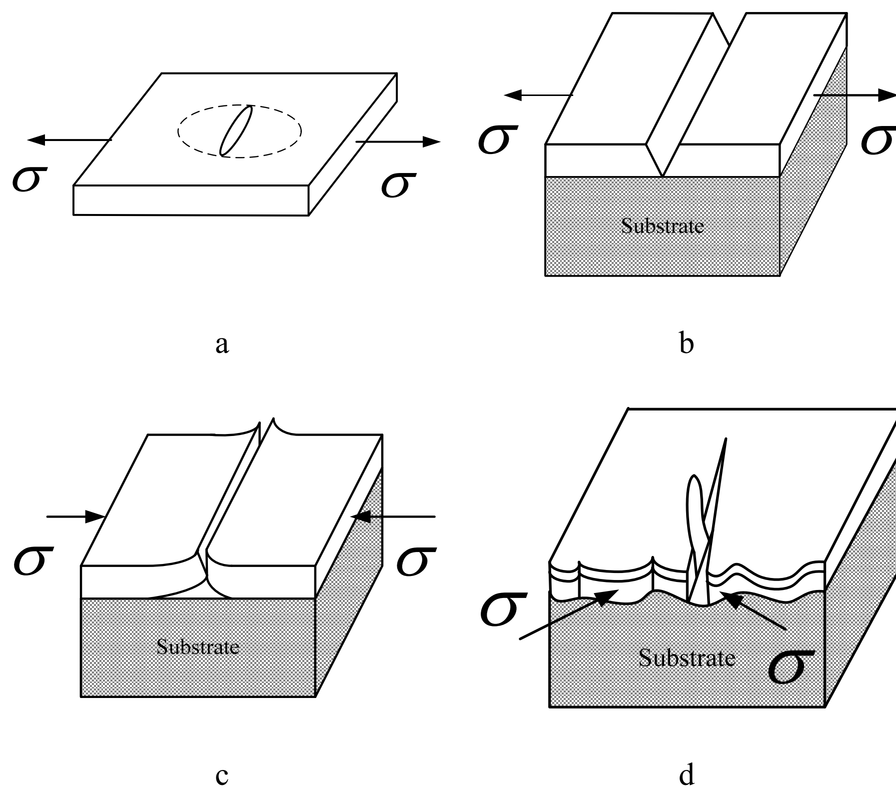

Figure 2. 1 Cracking of thin films (a) flat elliptical through-crack lying in the film plane loaded uniaxially in tension; (b) crack leading to coating fracture due to tensile stress; (c) crack leading to coating delamination due to compressive stress; (d) mechanism of metal whisker formation and cracking of overlying brittle film layer. (Adapted from Ohring 2002)

2.2 Stoney Equation

As mentioned above, the reliability and stability of multilayer structure are very much dependent on the level of stress induced in the structure. As such, attention has always been focused on it, in design and/or optimization of multilayer structures. In fact, considerable efforts have been devoted to this for over one hundred years.

The earliest equation to deal with the stress in a thin film coated on a beam is developed by Stoney (1909). Stoney observed that metallic films deposited by electrolysis on a thick substrate might be in a state of tension or compression even in the absence of any external loading. And they strained the substrate on which they were deposited by bending. Then he suggested a simple method of measuring the curvature (the amount of bending) together with the thickness of film to determine the stress in the film in 1909. With some minor modifications, the equation proposed by Stoney can be expressed as,

$$\sigma = \frac{E_s t_s^2}{6 t_f r} \tag{2. 1}$$

where E_s is the substrate's Young's modulus, t_s and t_f are the substrate and film thickness, and r is the radius of curvature of the film-substrate structure (refer to Appendix A for details of the derivation of Stoney equation). As we can see in Equation (2.1), film properties were not included in the relationship between radius of curvature and film stress. The only information of the film is its thickness. All others

about the substrate, such as the Young's modulus and thickness, is assumed to be known. Stoney equation is based on a model of the film-substrate structure, which involves several assumptions. The main assumptions are as follows (Freund et al 1999),

1. Both the film and substrate thicknesses are small compared to the lateral dimensions;
2. The film thickness is much less than the substrate thickness;
3. The substrate material is homogeneous, isotropic, and linearly elastic;
4. The film material is isotropic;
5. Edge effects near the periphery of the substrate are inconsequential and all physical quantities are invariant under change in position parallel to the interface;
6. All stress components in the thickness direction vanish through the material;
7. The strains and rotations are infinitesimally small.

Stoney equation was derived based on the beam theory. It serves as a cornerstone of experimental work in which film stress is obtained from the measured curvature (Freund and Suresh 2003). And it has been used without any doubt for several decades since it was developed. One of the merits of this equation is that it can be conveniently used to determine the residual stress in the thin film based on the measurement of the curvature. When Stoney equation is used to evaluate residual stress in thin film, Stoney equation should be corrected by subtracting the initial curvature ($1/r_0$) from the measured curvature ($1/r$) since some of the substrates may have initial curvature. So

the average film stress can be calculated from the change of the radius of curvature of the bilayer structure using the following form of Stoney equation,

$$\sigma = \frac{E_s t_s^2}{6t_f}\left(\frac{1}{r} - \frac{1}{r_0}\right) \quad (2.\ 2)$$

However, apart from the limit that it is only applicable to bilayer structures only, it also results in considerable error in thicker films (e.g., Klein 2000b, Chen and Ou 2002). This is a significant problem in many applications, for instance in actuators, where thick films are required for larger forces.

2.3 Recent Modifications of Stoney Equation

Stoney equation has been modified continuously for years due to its limitations (e.g., Kim et al 1999, Klein 2000c, and Hsueh and Paranthaman 2008). In 1925, Timoshenko presented the classic solution for the problem of a bimaterial strip subjected to uniform heating with various end conditions (Timoshenko 1925). Some simplifications were made in this solution: i.e. the difference in CTE remains constant during temperature variation; and the width of the strip is small as compared with the length of the beam. The analytical approach utilized by Timoshenko has been widely adopted at present. The next remarkable contribution is from Brenner and Senderoff (1949). They extended Stoney equation to the case of thicker films with various boundary conditions. As discussed later, this extended Stoney equation also introduces big error in the case of relatively thicker films. Some years later, an integral solution was proposed by

Davidenkov in 1961 (Townsend et al 1987). In Davidenkov's study, the approximations, which are applied in Brenner and Sennderoff (1949), are not required.

It was pointed out by Hoffman (1966) that plate theory should be used to study the film-substrate structure. He extended the Stoney equation to the case of a thin film deposited on a plate by utilizing a biaxial elastic modulus. When the plate theory is used, the Young's modulus of the substrate should be replaced by its biaxial elastic modulus, $E_s/(1-\upsilon_s)$, where υ_s is the Poisson's ratio of substrate. Subsequently, Saul (1969) and Reinhart and Logan (1973) calculated the stresses in particular within some regions of one-dimensional composites with multiple film layers coated on a substrate. Olsen and Ettenberg (1977) obtained an expression for stresses within individual layers of a multilayer composite as a function of position within the layer. Their calculation is based on the equilibrium of forces and moments, and equal and isotropic elastic constants are also assumed. Alternatively, Roll (1976) presented an analysis technique, which departs from the strength of materials approach and utilizes a field description of the material strain. Many approximate formulas for the radius of curvature and thermally induced stress obtained by above researchers have used the assumption that all layers of the multilayer structure have the same Young's modulus and deposition temperature.

Although analytical solutions have been proposed for thin films on a thick substrate based on the thin-film approximation, for multiple layers of arbitrary thickness and different properties, e.g. the Young's modulus and CTE, closed-form solutions are only obtained till 1980s (Feng and Liu 1983 and Townsend et al 1987). In 1983, Feng and Liu (1983) derived generalized formulas for the radius of curvature and stresses in

layers caused by thermally induced strain in semiconductor multilayer structure with different elastic moduli and growth temperatures. In Townsend et al (1987), the description of the stress distribution and state of elastic strain in a hypothetical composite plate consisting of layers with different elastic and/or thermal properties was presented. One example of such configuration is a structure resulting from the deposition of films onto a substrate. When these layers have CTEs that differ from that of the substrate, changes in the temperature lead to differential rates of thermal strain within the plate. However, the layers are confined at each interface, and this leads to elastic strains in the films and substrate resulting in end forces or applied moments. A description of the state of elastic strain and distribution of stresses within the plate must satisfy the requirement that total resultant end forces and total resultant bending moments must be zero (Townsend et al 1987). Suo et al (1999) presented the basic mechanics relations for externally forced and thermally induced bending of the film-on-foil devices.

As we can see, in most of those methods, both the number of unknowns and the number of boundary conditions increase with the number of layers in the multilayer structures. More recently, Freund et al (1999) has extended the Stoney equation to large deformations using a potential energy minimization analysis.

In 1999, Schäfer et al (1999) reported their study of film stress based on a formula developed by Atkinson (1995), i.e.,

$$\sigma_{At} = \frac{E_s t_s^3 K}{6t_f (t_f + t_s)} \quad (2.\ 3)$$

where K is the curvature of the structure. Compared with the classic Stoney equation, this equation is modified from Stoney equation with an additional correction factor which is $1/(1+t_f/t_s)$. This correction factor takes the thickness ratio of film over substrate into accounts. Hence, it is a great improvement in Stoney-type equation, especially since it also does not require information on the film's elastic properties (Klein 2000b).

Another modified Stoney equation used by Rats et al (1995), which they attributed to Brenner and Senderoff (1949), is

$$\sigma_{BS} = \frac{E_s t_s^2 K}{6t_f}[1+\frac{4t_f}{t_s}(\frac{E_f}{E_s}-1)] \qquad (2.4)$$

where E_f is the Young's modulus of the film. In 2000, Klein evaluated the correction of Stoney equation and the above two modified versions and concluded that (Klein 2000b):

1. The correct equation for the stress in the film of bilayer plates can be expressed in terms of Stoney equation and a correction factor equal to $(1+\gamma\lambda^3)/(1+\lambda)$, where γ designates the ratio of the biaxial moduli of thin film and substrate and λ is the ratio of the layer thicknesses;
2. Stoney equation does not cause any serious errors for thickness ratio $\lambda \le 0.1$;

3. The modification proposed by Atkinson, which does not require information of the film's modulus, is a great improvement which is applicable to a thickness ratio up to $\lambda \approx 0.4$;
4. Brenner and Senderoff-type expressions can be very misleading and should be avoided.

More recently, Zhang et al (2005) systematically investigated the errors involved in using some typically approximate solutions, such as Stoney equation (1909), Brenner-Sendroff modification (1949), Saul approximation (1969), Röll approximation (1976), Vilms-Kerps approximation (1982), and Teixeira approximation (2001). The comparison is interesting. However, the average film stress was taken as reference for comparison. This is only useful provided that the thickness of a film is much less than that of the substrate. In the case of relatively thick film, the maximum film stress should be more meaningful in engineering application instead of the average film stress because the maximum film stress can be much larger than the average film stress.

Hsueh (2002) proposed a model to study the elastic deformation of multilayer structure due to residual stresses and external bending. In that model, the strain distribution in the multilayer structure, ε, is decomposed into a uniform component and a bending component, i.e.,

$$\varepsilon = c + \frac{z - t_b}{r} \tag{2. 5}$$

where c is the uniform strain component, t_b dictates the location of the bending axis (which is defined as the line in the cross section of a structure where the bending strain component is zero), r is the radius of curvature of the structure, z is the coordinate axis which is defined such that the interface between the substrate and layer 1 of the film is located at $z = 0$. Note that the bending axis is different from the conventional neutral bending axis, which, in the classic beam bending theory, is defined as the line in the cross section of a structure where the normal stress is zero. The strain/stress distributions are contingent upon solutions of three parameters, c , t_b , and r , which can be determined from the following three boundary conditions:

a) The resultant force due to the uniform strain component is zero, i.e.,

$$\sum_{i=1}^{n} E_i (c - \alpha_i \Delta T) t_i = 0 \tag{2. 6}$$

b) The resultant force due to the bending strain component is zero, i.e.,

$$\sum_{i=1}^{n} \int \frac{E_i (z - t_b)}{r} dz = 0 \tag{2. 7}$$

c) The sum of the bending moment with respect to the bending axis is in equilibrium with the applied moment, i.e.,

$$\sum_{i=1}^{n} \int E_i (c + \frac{z - t_b}{r} - \alpha_i \Delta T)(z - t_b) = M \tag{2. 8}$$

where E is the Young's modulus, α is the CTE, ΔT is the temperature variation, M is the applied moment per unit width of the multilayer, and n is the number of layers of the multilayer structure, respectively. The subscript 'i' denotes the ith layer.

One of the advantages of this model is that there are always only three unknowns in spite of the number of layers of multilayer structure. However, it only focuses on the elastic deformation range. Furthermore, only the average film stress has been investigated, but not the maximum film stress. As we will see in Chapter 3, the difference between the average stress and maximum stress may be significant in some applications, such as actuators, where the thickness ratio is larger.

In 2003, Nikishkov (2003) developed a closed-form estimation for the curvature in hinged multilayer structures with initial strains based on Hsueh's three-parameter approach. In the case of small width, the hinged multilayer structure is in the plane stress state; while in the case of a wide strip with bending constraint in one direction, it is in the plane strain state.

2.4 Thermo-mechanical Properties of Thin Films

As mentioned above, many micro mechanical components have been used in a large variety of technological applications. Typically, such micro-components are thin film based plate/beam structures, fabricated by silicon bulk micro-machining or surface micro-machining (Ziebart 1999). Apart from the geometry, the mechanical behaviors of these structures are determined by the thermo-mechanical properties of these thin films.

Furthermore, the stability and reliability of these structures are very much dependent on their thermal-mechanical properties.

For example, elastic properties, such as the Young's modulus and Poisson's ratio, and the residual film stresses determine the static and dynamic mechanical behavior of the structures (Petersen 1978). As another example, the elastic property is one of the determinants of the deflection range of a micro-gripper. In addition, there are several problems resulting from the thermal expansion of thin film and substrate. The mismatch of thermal expansion strain between thin film and substrate may lead to residual stresses in thin film and substrate and then over-deformation and permanent damage of the structure may occur. On the other hand, the thermal expansion effect can be exploited to drive microgrippers and microactuators. To sum up, thermo-mechanical behavior of microstructures can be significantly influenced by the properties of materials (Feng and Wichert 1996 and Huang et al 2001).

Thus, the knowledge of these thermo-mechanical properties, namely, the Young's modulus, Poisson's ratio, CTE, yield start stress, and strain hardening modulus etc, is essential for design, development, and optimization of these structures.

Bearing in mind, the properties of a thin film may be significantly different from those of its bulk material. Some investigations addressed below are examples.

Lima et al (1999) observed that the CTE of tetrahedral amorphous thin films depends on the network strain in their work. They found that the CTE of tensile films is smaller than that of corresponding crystalline semiconductors, but it is higher for compressive

films and that the elastic biaxial modulus of the amorphous and metallic films is smaller than that of crystalline counterparts.

Fang and Lo (2000) found that CTE of aluminum film differs by up to 66% when the film thickness increases from 0.3 to 1.7 μm and CTE of Ti film differs by up to 60% when the film thickness increases from 0.1 to 0.3 μm. That is, CTE of thin film materials is very sensitive to the variation of film thickness. Fang and Lo (2000) also found that CTE of aluminum film is close to that of bulk aluminum when the film thickness is around 1 μm. However, the difference in CTE between the bulk and thin film of aluminum increases with the film thickness when it is over 1 μm.

Tada et al (2000) suggested that CTE of poly-Si thin films may be significantly higher than that of bulks based on their experimental results.

Zhao et al (2000b) revealed that the product of the biaxial modulus and CTE of film decreases with film thickness and assumed that CTE increases in ultrathin films. The modulus was found to be dramatically smaller than that of the bulk material.

Kalkman et al (2001) observed that the values of the moduli of polycrystalline aluminum and Au films are considerably smaller than the corresponding values of bulk materials but the modulus of polycrystalline W film is about the same as the bulk one.

Badawi et al (2002) used a technique coupling in situ tensile testing with x-ray diffraction to measure the Young's modulus and Poisson's ratio. In their study of

tungsten thin films, the obtained Young's modulus was close to that of bulk material whereas the Poisson's ratio was significantly larger.

In addition, the mechanical properties of thin films, both the elastic and plastic properties, can also depend upon the film thickness, the fabrication processes, and processing history (Fang and Wickert 1995, Fang et al 1999, Jain et al 2001 and Taylor et al 2003, Kalkman et al 2001).

Bulk materials usually have Poisson's ratio in a range $0 < \upsilon < 0.5$, although a negative Poisson's ratio is not forbidden by thermodynamics ($-1 < \upsilon < 0.5$). However, Renault et al (1998) has shown that the negative Poisson's ratio assumption proposed by Fullerton et al (1993) and Fartash et al (1993) was the result of an incorrect determination of strains from x-ray diffraction measurements.

It is therefore not a reliable approach to extrapolate the thermo-mechanical properties of bulk materials to thin films. It is more accurate to in-situ characterize the properties of thin films, i.e., with substrates untouched.

2.5 Determination of Thermo-mechanical Properties of Thin Films

Thermal-mechanical properties of thin films have received numerous attentions because of their strong influence on the behavior and performance of thin films, and implications on the reliable operation of thin film based micro components (Chang et al 2007 and Varguez et al 2008). At present, in MEMS design, elastic and elastic-plastic behaviors (although a few examples of anelastic and viscoelastic responses exist) are

mostly concerned and the mechanical properties of interest are, for instance, the Young's modulus, yield stress and residual stress etc (Srikar and Spearing 2003). There are several available techniques to measure the thermo-mechanical properties of bulk materials (e.g. Kinzly 1967, Jacobs et al 1970, Courtney 2000, and Aviles et al 2008). For example, one of the most widely used methods to measure CTE of a sample is optical method. This method involves the measurement of the change in dimension, due to a variation in temperature, with respect to the original size.

Unfortunately, most of the conventional techniques for characterization of bulk materials have tremendous difficulties in dealing with very thin films since thin films are easily deformed and broken. Experimental difficulties in dealing with thin films result in that most of conventional techniques become unreliable (Tien et al 2001).

On-wafer characterization of thermo-mechanical properties of thin films is an active field in both applied physics research and engineering applications (Zhao 2000). In fact, several methods dedicated to thermo-mechanical properties of thin films have been developed for decades (Nix 1989). Each method has its own advantages and disadvantages.

2.5.1 Bulge-testing method

One of the first methods to determine the Young's modulus and residual stress of thin films with submicron or micron thickness is bulge-testing technique, also referred to as membrane load-deflection method (e.g., Zheng et al 2000, Kalkman et al 2001), which is suitable for free-standing thin films.

In this method, the thin film is sealed to the end of a hollow cylindrical tube and pressurized with gas. The thin film is loaded by a differential pressure while the maximum height of the resulting deflection in the film is detected optically by a microscope or interferometer and then converted into strain. The relationship between the dome height (h) and the applied differential pressure (P_d) can be determined by (Hoffman 1966)

$$P_d = 4t_f h / r_{sp}^2[\sigma + 2E_f h^2 / 3(1-\upsilon_f)r_{sp}^2] \quad (2.9)$$

Here, the film thickness and specimen radius are t_f and r_{sp}, respectively; σ is the residual stress in the film under a zero pressure differential; E_f and υ_f are the Young's modulus and Poisson's ratio of the thin film, respectively.

Using above model, the residual stress and a combination of the Young's modulus and Poisson's ratio can be extracted from the linear and nonlinear membrane response, respectively. And Poisson's ratio can be extracted by further testing membranes with square and rectangular geometries.

Since the nonlinear response varies with the fourth power of the lateral membrane size, precise sample fabrication and accurate size determination are crucial. The bulge test is only sensitive to mechanical properties in the plane of the film. This makes the interpretation of the experimental data more straightforward than in other methods such as nanoindentation (will be discussed shortly).

A further advantage of this method is that precise bulge test samples can be fabricated by selective removal of the silicon substrate underneath the film using silicon micromachining techniques. This avoids the delicate handling of free-standing thin films (Ziebart 1999). Zheng et al (2000) even used the experimentally derived biaxial moduli, together with the thermal stress data of the film samples, to estimate CTE of dense and porous poly-arylethers films.

However, in bulge test technique, the extraction of elastic modulus involves many simplifications. In order to get accurate result, numerical methods, such as finite element analysis, are needed.

2.5.2 Gauge technique

Another method to determine the Young's modulus of thin films is the strain gauge technique (Chiu 1990). The formulas for calculating the in-plane elastic modulus are derived using beam theory. To apply these formulas, a strain gauge is used to measure the surface strain. However, since it is in a contact manner the strain gauge may have impact on the film and may introduce errors to the measurement of elastic modulus of thin film. Furthermore, it may be very difficult to bond a gauge onto the film, which is crucial to this technique.

Chae et al (1999) used microgauge method, which has some merits as compared with commonly used optical methods, to measure the CTE of poly-Si. In the process of measuring the CTE of thin films, the elastic modulus and CTE of the substrate are no longer needed in the microgauge method. CTE of a thin film was expressed as a

function of the average temperature of the microgauge and the measured displacement at the vernier gauge. However, this technique is limited to conductive thin film only.

2.5.3 Nanoindentation method

Nanoindentation is another widely used technique to determine material behavior of thin films on a substrate, such as the Young's modulus of thin films (e.g. Oliver and Pharr 1992, Caceres et al 1999, Kucheycv et al 2000, Bradby et al 2002, and Malzbender and Steinbrech 2003) and even plastic properties of thin films (Nowak et al 1999).

Nanoindentation is a characterization technique similar to the hardness test commonly used for bulk materials. In this method, a diamond indenter with well-defined geometry is pressed into the film (normally, there are two kinds of shapes of indenters, namely, spherical and sharp). The indentation load-displacement data obtained at each depth are analyzed to determine the hardness, H, and elastic modulus, E. In this method, the hardness and modulus are determined from (Tsui and Pharr 1999):

$$H = \frac{P_{\max}}{A} \tag{2. 10}$$

$$E = (1-\upsilon)[\frac{2}{\sqrt{\pi}}\beta\frac{\sqrt{A}}{S} - \frac{1-\upsilon_{ind}^2}{E_{ind}}]^{-1} \tag{2. 11}$$

where $P_{\max}$ is the peak indentation load, A is the indentation contact area, β is a constant which depends on the indenter geometry, S is a experimentally measured contact stiffness, υ is Poisson's ratio of the specimen, and υ_{ind} and E_{ind} are Poisson's ratio and the elastic modulus of the indenter.

However, plastic and elastic deformations occur simultaneously upon loading. Due to this reason, the elastic properties are extracted from the elastic unloading curve of the indentation process. In comparison with other methods, this method has proven to be a simple and easy technique, and sample preparation is relatively simple. The thin film has neither to be removed from the substrate nor to be structured. Another merit is that a sample area of a few square micrometers is sufficient.

However, as we know the stress state underneath the indenter tip is highly non-uniform. Thus, the elastic response of the film during unloading is a complicated function of the possibly anisotropic material properties of the tested sample (Ziebart 1999).

Another intrinsic problem in nanoindentation is that a complicated hydrostatic stress is applied instead of a directional stress. Moreover, it fails to provide the fundamental data needed for characterization and modeling of thin-film structures (Florando and Nix 2005). Also, the substrate influence cannot be negligible when the penetration depth of the indenter is greater than 10% of the film thickness (Tsui and Pharr1999). This makes the extraction of reliable elastic modulus of thin films difficult. Like bulge test, there are many simplifications in the process of extraction of elastic modulus. In order to get accurate result, a numerical method, e.g. finite element analysis, is required. Another

possibly fatal drawback of nanoindentation method is that what it can determine is the out-of-plane properties, while the in-plane properties are normally more of our interest from the application point of view.

In summary, the application of nanoindentation to thin films is complicated and affected by several factors, such as indentation size effects, substrate effects, sink-in and pile-up of material around the indenter, and surface conditions etc (Su 2004). As such, its application is rather limited.

2.5.4 Brillouin scattering technique

The Brillouin light scattering technique has been exploited in order to study the elastic properties of dielectric films used in microelectronics (Carlotti et al 2002). By means of the finite element method, the resultant elastic constants were used to reproduce the measured stress vs. temperature curve, from which estimations of both CTE and the viscosity of films were obtained, as shown in Carlotti et al (2002).

However, in the Brillouin light scattering technique, the elastic constants are obtained by fitting the experimental data to the dispersion relation deduced from the theoretical model. The number of parameters for fitting increases as the film thickness decreases. This raises the uncertainty of the determined elastic constants for the film. Furthermore, the elastic property obtained from Brillouin scattering, is actually the high frequency dynamic response but not the static elastic property.

2.5.5 X-ray diffraction technique

X-ray diffraction measures residual stress and the thermo-mechanical properties of thin films by detecting the slight changes in the inter-planar spacing of crystal planes in different directions with respect to the specimen surface. These changes are revealed as shifts in angular positions of respective diffraction peaks. The variation of the crystal plane spacing has a certain relationship with the angle made by the normal of the specimen surface and that of the crystal plane. X-ray stress measurement devices measure this variation and subsequently determine the stress.

An alternative analytical method has been proposed by Ohring (2002). As an example, consider a polycrystalline film with an isotropically distributed biaxial tensile stress in the $x-y$ plane ($\sigma_z = 0$). The film contracts in the z direction by,

$$\varepsilon_z = (-\upsilon / E_f)(\sigma_x + \sigma_y) = -\upsilon_f(\varepsilon_x + \varepsilon_y) \tag{2. 12}$$

Here, υ_f is Poisson's ratio, E_f is the Young's modulus, σ is stress, and ε is strain (x and y denote directions). By measuring the lattice spacing (d_l) in a stressed film relative to the unstressed bulk lattice (d_{l0}) in the z direction using x-rays, Bragg's law yields $\varepsilon_z\,[=(d_l - d_{l0})/d_{l0}]$. Since $\sigma_x = \sigma_y = \sigma_f$, one has

$$\sigma_f = -\frac{E_f(d_l - d_{l0})}{2\upsilon_f d_{l0}} \tag{2. 13}$$

Zhou et al (1999) proposed two methods to measure CTE of anodic films, which are based on the x-ray diffraction. One method is to detect the change of the lattice spacing (d_l) of crystalline phase as the temperature increases. The measured d_l is plotted as a function of temperature. CTE, α, can be evaluated as

$$\alpha = \frac{\Delta d_l}{\Delta T} \frac{1}{d_{l0}} \quad (2.\ 14)$$

where $\Delta d_l / \Delta T$ is the slope of the $d_l - T$ curve, d_{l0} is the original lattice spacing of the specified plane. The other method is to determine the thermal stress in the film, which allows CTE to be determined numerically (Zhou et al 1999).

Cornella et al (1997) used non-symmetric x-ray diffraction technique to determine Poisson's ratio of crystalline thin films without any knowledge of the elastic properties of the thin film material.

Badawi et al improved this method and proposed a technique coupling x-ray diffraction measurements with in-situ tensile test to determine the Young's modulus and Poisson's ratio of a polycrystalline tungsten thin film (Renault et al 1998, Badawi et al 2002).

However, there are several drawbacks with x-ray diffraction technique in determination of thermo-mechanical properties of thin films. First, it needs an intense x-ray source to obtain enough signals. Second, only the out-of-plane CTE can be worked out by x-ray method. Third, x-ray diffraction is only applicable to crystalline films. Unfortunately, many low *k* dielectric films, which are very popular at present, are non-crystalline

(Zhao 2000). Furthermore, it is time consuming and only a slow strain rate can be applied (Hommel and Kraft 2001).

2.5.6 Microtensile test

Tensile test is a standard approach to evaluate elastic/plastic response of bulk materials. Microtensile test is a miniaturized version. Unlike its bulk counterpart, microtensile test on thin films is far from routine.

Microtensile test on free-standing thin films produces straightforward data to determine their stress versus strain relationships without any additional assumptions. For thin films coated atop a substrate, the extreme delicacies required in handling and detaching thin films from the substrate, gripping and aligning them, applying load, and measuring the mechanical response are experimental challenges. Loading is normally achieved by an electromagnetic force transducer, and strain is typically measured by an optical method in a contactless fashion. Some novel microtensile testing devices have been incorporated within electron microscopes, enabling direct observation of defects and recording of diffraction patterns during straining (Ohring 2002).

The main advantage of this method is that the stress state of a sample is nearly uniaxial, making interpretation of the experimental data straightforward. As compared with curvature methods, it can not only obtain but also control stress/strain in the film without thermal loading/unloading of the film-substrate system (Haque and Saif 2003).

However, sample fabrication, handling, and alignment in testing preparation are crucial. If the sample is not properly aligned, the applied force is not uniformly distributed within the film and wrinkling may occur. These problems are partially solved in some new sample design and preparation techniques based on silicon micromachining (Ziebart 1999). Measurements on a free-standing film can separate intrinsic thin film properties from substrate contributions. We should bear in mind that a free-standing film may have different properties from that coated on a substrate due to the interface effects.

2.5.7 Microstructures technique

Various techniques based on microstructures to determine properties of thin films as well as the residual stress have been developed (e.g. Fang and Wichert 1995, Fang and Wickert 1996, Fang et al 1999, Godin et al 2001, and Xu and Zhang 2003).

Fang et al exploited single layer and bilayer microcantilevers to determine CTE of thin films. The single layer and bilayer cantilevers would exhibit an out-of-plane deflection after subjected to a temperature change. Thus, thermal expansion of thin film materials can be determined using optical interferometric technique on thermally loaded microcantilevers (Fang et al 1999, Fang and Lo 2000).

The main inconvenience of this method is that the relationship between angular deflection of a microcantilever and the CTE is required to be determined by the finite element analysis. In addition, since a microcantilever beam has a free end, residual stress in the film may be released through the free end before testing (Xu and Zhang

2003). In general, it is impossible to determine residual stresses and the Young's modulus simultaneously from such a microcantilever beam test.

Beam buckling technique is based on principle of Euler buckling, which depends on compressive stress, and the beam size and shape (Gckel et al 1985). Fabricating an array of beams with different sizes, the critical beam length at which a beams starts to buckle can be determined. Subsequently, the film strain is obtained. This method is very sensitive to the film stress which is compressive. However, it has the disadvantage that a large number of different sized beams are required in order to obtain high accuracy (Ziebart 1999).

Su et al (2000) used bilayer microbridge method to characterize films. Zhang et al (2000) and Xu and Zhang (2003) extended the microbridge method to trilayer samples, which consist of SiO2/Si3N4/SiO2 and Si3N4/SiO2/ Si3N4, to estimate residual stress and the Young's modulus in each layer.

2.5.8 Beam bending method

Various bending beam methods (four-point bending, three-point bending, and bending a cantilever beam, etc) have also been used to determine the elastic modulus (Kim et al 2007, Tsai et al 2009). For example, in a four-point bending test (refer to Figure 2.2), the elastic modulus of a thin film can be determined from the slope of a load (P)-deflection (δ) curve by (Malzbender and Steinbrech 2004)

$$E = \frac{a(3Lx - 3x^2 - a^2)}{12I}\frac{\Delta P}{\Delta \delta} \quad (2.\ 15)$$

where I is the moment of inertia and x indicates the position, $a \le x \le L/2$ at which the deflection δ is measured. Most likely, δ is measured either at center, $x = L/2$ or at the position where load is applied, $x = a$.

Four-point bending is also applicable to bilayer or multilayer structure (refer to Figure 2.3). The formula to determine elastic modulus is more complicated (Malzbender and Steinbrech 2004a).

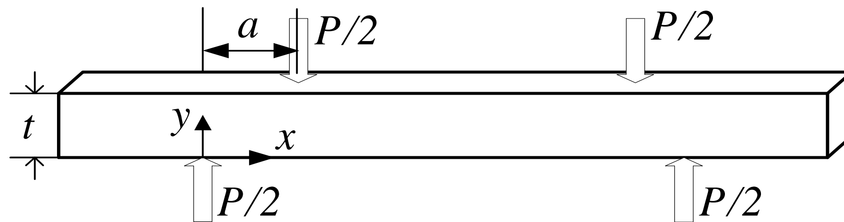

Figure 2. 2 Four-point bending of a monolithic material.

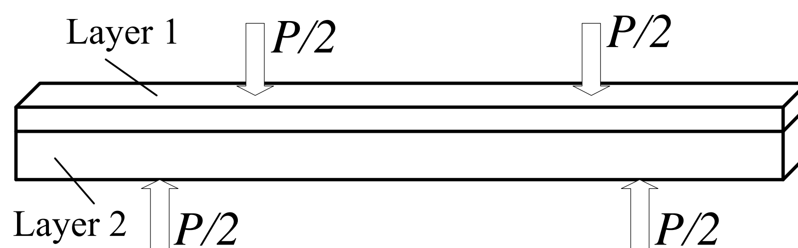

Figure 2. 3 Four-point bending of a bi-layer material.

Florando and Nix (2005) proposed a microbeam bending method to study the stress versus strain relationship of metallic thin films deposited atop a silicon substrate, in which triangular silicon microbeams were used instead of the common rectangular beams. The advantage of triangular beam is that the entire film on the top surface of the beam is subjected to a uniform plane strain when the beam is deformed.

2.5.9 Curvature measurement method

Curvature measurement method is one of the most widely adopted techniques to determine the residual stress. In the case of thin films, based on Stoney equation, the change in substrate curvature induced either during film deposition or temperature variation provides insight into the evolution of residual stress. One merit of curvature measurement method is that it does not require the material properties of the film. Other advantages of the curvature measurement method are:

1) It is fast, cheap and uncomplicated measurement;
2) It has a high accuracy;
3) It is applicable to amorphous materials.

Curvature measurement method can also be utilized to extract the Young's modulus and CTE of films (Lima et al 1999, Zhao et al 2000 and Gunnars and Wiklund 2002). Apart from the elastic properties of films, curvature measurement method also provides useful information about the plastic response of films. The main disadvantages of curvature measurement method are:

1) Large temperature change is required in the experiment;
2) Only averaged properties of a film can be obtained (Florando and Nix 2005);

3) It is not applicable to free-standing films.

There are a lot of mature techniques available for curvature measurement. Freund and Suresh (2003) categorized them broadly into four groups, namely, mechanical method, capacitance method, x-ray diffraction method, and optical method. Among them, mechanical method is usually a contact approach, while the rest three are contactless methods. Except x-ray diffraction method, which is only applicable to crystalline films, all others measure the out-of-plane deflection of a curved bilayer structure. The most commonly used method is optical method, which offers the convenience, accuracy and flexibility in measuring curvature through remote sensing. There are several different types of optical techniques, such as scanning laser method, multi-beam optical stress sensor, grid reflection method, and coherent gradient sensor method. For their advantages and limitations, one may refer to Freund and Suresh (2003) for details.

2.5.10 Other techniques

Yuan et al (1998) measured the coefficient of linear thermal expansion of ZnSe thin films with a temperature regulated spectroscopic ellipsometer. They found that the coefficient of linear thermal expansion varies linearly within a certain temperature range.

Carmen et al (2002) used narrow band photoacoustics to characterize mechanical properties and residual stress of free-standing nanometer-sized thin films. However, the results have to be analyzed numerically since in general it is not possible to obtain

simple analytical expressions for the phase velocities of the various modes in terms of the material properties and the waveguide dimensions.

A technique based on resonant frequency analysis of beam or plate structures has been developed (e.g. Harms et al 2001). The structures are excited to vibrate and the variation of excitation frequency enables the resonant frequencies to be measured. For evaluation of mechanical properties, the mass density of the materials has to be pre-determined separately. The Young's modulus also depends strongly on sample geometry. Therefore a precise geometrical characterization of the tested sample is crucial.

Tien et al (2001) proposed a method associated with an image processing technique to determine the mechanical properties of thin films. In that method, the change of deflection of a substrates coated with a thin film was obtained by digital phase shifting interferometry. The main drawback of that method is that image processing is necessary to determine the properties.

Electrostatic beam bending is also a popular technique to measure the Young's modulus and residual stress of free-standing and thin structures (Osterberg and Senturia 1997). In this technique, it is crucial to measure the gap size and beam thickness accurately. Finite element simulation is required to work out the Young's modulus (Srikar and Spearing 2003).

The recent development in microelectromechanical systems has brought forward many useful microdevices. The performance and reliability of these microdevices are largely

dependent on the thermo-mechanical properties of materials involved, especially those of thin films. The decrease in size of these devices with features at micro/submicron scale requires new testing methods to determine their mechanical properties.

As a result, many new microscale mechanical testing techniques have been developed. Mentioned above are a couple of typical examples. Most of them have advantages as well as disadvantages. The selection of a testing technique depends on the thermo-mechanical properties of our concern, such as the Young's modulus, yield stress, CTE, strain hardening modulus, and Poisson's ratio; and also depends on the film structure, loading/supporting conditions and etc.

CHAPTER 3 ELASTIC AND ELASTIC-PLASTIC ANALYSIS OF MULTILAYER THIN FILMS

3.1 Introduction

Maybe the earliest mathematic expression for the stress in a thin film on top of a thick substrate was presented by G. G. Stoney in 1909, known as "Stoney equation" at present (Stoney 1909). It has been modified continuously since then to overcome its limitation, e.g., one layer of very thin film. In the cases of multilayer thin films, several researchers have obtained closed-form solutions independently following a variety of approaches (e.g., Feng and Liu 1983, Townsend et al 1987). However, as mentioned in Chapter 2, in those methods the number of unknowns and boundary conditions increases dramatically as the number of layers increases. For instance, there are three unknowns to solve in Hsueh et al (2003). On the other hand, only the average film stress has been the focus in most of the previous investigation, while the maximum film stress, which might be considerably higher than the average stress in thicker films, has not yet been studied carefully. Furthermore, all previous closed-form solutions are limited to within the elastic deformation range. Elastic-plastic analysis has only been done by means of finite element analysis (FEA) (Trochu and Qian 1997).

The purpose of this chapter is to investigate the stress in multilayer thin films in the whole elastic-plastic deformation range. Section 3.2 presents an elastic analysis based on the linear strain assumption, which results in the identical closed-form solution and approximation (in very thin films) as those reported in the literature. Section 3.3 is the elastic analysis of bilayer structures as they are more of practical interest. The error between the precise solutions of the average and maximum film stresses against the ratios of thickness and Young's modulus of film and substrate is systematically investigated. Section 3.4 presents an analysis in neutral axis in bilayer structures. Section 3.5 extends the study into the elastic-plastic deformation range in bilayer structures. A case study is presented in Section 3.6. Section 3.7 is numerical simulation. Section 3.8 is conclusions.

3.2 Multilayer Thin Film on Substrate (Elastic Analysis)

Assume that a sample is long enough as compared with its total thickness and the strains are isotropic and uniform. Consider the case of a *n*-layer thin film atop a substrate as shown in Figure 3. 1. The thickness, Young's modulus, and coefficient of thermal expansion of layer i are denoted as t_i, E_i, and α_i, and those of substrate are t_s, E_s and α_s, respectively. Note that in the case of biaxial stress, biaxial modulus, $\overline{E_i}$ [$= E_i/(1-\upsilon_i)$, where υ_i is Poisson's ratio], should be used instead of E_i . For convenience, the coordinate system is defined as that shown in Figure 3. 1(a), where the bottom of the substrate is located at $y=0$, and the interface between the substrate and layer 1 of the film is located at $y = t_s$.

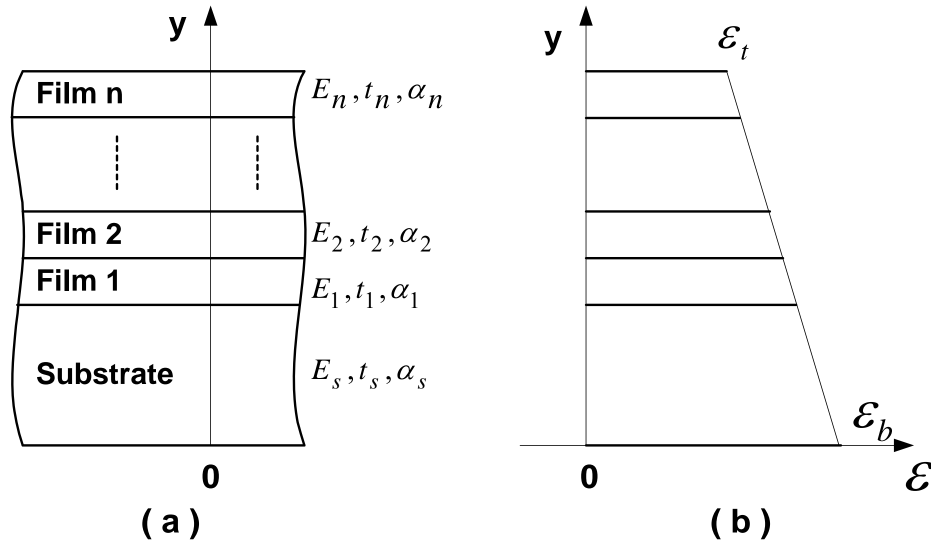

Figure 3. 1 Thin film and substrate. (a) Coordinate system; (b) illustration of strain distribution.

Upon temperature fluctuation, the multilayer structure tends to bend due to the difference in CTE. Since the strain, ε, is continuous in the thickness direction and may be assumed as linearly dependent on *y*, it can be expressed in terms of the strain at the top, ε_t, and the strain at the bottom, ε_b [refer to Figure 3. 1(b)], i.e.,

$$\varepsilon = \frac{\varepsilon_t - \varepsilon_b}{\sum_{i=1}^{n} t_i + t_s} y + \varepsilon_b \tag{3. 1}$$

For convenience in the expressions followed, $\sum_{i=1}^{k} t_i$ is defined as h_k (*k*=1, 2… *n*), i.e., the distance from the upper face of the *k*th film to the upper face of substrate. Additionally

define $h_0 = 0$. For small deformation cases, the radius of the curvature, *r*, can be calculated by $(h_n + t_s)/(\varepsilon_t - \varepsilon_b)$. The total strain, ε, includes two parts, namely, thermal strain ε_T (=$\alpha\Delta T$), and elastic strain ε_e, i.e., $\varepsilon = \varepsilon_T + \varepsilon_e$. Excluding the thermal strains, the induced normal stresses in the substrate and the films, σ_s and σ_i, can be expressed as,

$$\sigma_s = E_s(\varepsilon - \alpha_s \Delta T) \tag{3. 2}$$

$$\sigma_i = E_i(\varepsilon - \alpha_i \Delta T) \tag{3. 3}$$

where subscripts "*s*" and "*i*" stand for the substrate and the *i*th film, respectively, and ΔT is the variation of temperature. The equilibrium conditions of the multilayer structure are the total resultant in-plane force must be zero and the total moment must be null, i.e.,

$$\int_0^{t_s} \sigma_s dy + \sum_{i=1}^{n} \int_{t_s+h_{i-1}}^{t_s+h_i} \sigma_i dy = 0 \tag{3. 4a}$$

$$\int_0^{t_s} \sigma_s (y - y_e) dy + \sum_{i=1}^{n} \int_{t_s+h_{i-1}}^{t_s+h_i} \sigma_i (y - y_e) dy = 0 \tag{3. 4b}$$

where y_e is the location of moment equilibrium axis, which depends only on the properties of the structure and is independent of *y*. Rearranging Equation (3.4b) results in,

$$\int_0^{t_s}\sigma_s ydy+\sum_{i=1}^{n}\int_{t_s+h_{i-1}}^{t_s+h_i}\sigma_i ydy-y_e\left(\int_0^{t_s}\sigma_s dy+\sum_{i=1}^{n}\int_{t_s+h_{i-1}}^{t_s+h_i}\sigma_i dy\right)=0 \qquad (3.\ 4c)$$

Referring to Equation (3.4a), Equation (3.4c) can be reduced to,

$$\int_0^{t_s}\sigma_s ydy+\sum_{i=1}^{n}\int_{t_s+h_{i-1}}^{t_s+h_i}\sigma_i ydy=0 \qquad (3.\ 4d)$$

With Equations (3.1)-(3.3), (3.4a) and (3.4d), the explicit expressions for ε_t and ε_b can be obtained. They are too long to be included here (refer to Appendix B for expressions for ε_t and ε_b). Given ε_t and ε_b, *1/r* can be conveniently obtained as,

$$\frac{1}{r}=\frac{6\Delta TE_s t_s\sum_{i=1}^{n}E_i t_i(\alpha_i-\alpha_s)(h_{i-1}+h_i+t_s)}{E_s^2t_s^4+\sum_{i=1}^{n}\sum_{j=1}^{n}E_i t_i E_j t_j(h_j-h_{j-1})^2+2E_s t_s\sum_{i=1}^{n}E_i t_i(2(h_i^2-h_ih_{i-1}+h_{i-1}^2+t_s^2)+3(h_i+h_{i-1})t_s)}$$

(3. 5)

Equation (3.5) is a closed-form solution, which is identical to that reported in the literature solved by other approaches (e.g. Feng and Liu1983, Townsend et al 1987, Hsueh 2002, Nikishkov 2003).

In the case that the total thickness of thin films is much less than that of the substrate, i.e. $\sum_{i=1}^{n}t_i << t_s$, and $\sum_{i=1}^{n}E_i t_i << E_s t_s$, ε_t, ε_b and $1/r$ can be estimated as,

$$\varepsilon_t = 4\Delta T \sum_{i=1}^{n} E_i t_i (\alpha_i - \alpha_s) / E_s t_s + \alpha_s \Delta T \tag{3. 6a}$$

$$\varepsilon_b = 2\Delta T \sum_{i=1}^{n} E_i t_i (\alpha_s - \alpha_i) / E_s t_s + \alpha_s \Delta T \tag{3. 6b}$$

$$\frac{1}{r} = 6\Delta T \sum_{i=1}^{n} E_i t_i (\alpha_i - \alpha_s) / E_s t_s^2 \tag{3. 6c}$$

Then, the distribution of strain ε may be expressed as,

$$\varepsilon = 6\Delta T (\sum_{i=1}^{n} E_i t_i (\alpha_i - \alpha_s) / E_s t_s^2) y + 2\Delta T \sum_{i=1}^{n} E_i t_i (\alpha_s - \alpha_i) / E_s t_s + \alpha_s \Delta T \tag{3. 7}$$

Equation (3.6c) is identical to, for example, Equation (9c) in Hsueh (2002) and Equation (31b) in Townsend et al (1987). The location of the neutral axis is where ε_e is zero. According to Equation (3.7), the neutral axis in the substrate is located at $y_s^n = t_s / 3$, where $\varepsilon = \alpha_s \Delta T$ and $\varepsilon_e = 0$. Similarly, $\varepsilon = \alpha_i \Delta T$ at $y = y_i^n$, where

$$y_i^n = \frac{E_s t_s^2 (\alpha_i - \alpha_s)}{6 \sum_{j=1}^{n} E_j t_j (\alpha_j - \alpha_s)} + t_s / 3 \tag{3. 8a}$$

The condition that the neutral axis is in the *i*th film is $t_s + h_{i-1} \le y_i^n \le t_s + h_i$. Equation (3.8a) can also be expressed in terms of radius of curvature and thermal mismatch by substituting Equation (3.6c) into Equation (3.8a), i.e.,

$$y_i^n = r(\alpha_i - \alpha_s)\Delta T + t_s / 3 \tag{3. 8b}$$

Thus, the general expression for the location of neutral axis in a layer if existing is

$$y^n = r(\alpha - \alpha_s)\Delta T + t_s / 3 \qquad (\alpha = \alpha_i\,,\ \alpha_s) \tag{3. 9}$$

This expression reveals that in the case of very thin films the location of neutral axis in a layer depends on the radius of curvature and the thermal mismatch between the layer and the substrate.

Upon defining $\frac{1}{r_i} = 6\Delta T E_i t_i (\alpha_i - \alpha_s) / E_s t_s^2$, based on Equation (3.6c), we have,

$$\frac{1}{r} = \sum_{i=1}^{n} \frac{1}{r_i} \tag{3. 10}$$

This expression shows that the resultant curvature, $1/r$, can be expressed in terms of the components contributed by the thermal mismatch between the substrate and each thin film layer. Equation (3.10) has also been reported by Hsueh (2002) and Townsend et al (1987).

3.3 Bilayer Structures (Elastic Analysis)

Now consider bilayer structures, which consist of only one layer of thin film atop a substrate. They are the special case of multilayer thin films. For convenience, subscript

"*f*" is used standing for the thin film. Therefore, the expressions for ε_t, ε_b and *r* can be reduced to,

$$\varepsilon_t = \frac{\Delta T(E_f^2 t_f^4 \alpha_f + E_s^2 t_s^4 \alpha_s + E_f E_s t_f t_s ((6t_f^2 + 9t_f t_s + 4t_s^2)\alpha_f - t_f(2t_f + 3t_s)\alpha_s))}{E_f^2 t_f^4 + E_s^2 t_s^4 + 2E_f E_s t_f t_s (2t_f^2 + 3t_f t_s + 2t_s^2)} \quad (3.11a)$$

$$\varepsilon_b = \frac{\Delta T(E_f^2 t_f^4 \alpha_f + E_s^2 t_s^4 \alpha_s + E_f E_s t_f t_s ((6t_s^2 + 9t_f t_s + 4t_f^2)\alpha_s - t_s(2t_s + 3t_f)\alpha_f))}{E_f^2 t_f^4 + E_s^2 t_s^4 + 2E_f E_s t_f t_s (2t_f^2 + 3t_f t_s + 2t_s^2)} \quad (3.11b)$$

$$r = \frac{E_f^2 t_f^4 + E_s^2 t_s^4 + 2E_f E_s t_f t_s (2t_f^2 + 3t_f t_s + 2t_s^2)}{6\Delta T E_f E_s t_f t_s (t_f + t_s)(\alpha_f - \alpha_s)} \quad (3.11c)$$

Equation (3.11c) is identical to Equation (6) in Freund et al (1999), which was obtained using a potential energy method. With Equations (3.1)-(3.3), (3.11a) and (3.11b), we can obtain the stress distribution in the thickness direction as,

$$\sigma_s = \frac{\Delta T E_s E_f t_f (E_f t_f^3 + E_s t_s (6 y t_f - 3(t_f - 2y)t_s - 2t_s^2))(\alpha_f - \alpha_s)}{E_f^2 t_f^4 + E_s^2 t_s^4 + 2E_f E_s t_f t_s (2t_f^2 + 3t_f t_s + 2t_s^2)} \quad (0 \le y \le t_s)$$

(3. 12a)

$$\sigma_f = \frac{\Delta T E_s E_f t_s (E_s t_s^3 + E_f t_f (4t_f^2 + 6(t_s - y)t_s + t_f(9t_s - 6y)))(\alpha_s - \alpha_f)}{E_f^2 t_f^4 + E_s^2 t_s^4 + 2E_f E_s t_f t_s (2t_f^2 + 3t_f t_s + 2t_s^2)} \quad (t_s \le y \le t_s + t_f)$$

(3. 12b)

In some applications, the film is so thin that the average stress in the film, which can be obtained by,

$$\sigma_f^{mean} = \frac{1}{t_f}\int_{t_s}^{t_s+t_f} \sigma_f dy \tag{3. 13}$$

is of the interest.

Substituting Equation (3.12b) into Equation (3.13) results in that

$$\sigma_f^{mean} = \frac{\Delta T E_s E_f t_s (E_s t_s^3 + E_f t_f^3)(\alpha_s - \alpha_f)}{E_f^2 t_f^4 + E_s^2 t_s^4 + 2E_f E_s t_f t_s (2t_f^2 + 3t_f t_s + 2t_s^2)} \tag{3. 14}$$

By substituting Equation (3.11c) into Equation (3.14), σ_f^{mean} also can be expressed as,

$$\sigma_f^{mean} = \frac{-(E_f t_f^3 + E_s t_s^3)}{6r(t_f + t_s)t_f} \tag{3. 15}$$

Equations (3.14) and (3.15) are identical to those in Huseh (2002).

In many other applications, such as micro actuators in MEMS, where a large deflection is the major concern, the thickness of the film may be of the same order as that of the substrate. Hence, it is important to find the maximum stress in the film and the location of the maximum stress as well. According to Equation (3.12), it is obvious that both the maximum stress in the film and the maximum stress in the substrate always appear in the interface between them, i.e.,

$$\sigma_f^{\max} = \sigma_f \,|_{y=t_s} = \frac{\Delta T E_s E_f t_s (E_s t_s^3 + 4E_f t_f^3 + 3E_f t_f^2 t_s)(\alpha_s - \alpha_f)}{E_f^2 t_f^4 + E_s^2 t_s^4 + 2E_f E_s t_f t_s (2t_f^2 + 3t_f t_s + 2t_s^2)} \quad (3.16a)$$

$$\sigma_s^{\max} = \sigma_s \,|_{y=t_s} = \frac{\Delta T E_f E_s t_f (E_f t_f^3 + 4E_s t_s^3 + 3E_s t_s^2 t_f)(\alpha_f - \alpha_s)}{E_f^2 t_f^4 + E_s^2 t_s^4 + 2E_f E_s t_f t_s (2t_f^2 + 3t_f t_s + 2t_s^2)} \quad (3.16b)$$

Apart from that, according to Equation (3.12), the stress at the top surface of film, σ_f^{top}, can be expressed by,

$$\sigma_f^{top} = \sigma_f \,|_{y=t_f+t_s} = \frac{\Delta T E_s E_f t_s (E_s t_s^3 - 2E_f t_f^3 - 3E_f t_f^2 t_s)(\alpha_s - \alpha_f)}{E_f^2 t_f^4 + E_s^2 t_s^4 + 2E_f E_s t_f t_s (2t_f^2 + 3t_f t_s + 2t_s^2)} \quad (3.17)$$

Comparing Equation (3.17) with Equation (3.16), the condition for the film stress to be of the same sign is $E_s t_s^3 - 2E_f t_f^3 - 3E_f t_f^2 t_s \geq 0$, which can be rewritten in terms of the Young's modulus ratio and thickness ratio as,

$$1 - 2\frac{E_f}{E_s}\left(\frac{t_f}{t_s}\right)^3 - 3\frac{E_f}{E_s}\left(\frac{t_f}{t_s}\right)^2 \geq 0 \quad (3.18)$$

Figure 3.2 plots the contour of [$1 - 2\frac{E_f}{E_s}(\frac{t_f}{t_s})^3 - 3\frac{E_f}{E_s}(\frac{t_f}{t_s})^2$] against the Young's modulus ratio and thickness ratio. If Equation (3.18) is satisfied, σ_f^{top} is the minimum film stress. We will only focus on the case that Equation (3.18) is satisfied, since for ordinary materials and under most of the situations, according to Figure 3.2, Equation 3.18 should be always satisfied.

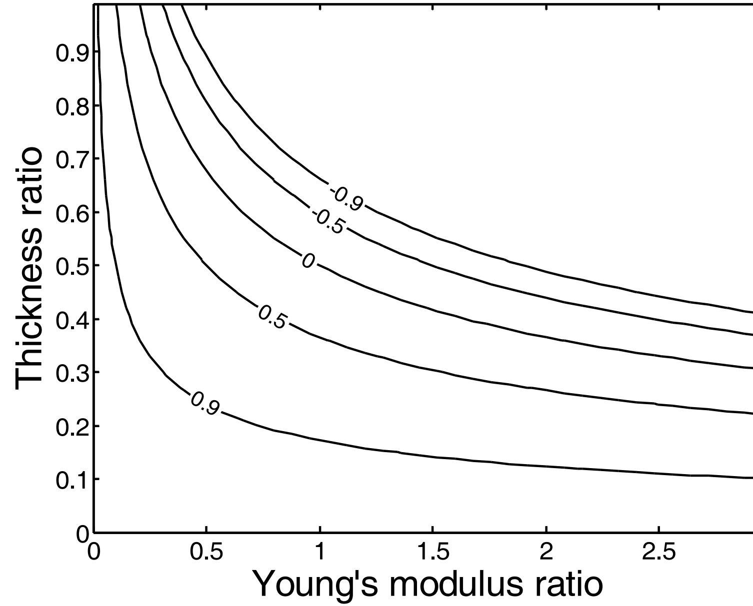

Figure 3. 2 Contour of $[1-2\frac{E_f}{E_s}(\frac{t_f}{t_s})^3-3\frac{E_f}{E_s}(\frac{t_f}{t_s})^2]$ against thickness ratio (t_f/t_s) and modulus ratio (E_f/E_s). When $E_s t_s^3-2E_f t_f^3-3E_f t_f^2 t_s \geq 0$, the film stress is of the same sign.

For easy comparison, the result of the Stoney equation (Stoney stress) is labeled as σ_0, i.e.,

$$\sigma_0=-E_s t_s^2/6t_f r \tag{3. 19}$$

As such, σ_f^{mean} and $\sigma_f^{\max}$ in Equations (3.15) and (3.16a) can be rewritten as,

$$\sigma_f^{mean} = \sigma_0 \frac{1 + E_f t_f^3 / E_s t_s^3}{1 + t_f / t_s} \tag{3. 20}$$

$$\sigma_f^{\max} = \sigma_0 \frac{1 + 4E_f t_f^3 / E_s t_s^3 + 3E_f t_f^2 / E_s t_s^2}{1 + t_f / t_s} \tag{3. 21}$$

Assuming that $E_s = 162\,\text{GPa}$ (for silicon) and $E_f = 83\,\text{GPa}$ (for silver), σ_f^{mean} and $\sigma_f^{\max}$ are plotted against the thickness ratio of the film over the substrate (t_f / t_s) in Figure 3.3 using Equations (3.20) and (3.21). As we can see, the Stoney equation is a good estimation for a thickness ratio up to about 0.1.

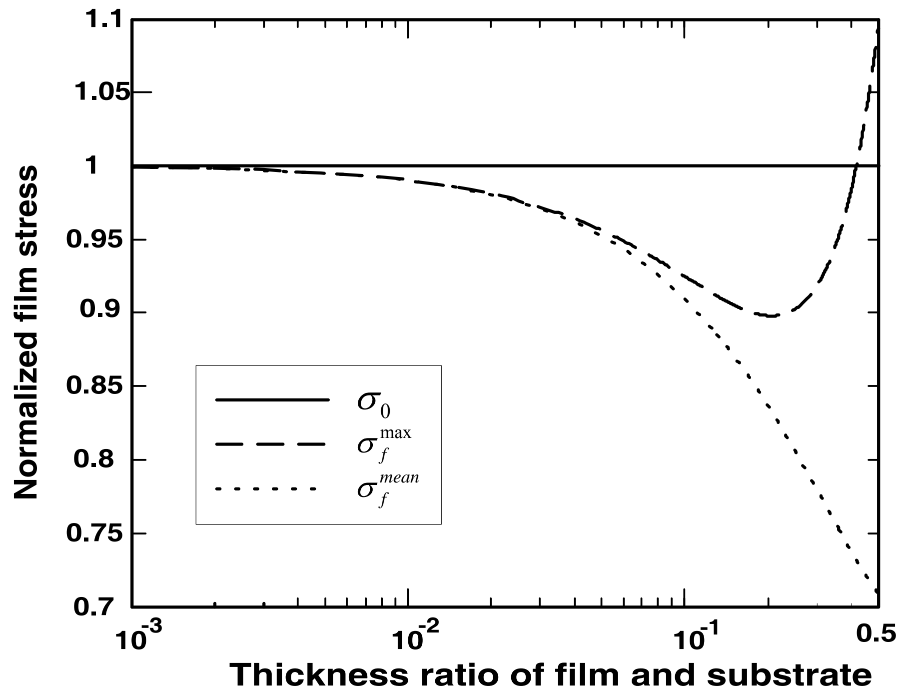

Figure 3. 3 Normalized stress against thickness ratio (t_f / t_s).

In order to compare the difference between σ_f^{mean} and $\sigma_f^{\max}$, we may define $\eta = (\sigma_f^{\max} - \sigma_f^{mean}) / \sigma_f^{\max}$ as a parameter. Hence,

$$\eta = \frac{3E_f t_f^3 / E_s t_s^3 + 3E_f t_f^2 / E_s t_s^2}{1 + 4E_f t_f^3 / E_s t_s^3 + 3E_f t_f^2 / E_s t_s^2} \tag{3. 22}$$

η is plotted against the thickness ratio and the ratio of Young's modulus in Figure 3.4. It reveals that the difference between σ_f^{mean} and $\sigma_f^{\max}$ can be significant for relatively thick films and in particular for hard films. Depending on the precision requirement, one may refer to Figure 3.4 to determine whether the average stress is good enough in the stress analysis.

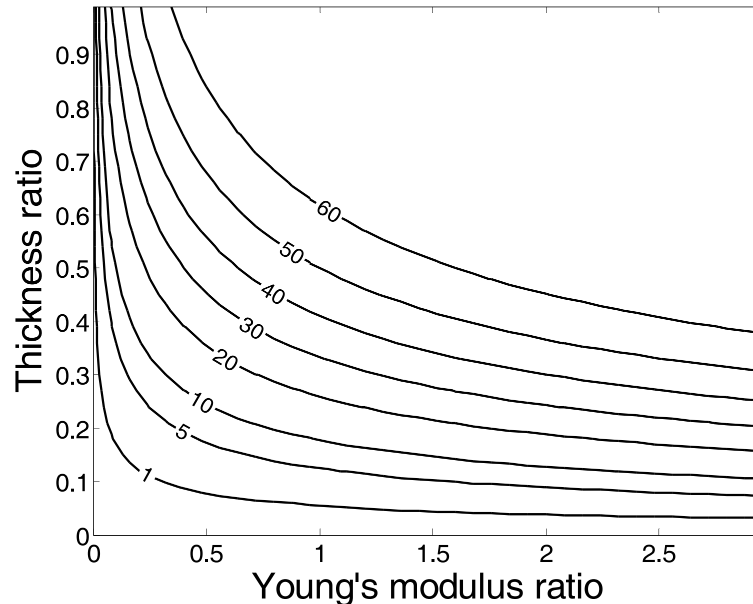

Figure 3. 4 Contour of η (%) against thickness ratio (t_f / t_s) and modulus ratio (E_f / E_s).

3.4 Neutral Axis in Bilayer Structures (Elastic Analysis)

There are a few different definitions of neutral axis in the literature. For instance, Klein (2000a) defined the position where the bending-force is zero as neutral axis and the position where the normal stress is zero as null axis. In Hsueh (2002), the position of zero stress is defined as neutral axis. We take the latter definition in the course of current study.

For convenience, a new coordinate system as illustrated in Figure 3.5 is adopted here. The interface between the film and substrate is therefore located at $y = 0$.

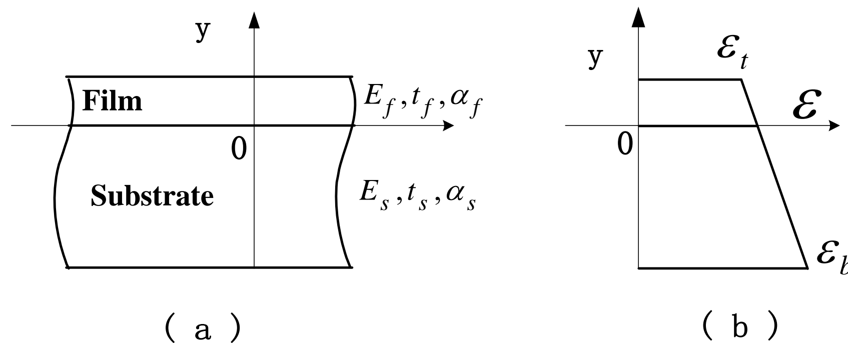

Figure 3. 5 Bilayer structure. (a) Coordinate system; (b) illustration of strain distribution.

Following the same method as mentioned above, the stress distributions in the film and substrate in the thickness direction can be expressed as,

$$\sigma_s = \frac{\Delta T E_s E_f t_f (E_f t_f^3 + E_s t_s (6 y t_f + 3(t_f + 2y) t_s + 4 t_s^2))(\alpha_f - \alpha_s)}{E_f^2 t_f^4 + E_s^2 t_s^4 + 2 E_f E_s t_f t_s (2 t_f^2 + 3 t_f t_s + 2 t_s^2)} \qquad (-t_s \le y \le 0)$$

(3. 23a)

$$\sigma_f = \frac{\Delta T E_s E_f t_s (E_s t_s^3 + E_f t_f (4 t_f^2 - 6 y t_s - t_f (6y - 3t_s)))(\alpha_s - \alpha_f)}{E_f^2 t_f^4 + E_s^2 t_s^4 + 2 E_f E_s t_f t_s (2 t_f^2 + 3 t_f t_s + 2 t_s^2)} \qquad (0 \le y \le t_f)$$

(3. 23b)

By setting $\sigma_s = 0$ and $\sigma_f = 0$, we can obtain the locations of neutral axes in the film and the substrate ($y = t_{f,\,n}$ and $y = t_{s,\,n}$) from Equation (3.23) as follows,

$$t_{f,\,n} = \frac{E_s t_s^3 + E_f t_f^2 (4 t_f + 3 t_s)}{6 E_f t_f (t_f + t_s)} \qquad (3.\ 24a)$$

$$t_{s,\,n} = -\frac{E_f t_f^3 + E_s t_s^2 (4 t_s + 3 t_f)}{6 E_s t_s (t_f + t_s)} \qquad (3.\ 24b)$$

The condition for the existence of neutral axis in the film is $0 \le t_{f,\,n} \le t_f$, while that in the substrate is $-t_s \le t_{s,\,n} \le 0$. Equation (3.24) also reveals that the locations of the neutral axes in the film and the substrate are dependent upon the elastic modulus and thickness of the film and substrate, and independent on CTE and temperature variation.

To show the location of neutral axis, consider a case that an aluminum film is deposited atop a silicon substrate. Parameters used in this case study are listed in Table 3.1.

Parameter	Young's Modulus	CTE	Thickness
Aluminum	70 GPa	23×10^{-6} /^{o}C	5 μm
Silicon	162 GPa	2.6×10^{-6} /^{o}C	15 μm

Table 3. 1 Parameters used in neutral axis case study.

Figure 3.6 shows the stress distributions at two temperatures, namely, $\Delta T = 10\ ^{o}C$ and $\Delta T = 15\ ^{o}C$. It is clear that the location of the neutral axes is independent on the exact temperature variation.

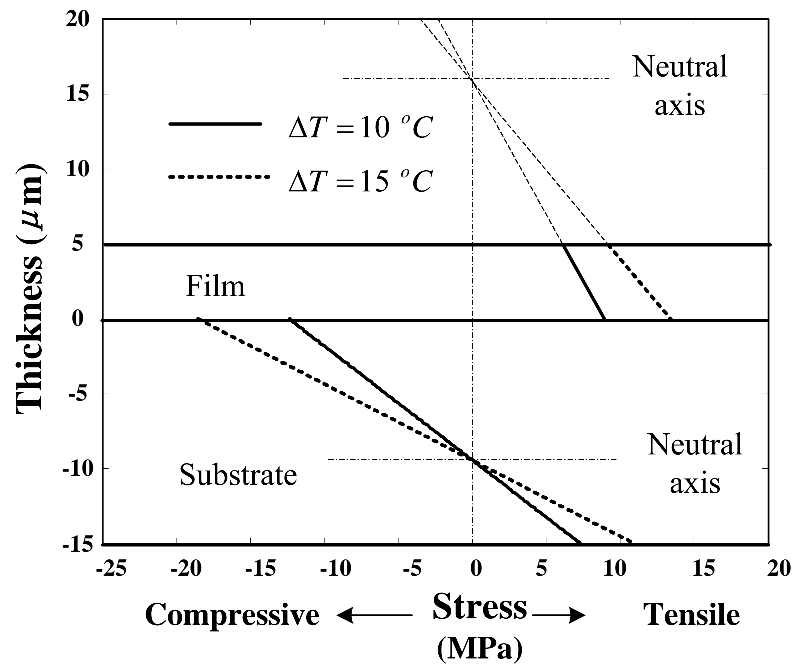

Figure 3. 6 Locations of neutral axes in film and substrate.

3.5 Bilayer Structures (Elastic-Plastic Analysis)

In the case that the temperature fluctuation is significant, the film may go beyond its elastic deformation range partially or even fully. However, in most cases, it might be reasonable to assume that the plastic strain is well limited within a regime slightly over the yield start point.

For convenience in the discussion hereinafter, we assume that the materials constants are temperature independent and the substrate is always within the elastic deformation range. The stress vs. strain relationship of most engineering materials in a range slightly over the elastic limit may be estimated using a bilinear model as illustrated in Figure 3.7, where E, H_f and σ_Y are the Young's modulus, strain hardening modulus and yield start stress, respectively.

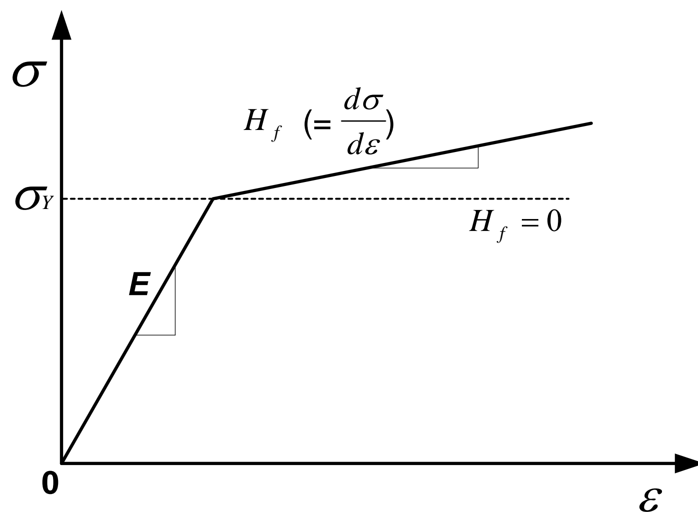

Figure 3. 7 Bilinear strain vs. stress model.

Let us start from the stress-free state. With the increase of temperature fluctuation, the film stress and the maximum film stress will increase accordingly. At a critical temperature, namely, ΔT_1, plastic deformation will appear in the film-substrate interface first. ΔT_1 can be solved by substituting $\sigma_f^{\max} = \sigma_Y$ into Equation (3.16a), i.e.,

$$\Delta T_1 = \frac{\sigma_Y (E_f^2 t_f^4 + E_s^2 t_s^4 + 2E_f E_s t_f t_s (2t_f^2 + 3t_f t_s + 2t_s^2))}{E_s E_f t_s (E_s t_s^3 + 4E_f t_f^3 + 3E_f t_s t_f^2)(\alpha_s - \alpha_f)} \tag{3. 25}$$

With further increase in temperature variation, more part of the film reaches the plastic state, until the whole film is in plastic range at another critical temperature, denoted by ΔT_2 (which will be solved later), as illustrated in Figure 3.8.

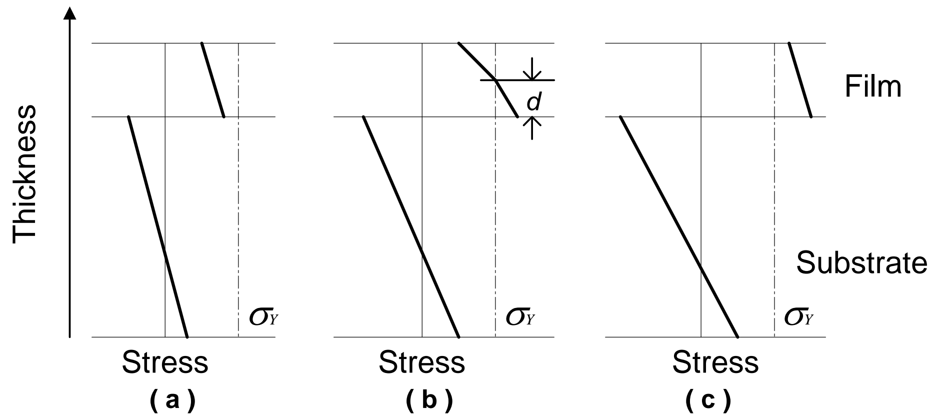

Figure 3. 8 Film stress development. (a) Pure elastic; (b) partially in plastic; (c) pure plastic.

Consider the case of pure plastic deformation, i.e., temperature variation> ΔT_2. The stress vs. strain relationship of the film can be expressed as (Shames 1989),

$$\sigma_f^{'} = H_f(\varepsilon - \alpha_f \Delta T - \frac{\sigma_Y}{E_f}) + \sigma_Y \tag{3. 26}$$

Then, the conditions for equilibrium (both the total resultant force and the total moment must be zero) are,

$$\int_0^{t_s} \sigma_s dy + \int_{t_s}^{t_s+t_f} \sigma_f^{'} dy = 0 \tag{3. 27a}$$

$$\int_0^{t_s} \sigma_s y dy + \int_{t_s}^{t_s+t_f} \sigma_f^{'} y dy = 0 \tag{3. 27b}$$

With Equations (3.1), (3.2), (3.26), and (3.27), one has,

$$\sigma_f^{mean} = \frac{-E_s t_s (E_s t_s^3 + H_f t_f^3)(E_f(\Delta T H_f(\alpha_f - \alpha_s) - \sigma_Y) + H_f \sigma_Y)}{E_f(H_f^2 t_f^4 + E_s^2 t_s^4 + 2H_f E_s t_f t_s (2t_f^2 + 3t_f t_s + 2t_s^2))} \tag{3. 28a}$$

$$\sigma_f^{\max} = \frac{-E_s t_s (E_s t_s^3 + H_f t_f^2(4t_f + 3t_s))(E_f(\Delta T H_f(\alpha_f - \alpha_s) - \sigma_Y) + H_f \sigma_Y)}{E_f(H_f^2 t_f^4 + E_s^2 t_s^4 + 2H_f E_s t_f t_s (2t_f^2 + 3t_f t_s + 2t_s^2))} \tag{3. 28b}$$

$$\sigma_f^{\min} = \frac{E_s t_s (-E_s t_s^3 + H_f t_f^2(2t_f + 3t_s))(E_f(\Delta T H_f(\alpha_f - \alpha_s) - \sigma_Y) + H_f \sigma_Y)}{E_f(H_f^2 t_f^4 + E_s^2 t_s^4 + 2H_f E_s t_f t_s (2t_f^2 + 3t_f t_s + 2t_s^2))} \tag{3. 28c}$$

Rewriting them in terms of the radius of curvature and σ_0 yields

$$\sigma_f^{mean} = -\frac{E_s t_s^3 + H_f t_f^3}{6t_f(t_s + t_f)r} = \sigma_0 \frac{1 + H_f t_f^3 / E_s t_s^3}{1 + t_f / t_s} \tag{3. 29a}$$

$$\sigma_f^{\max} = -\frac{E_s t_s^3 + 4H_f t_f^3 + 3H_f t_f^2 t_s}{6t_f(t_f + t_s)r} = \sigma_0 \frac{1 + 4H_f t_f^3 / E_s t_s^3 + 3H_f t_f^2 / E_s t_s^2}{1 + t_f / t_s} \tag{3. 29b}$$

$$\sigma_f^{\min} = -\frac{E_s t_s^3 - 2H_f t_f^3 - 3H_f t_f^2 t_s}{6t_f(t_f + t_s)r} = \sigma_0 \frac{1 - 2H_f t_f^3 / E_s t_s^3 - 3H_f t_f^2 / E_s t_s^2}{1 + t_f / t_s} \tag{3. 29c}$$

where σ_0 is the result of Stoney equation, in which r may be expressed as

$$r = \frac{E_f(H_f^2 t_f^4 + E_s^2 t_s^4 + 2H_f E_s t_f t_s (2t_f^2 + 3t_f t_s + 2t_s^2))}{6E_s t_f t_s (t_f + t_s)(E_f(\Delta T H_f(\alpha_f - \alpha_s) - \sigma_Y) + H_f \sigma_Y)} \tag{3. 30}$$

Note that here, subscript “min” stands for minimum.

Comparing Equations (3.20) and (3.21) (pure elastic solution) with Equations (3.29a) and (3.29b) (pure plastic solution), the only difference is that E_f is replaced by H_f.

Figure 3.9 shows the difference between $\sigma_f^{\max}$ and σ_0 when the whole film is in plastic deformation, while Figure 3.10 is for the difference between σ_f^{mean} and σ_0.

As mentioned above, the only difference between the pure elastic solution and pure plastic solution is that E_f is replaced by H_f if they are presented in terms of *r* (which is different in the elastic or pure plastic analysis). Thus, Figure 3.9 and Figure 3.10 can also be used for the pure elastic case after replacing H_f / E_s by E_f / E_s. Furthermore,

Figure 3.4 can be used in pure plastic deformation for the difference between σ_f^{mean} and $\sigma_f^{\max}$, after replacing E_f / E_s by H_f / E_s.

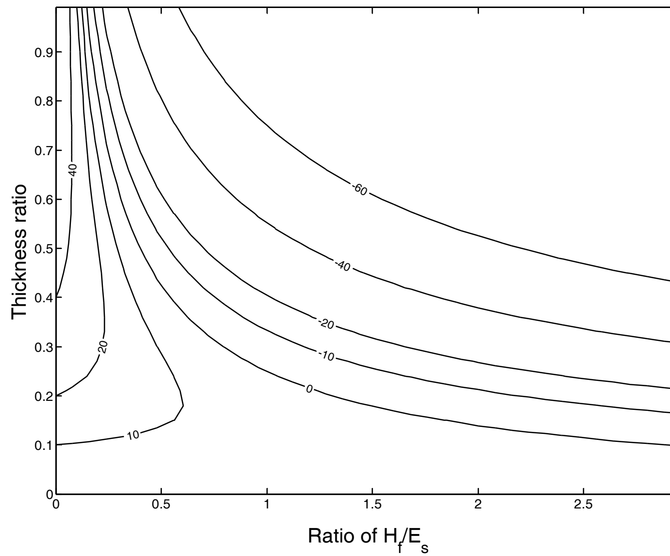

Figure 3. 9 Contour of difference ($\frac{\sigma_0 - \sigma_f^{\max}}{\sigma_f^{\max}}$, in %) against H_f / E_s and thickness ratio (t_f / t_s) when the whole film is in plastic deformation.

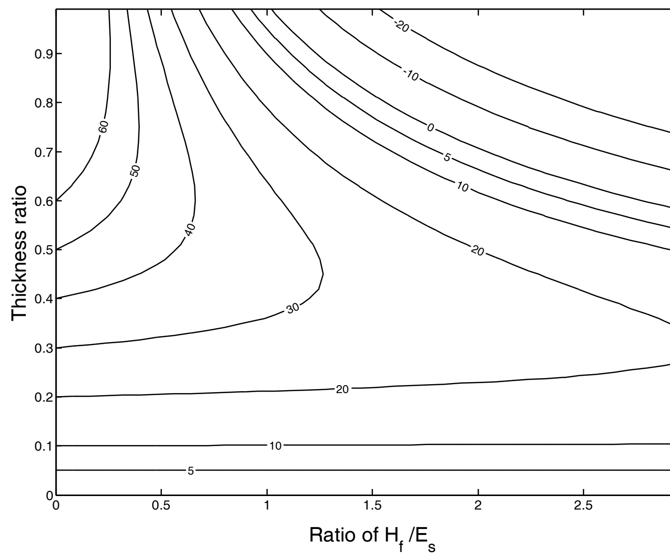

Figure 3. 10 Contour of difference ($\frac{\sigma_0 - \sigma_f^{mean}}{\sigma_f^{mean}}$, in %) against H_f / E_s and t_f / t_s when the whole film is in plastic deformation.

Figures 3.9 and 3.10 reveal the limit of the Stoney equation in stress analysis. According to Figure 3.9, for a difference within ±10% between σ_0 and $\sigma_f^{\max}$, the thickness ratio is recommended to be about 0.1 or less.

As shown in Figure 3.10, which is identical to Figure 1 in Klein (2000b) (note: that is for elastic analysis), the difference between σ_0 and σ_f^{mean} is $\leq 10\%$ for a thickness ratio ≤ 0.1, independent on the modulus ratio. Hence, we may conclude that as compared with the Stoney stress, for a precision within ±10%, the only requirement is that the thickness ratio is less than about 0.1.

As defined previously, ΔT_2 is the temperature at which plastic deformation is within the whole film. Now substituting $\sigma_f^{\min} = \sigma_Y$ into Equation (3.28c), one has,

$$\Delta T_2 = \frac{\sigma_Y (E_s t_s (E_s t_s^3 - H_f t_f^2 (2t_f^2 + 3t_s)) + E_f t_f (H_f t_f^3 + E_s t_s (6t_f^2 + 9t_f t_s + 4t_s^2)))}{E_f E_s t_s (E_s t_s^3 - H_f t_f^2 (2t_f + 3t_s))(\alpha_s - \alpha_f)} \tag{3. 31}$$

At a temperature between ΔT_1 and ΔT_2, only part of the film is deformed plastically. The condition of equilibrium (the total resultant force and the total moment must be zero) requires

$$\int_0^{t_s} \sigma_s dy + \int_{t_s}^{t_s+d} \sigma_f' dy + \int_{t_s+d}^{t_s+t_f} \sigma_f dy = 0 \tag{3. 32a}$$

and

$$\int_0^{t_s} \sigma_s y dy + \int_{t_s}^{t_s+d} \sigma_f^{'} y dy + \int_{t_s+d}^{t_s+t_f} \sigma_f y dy = 0 \qquad (3.\ 32b)$$

where d is the location of the yield start point in the film at a certain temperature between ΔT_1 and ΔT_2 [refer to Figure 3.8(b)]. In this case, $\sigma_f |_{y=t_s+d} = \sigma_f^{'} |_{y=t_s+d} = \sigma_Y$. Note that Equations (3.32a) and (3.32b) are difficult to solve analytically. Numerical solution can be obtained if the values of the parameters are available.

The difference among all the solutions within this temperature range should be between those of the elastic solution and pure plastic solution.

3.6 A Case of Elastic-Plastic Analysis

To show the difference of $\sigma_f^{\max}$, σ_f^{mean} and $\sigma_f^{\min}$ as compared with σ_0 in the whole temperature range, consider the case that an aluminum film is deposited atop a silicon substrate. Ignore the possible intermediate layer between them formed upon deposition. Most of the parameters listed in Table.3.2 are taken from Gere et al (1991). Three values for H_f, namely, 15 GPa (strain hardening), 0 GPa (i.e., ideal elastic-plastic material), and -15 GPa (strain softening) are used for analysis and comparison. ΔT_1 and ΔT_2 of three situations are listed in Table 3.3.

Parameter	Young's Modulus	CTE	Thickness	Yield start stress	H_f
Aluminum	70 GPa	23×10^{-6} /°C	5 μm	20 MPa	15 GPa
					0 GPa
					-15 GPa
Silicon	162 GPa	2.6×10^{-6} /°C	15 μm		

Table 3. 2 Parameters used in elastic-plastic case study.

	$H_f = 15$ GPa	$H_f = 0$ GPa	$H_f = -15$ GPa
ΔT_1 (^oC)	22.38	22.38	22.38
ΔT_2 (^oC)	30.08	29.47	28.90

Table 3. 3 ΔT_1 and ΔT_2 of three kind films with different H_f.

The stress distributions in the film and substrate at two temperatures of 25^oC and 35^oC are shown in Figure 3.11.

Film stresses (maximum, average, minimum stress) are plotted against temperature variation in Figure 3.12. We can see that the film stresses have linear relationships against temperature at a ΔT below ΔT_1 or above ΔT_2. Between them, i.e., the film is partially in plastic deformation, the relationship is non-linear. When the whole film is in the plastic range, the difference between $\sigma_f^{\max}$ and σ_f^{mean} , η

($= \dfrac{3H_f t_f^3 / E_s t_s^3 + 3H_f t_f^2 / E_s t_s^2}{1 + 4H_f t_f^3 / E_s t_s^3 + 3H_f t_f^2 / E_s t_s^2}$), becomes smaller. However, the difference between σ_0 and $\sigma_f^{\max}$ or σ_f^{mean} becomes larger as H_f is smaller than E_f.

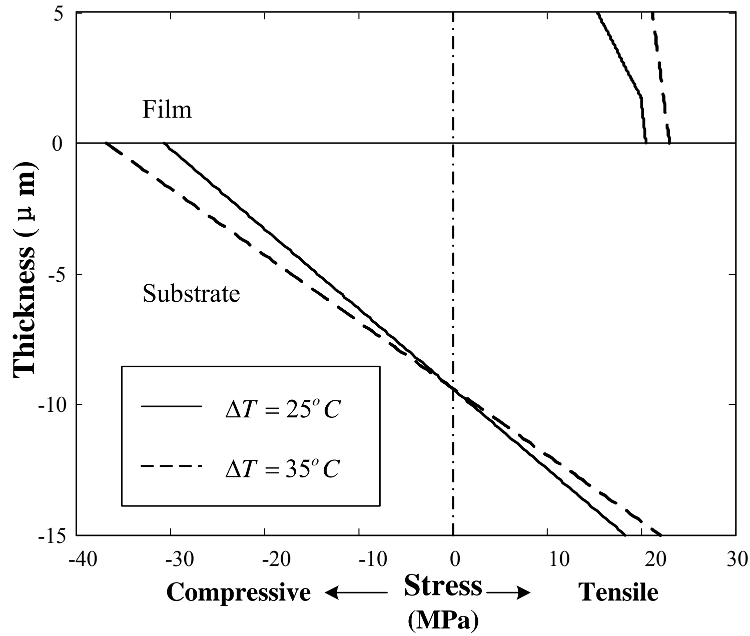

(a)

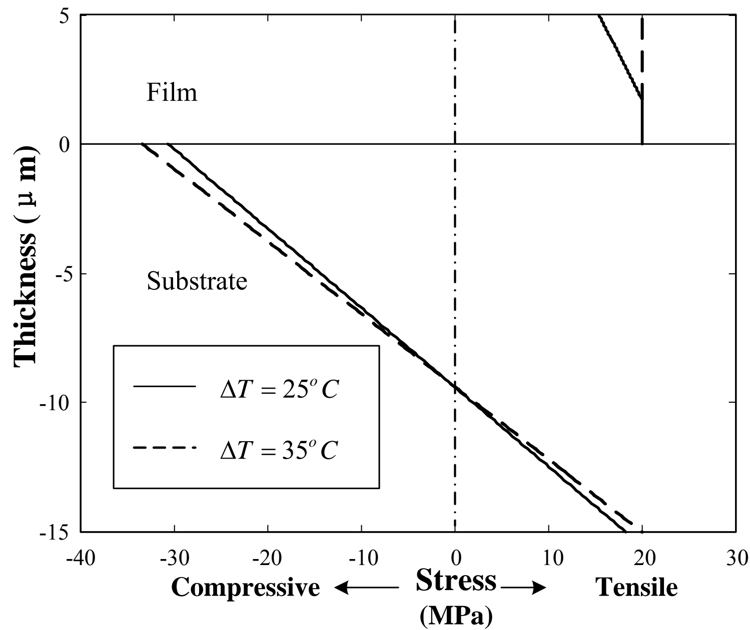

(b)

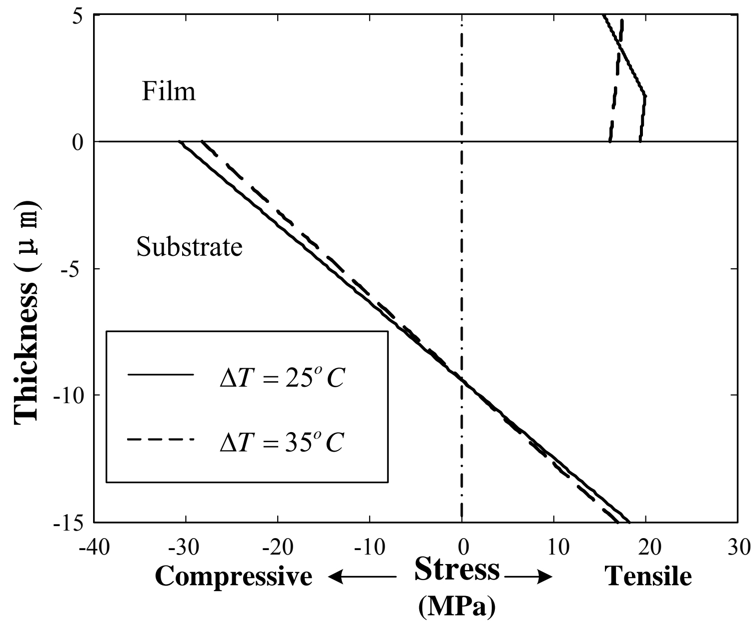

(c)

Figure 3. 11 Stress distributions in the film and substrate at $25^o C$ and $35^o C$. (a) $H_f = 15$ GPa; (b) $H_f = 0$; (c) $H_f = -15$ GPa.

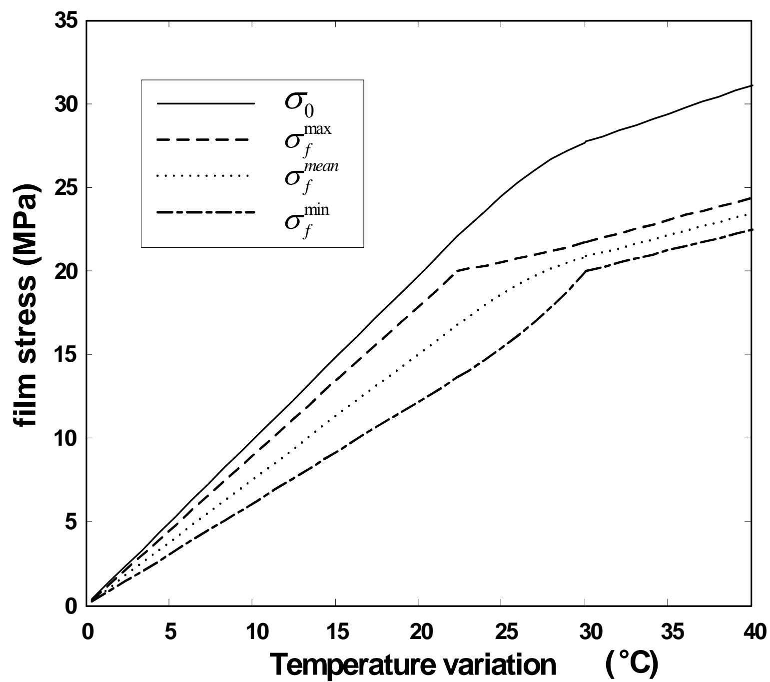

(a)

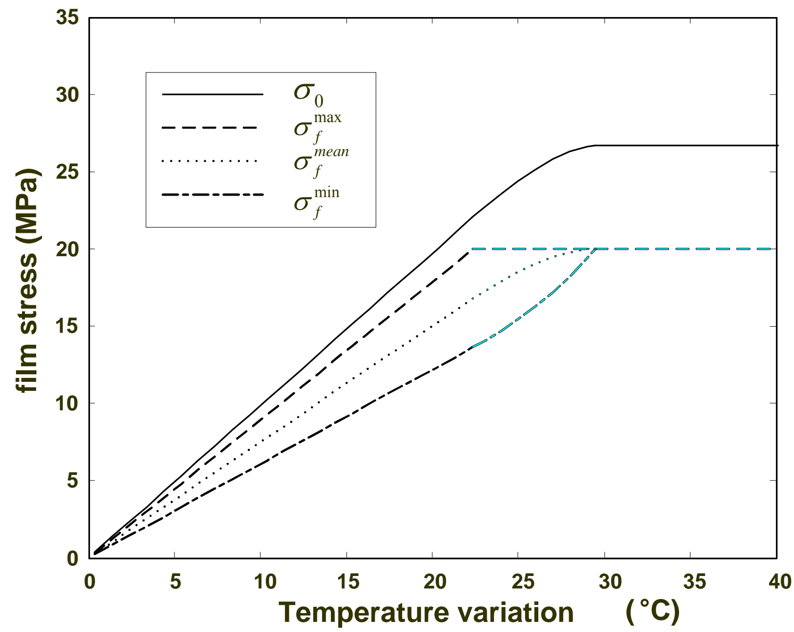

(b)

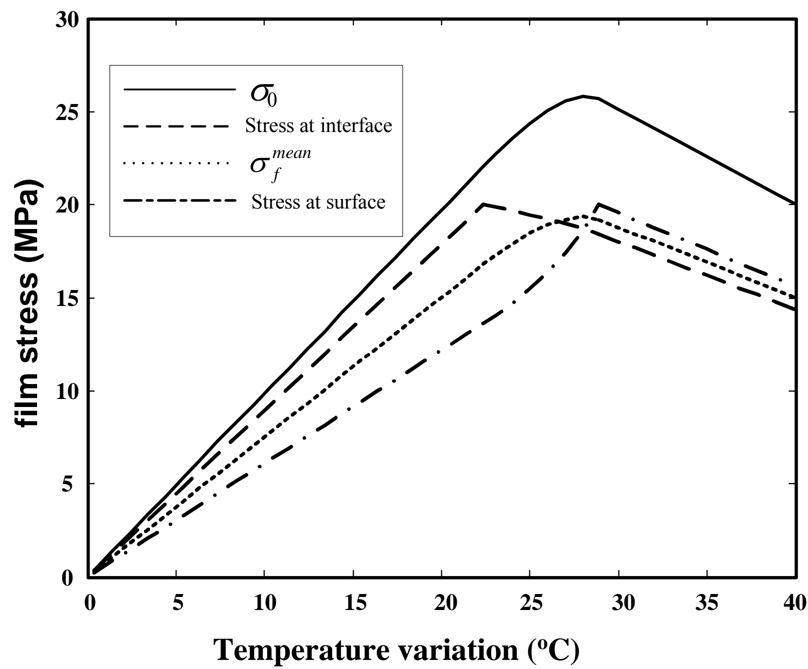

(c)

Figure 3. 12 Film stresses as function of temperature variation. (a) $H_f = 15$ GPa ; (b) $H_f = 0$; (c) $H_f = -15$ GPa .

Note that in the case of $H_f = -15$ GPa, the stress at the interface is not the maximum stress of the film after the yield start stress is reached due to softening. For the same reason, the minimum stress is not at the top surface of the film. Hence, the minimum and maximum stress presented in Figure 3.12(c) should be read as the film stress at the top surface and the interface, respectively, to reflect the true physical meaning of them.

Figure 3.13 shows the exact value of d in the temperature range from ΔT_1 to ΔT_2 together with that determined by a linear estimation, i.e.,

$$d = \frac{\Delta T - \Delta T_1}{\Delta T_2 - \Delta T_1} \times t_f \tag{3. 33}$$

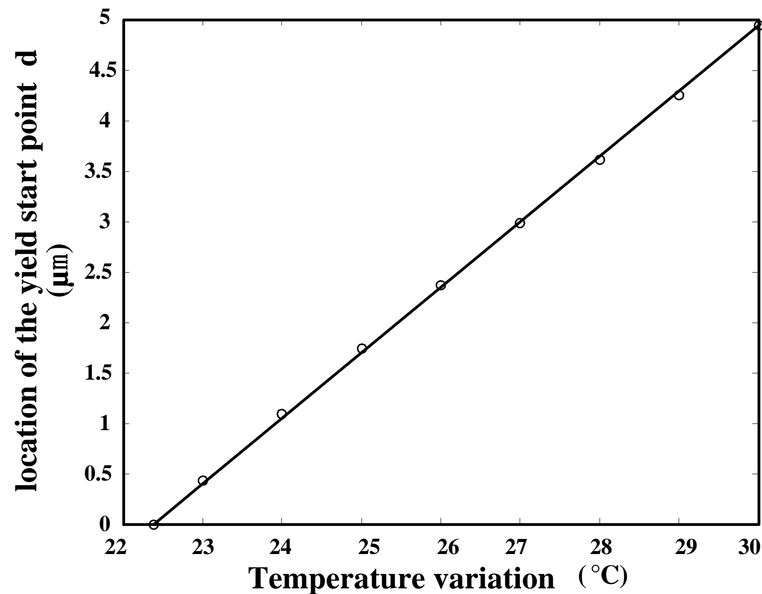

(a)

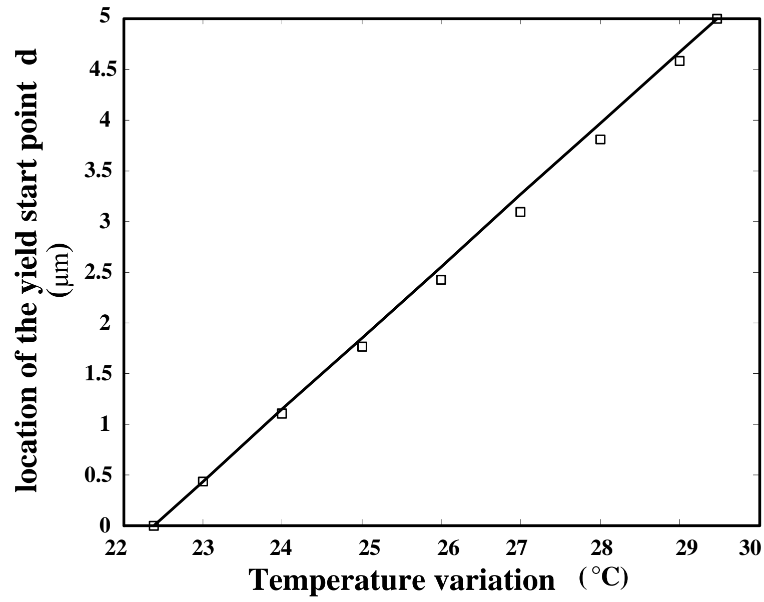

(b)

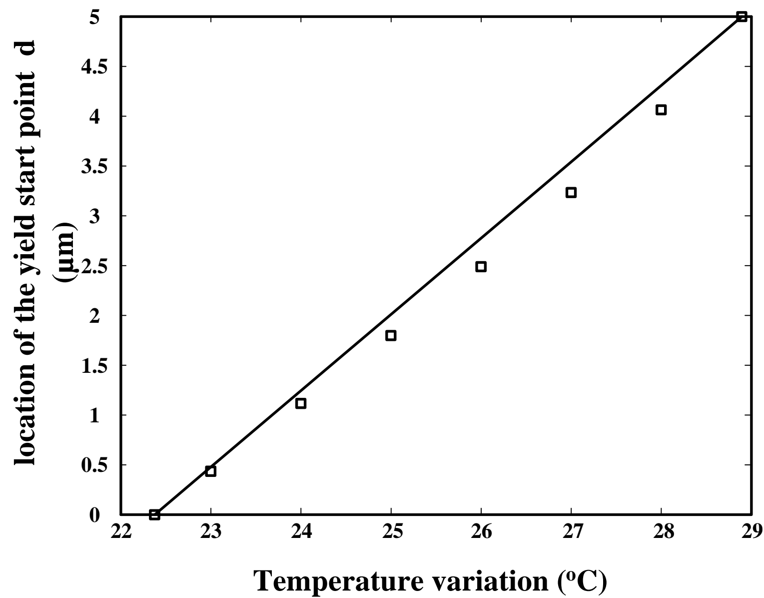

(c)

Figure 3. 13 Location of d against ΔT in the range between ΔT_1 and ΔT_2. Symbol: exact solution; line: determined by Equation (3.33). (a) $H_f = 15$ GPa ; (b) $H_f = 0$; (c) $H_f = -15$ GPa .

The errors in stress between the exact solution and that of Equation (3.33) in percentage (taking the exact solution as reference) are shown in Figure 3.14. It reveals that the maximum error in stress in percentage in all three H_f is less than 0.1%. Therefore, in this particular case d can be estimated as a linear function of ΔT.

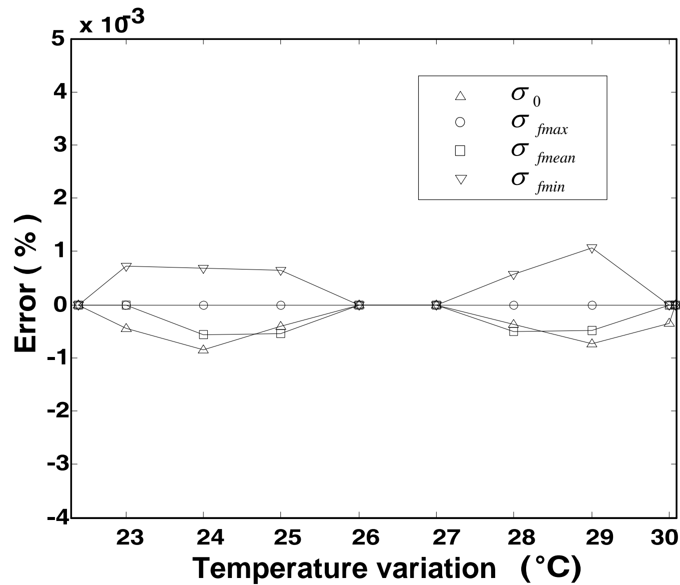

(a)

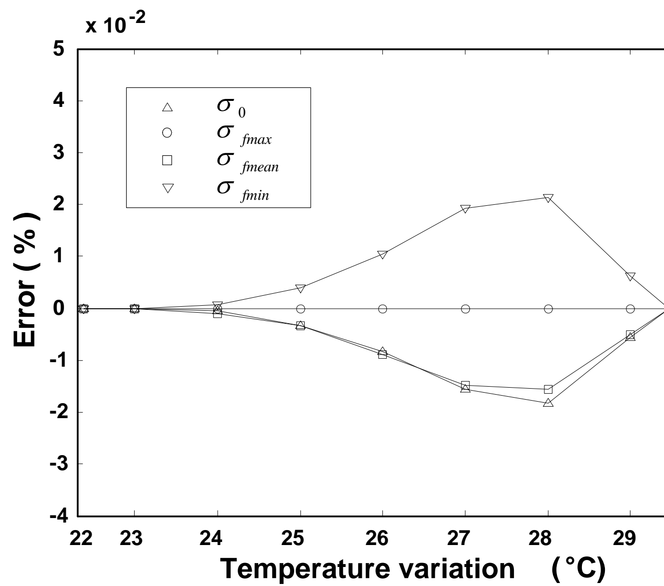

(b)

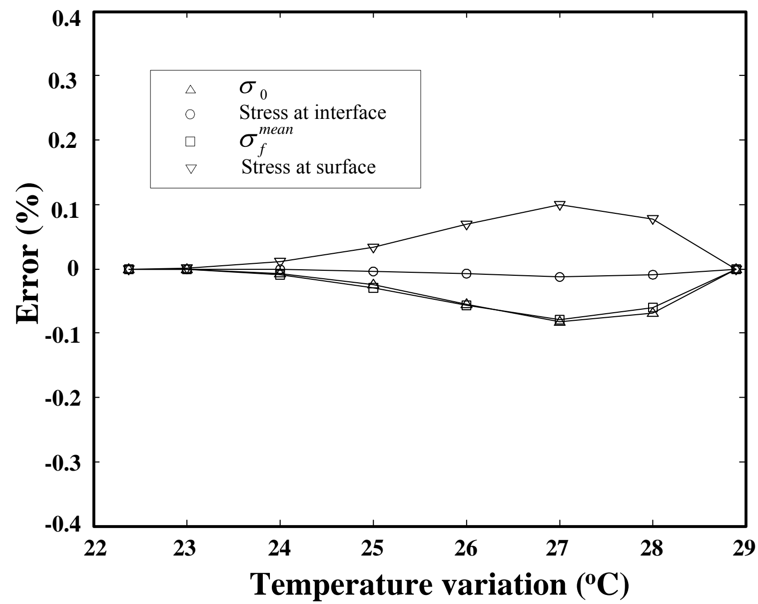

Figure 3. 14 Difference between exact solution and approximate solution (in %). (a) $H_f = 15$ GPa ; (b) $H_f = 0$; (c) $H_f = -15$ GPa .

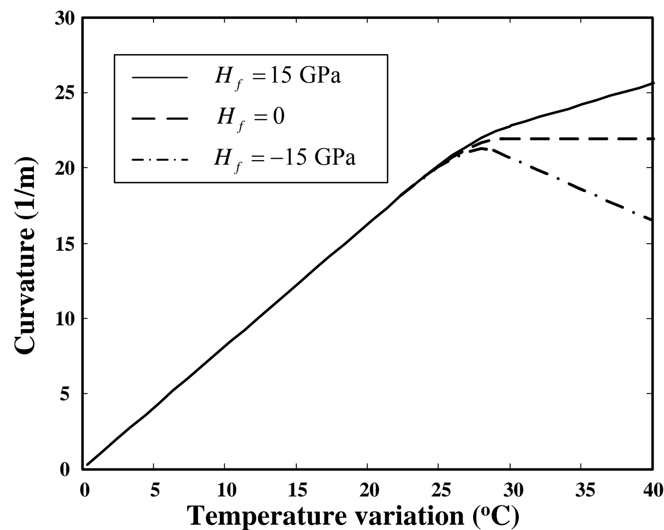

Figure 3. 15 Curvature as a function of temperature variation.

Figure 3.15 plots the curvature as a function of temperature variation. As we can see, the curvature slope decreases sharply after the film reaches plastic deformation. In the

case that $H_f = 0$, it becomes a constant after the whole film is over its elastic limit, while in the case that $H_f = -15$ GPa, it drops down linearly.

3.7 Numerical Simulation

In this section, thermal stress in bilayer strip is investigated by numerical simulation not only in the elastic deformation range but also in the elastic-plastic deformation range of film. The effects of parameters of film, such as thickness, strain hardening modulus, on thermal stress (normal stress, shear stress, etc) are also studied.

Consider the same case that an aluminum film is deposited atop a silicon substrate as assumed in Section 3.6. However, now three values of H_f, namely, 15 GPa (strain hardening), 5 GPa (strain hardening) and 0 GPa (ideal elastic-plastic material) are used for analysis and comparison, which are different from those in Section 3.6. The thickness of substrate is 15 μm, while that of film is 5 μm except the cases that the effect of film thickness is studied in which film thickness varies from 1 μm to 5 μm. The length of the bilayer structure is 240 μm.

Commercial finite element analysis package ANSYS 8.0 was utilized to simulate the thermal mismatch induced stress in a steady-state analysis. The substrate is modeled as isotropic and perfectly elastic. The plastic behavior of film is assumed to be isotropic. Hence, its stress versus strain relationship is modeled using bilinear isotropic hardening (BISO). In isotropic hardening, the yield surface remains centered at its initial centerline and expands in size as the plastic strains develop. The interface between the

film and substrate is assumed to be perfectly bonded at all times during simulation. The simulation is simplified as a two dimensional model using eight-node quadrilateral elements (PLANE82 with plane stress option) with two degrees of freedom at each node: translations in the nodal X and Y directions. The element size of the film is minimized gradually from top to interface, as interface is most likely to be with high stress concentration since both the maximum stress in the film and maximum stress in the substrate could appear at the interface as found in the previous studies. Due to the fact that film stress is more of our interest, coarser mesh is used for the substrate except in the area near the edge where stress concentration may also happen. The bilayer strip is symmetrical about its mid-point in the length direction and hence only half of it needs to be modeled. Finally, a two-dimensional rectangular mesh for the right half of the bilayer strip consists of 576 elements and 1849 nodes (in the case of 5 μm film).

The boundary and initial conditions are as follow: a) the middle line in X direction (left boundary of the model) is treated as symmetrical axis and hence all nodes on it are constrained from moving in X direction (X direction is along length of the bilayer structure); b) the node at the lower left corner is fixed to prevent from moving in both X and Y directions in a rigid body fashion (Y direction is along thickness of the bilayer structure); c) all other nodes are free to move; d) the bilayer strip is in free stress state during deposition. The simulation assumes a uniform temperature distribution in the strip and the temperature variation (ΔT) starts from cooling from the deposition temperature. Refer to Appendix C for the details of the FEA model.

Film stresses (σ_x) are plotted against temperature variation in Figure 3.16. For finite element method (FEM), stress in the area far away from edge is plotted, as we can see later, film stresses may change significantly at the edge.

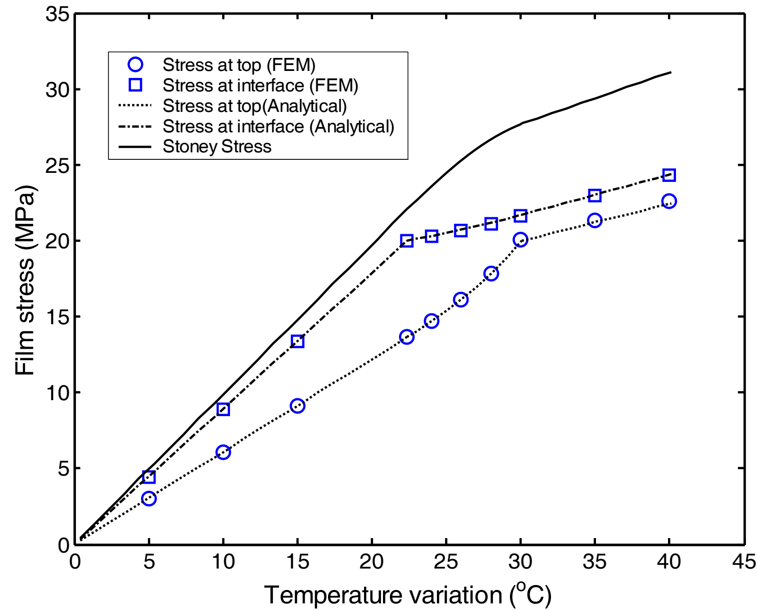

Figure 3.16 Film stresses σ_x as function of temperature variation (H_f =15 GPa).

Figure 3.16 shows that thermal stress (both at top and at interface) increases with the increase of temperature variation and the analytical result agrees well with that of FEM. In the range that the film is fully elastic or plastic, the relationships between film stresses and temperature variation are linear, which agree well with the analytical results. As mentioned earlier, a linear variation in film stress over the thickness direction occurs when the film is fully elastic state, with the maximum film stress located at the interface. The film starts to yield at the interface first (in this studied case, at a temperature variation of about 22.4^{o}C) and then yielding part expands along the thickness direction upon further increase in temperature variation till the whole film is

in plastic state. Therefore, the relationship of film stress versus temperature variation is non-linear when film is partially in plastic deformation. There is no sudden turning point in average film stress versus temperature curve (for a clear view, average film stress is not plotted in Figure 3.16, refer to Figure 3.12) even the film has an obvious yield point in its stress versus strain relationship. Similar phenomenon has been reported in bending of a bilayer micro beam (Florando and Nix 2005).

Figure 3.17 shows FEM results of film stresses both at top and at interface versus film thickness when temperature variation is 15°C and H_f=15 GPa. Both stress at top and stress at interface increase as film thickness decreases. On the other hand, the thinner is the film, the closer the stress at top and the stress at interface are. That is to say in the case that substrate is much thicker than the film, the film stress is approximately uniform over the thickness direction.

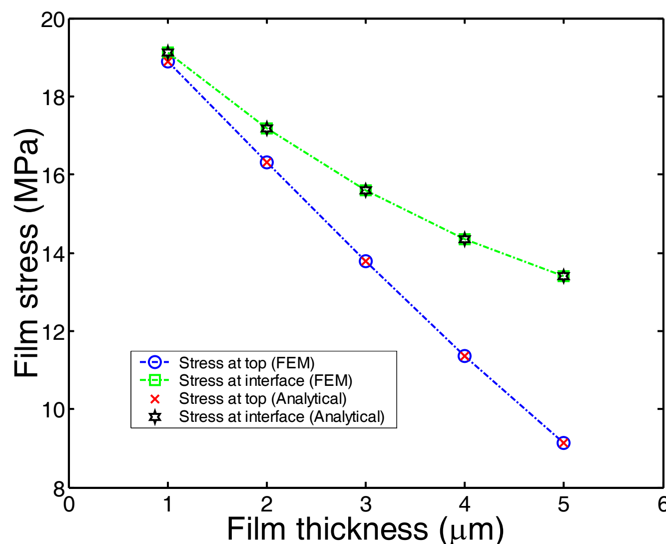

Figure 3.17 Film stress σ_x versus film thickness (temperature variation is 15°C and H_f=15 GPa).

Figure 3.18 shows the film stress (σ_x) at the interface at three different temperature variations, namely, 20°C, 26°C and 35°C. Note here, at ΔT=20°C, the film is in elastic range, while at ΔT=35°C, it is in whole plastic range. Between them, at ΔT=26°C, it is partially in plastic deformation range. From Figure 3.18, we can see that at a place which is far away from the edge, the FEM results agree well with the analytical values. However, FEM results show gradual decrease starting from about 100 μm due to the edge effect, and it becomes dramatic near the edge. The range of edge effect in in-plane is around the total thickness of the bilayer strip (20 μm). On the other hand, the larger is the temperature variation, the bigger the σ_x is. However, the rate of increase of σ_x is smaller after yielding.

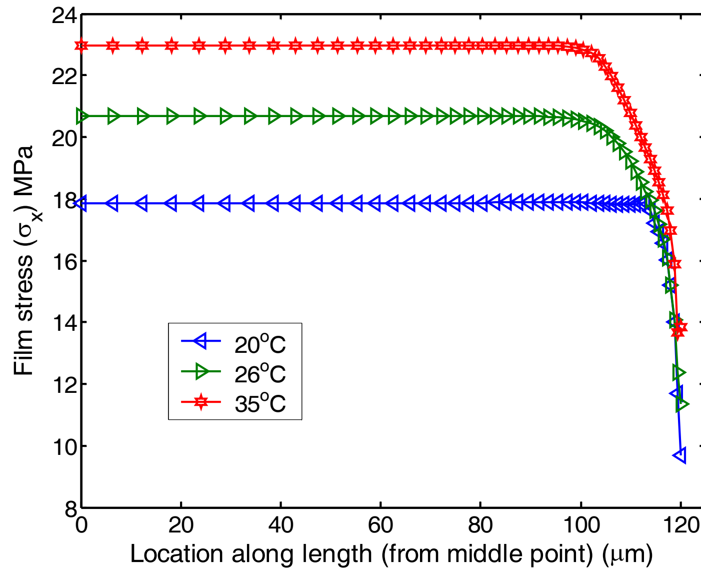

Figure 3.18 Film stress (σ_x) at the interface at three different temperature variations (H_f=15 GPa).

Figure 3.19 shows film stress (σ_y) at the interface at three different temperature variations. While σ_y is nearly zero in the area far away from the edge, it increases suddenly in the area near the edge till reaching the maximum. For instance, when temperature variation is 35°C, the maximum σ_y is 22.51 MPa, which is about the same as the maximum σ_x (22.95 MPa). Hence, σ_y may also cause failure of adhesion at the interface and/or spallation of the film. In addition, the range for the edge effect is also about 20 μm from edge.

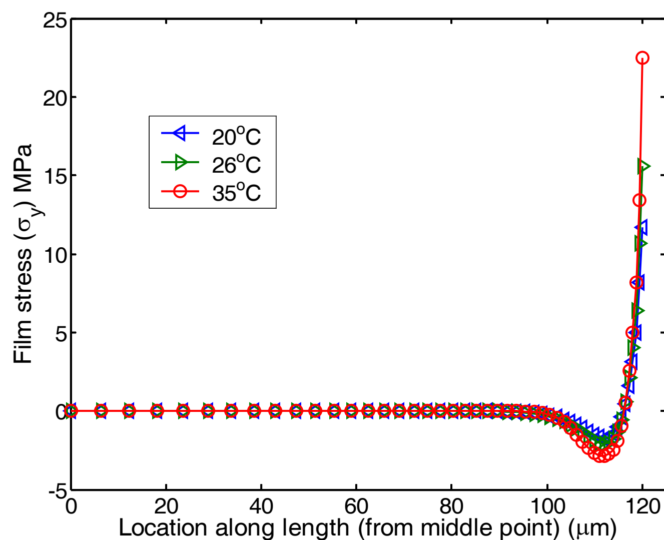

Figure 3.19 Film stress (σ_y) at the interface at three different temperature variations (H_f =15 GPa).

Film shear stress (σ_{xy}) at the interface is shown in Figure 3.20. Like σ_y, σ_{xy} is almost zero in the part far away from edge. At the edge, it increases significantly following the same trend at three temperature variations. Besides σ_x, σ_y and σ_{xy} may also be the

reasons for the failure of film due to the fact that σ_y and σ_{xy} may concentrate at the edge or at the area near the edge as shown in Figure 3.19 and Figure 3.20.

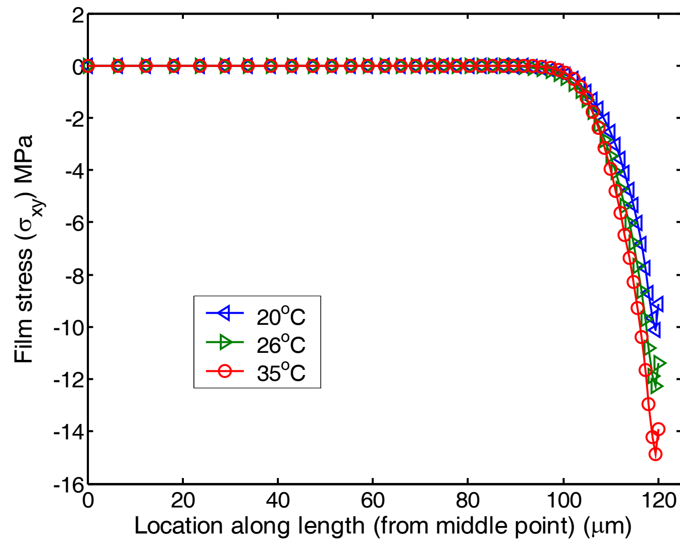

Figure 3.20 Film shear stress (σ_{xy}) at the interface at three different temperature variations (H_f =15 GPa).

Figure 3.21 shows film shear stresses (σ_{xy}) distribution through film thickness at different locations, namely, (x=100, 110, and 120 μm) and with different strain hardening moduli (H_f =15, 5, and 0 GPa, respectively) when temperature variation is 35°C. It can be seen that at x=100 μm from the middle point, the film shear stresses are almost zero through thickness of film in all three strain hardening moduli cases. At x=110 μm, the maximum shear stress occurs at the interface, but it almost remains the same in three strain hardening moduli cases. While at x=120 μm, i.e., the edge, the less the strain hardening modulus is, the smaller the maximum shear stress is, which is located at the interface.

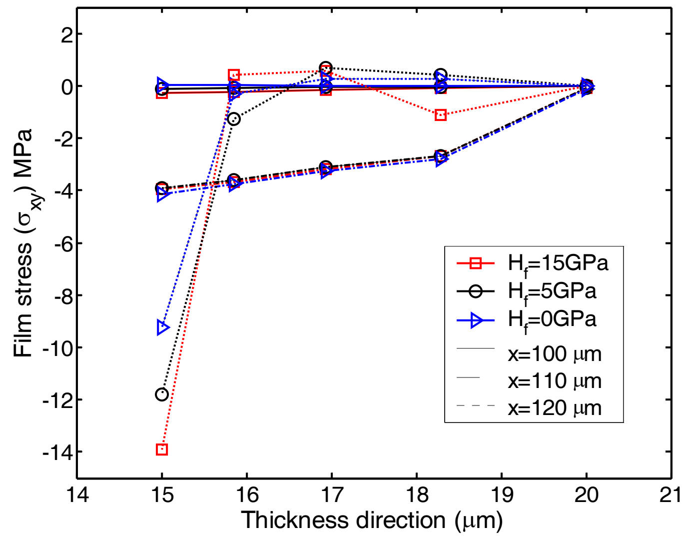

Figure 3.21 Film shear stress (σ_{xy}) distribution through film thickness at different locations (x=100, 110, and 120 μm) and with different strain hardening moduli (H_f =15, 5, and 0 GPa, respectively) when temperature variation is 35°C.

3.8 Conclusions

This chapter presents detailed elastic and elastic-plastic analysis of the stress in multilayer thin film structures.

1. The elastic analysis based on the linear strain assumption results in the identical closed-form solution and approximation (for very thin films) as those reported in the literature.

2. Closed-form solutions are obtained for full-plastically deformed films.

3. The difference among the maximum stress, average stress and Stoney stress in films is investigated systematically. It is concluded that taken Stoney stress as reference, for an error within ±10%, it is required that the thickness ratio should be about 0.1 or less in whatever elastic or elastic-plastic analysis.

4. The location of the neutral axes can be determined by the Young's modulus and the thickness of the film and substrate.

5. The result of a case study reveals that the yield start point may be estimated as a linear function of temperature in the elastic-plastic deformation range.

6. Although our current investigation is more focused on bilayer structures, the approach presented here can be easily extended into multilayer thin films.

CHAPTER 4 DETERMINATION OF THERMO-MECHANICAL PROPERTIES

4.1 Introduction

A lot of dedicated techniques have been developed to determine the thermo-mechanical properties of thin films, such as, the Young's modulus, coefficient of thermal expansion (CTE), Poisson's ratio etc, as discussed briefly in Chapter 2. Despite of these previous efforts, most of these techniques require either a very dedicated equipment (and normally very expensive as well) or a complicated procedure in testing and analysis, and have some difficulties in dealing with a few properties by just a couple of tests.

In 1980, Retajczyk and Sinha (1980) proposed the so-called "thermally induced bending method", in which two different materials were used as the substrate, to simultaneously determine two in-plane properties of thin films, namely, biaxial modulus and CTE. Continuous improvement has been made since then (e.g., Lima et al 1999, Thurn et al 2004). For examples, Zhao et al (1999) improved this method to determine the Young's modulus and CTE of thin films by measuring thermal stress in thin films deposited atop Si and GaAs substrates. Extensions of this technique even allow to estimate the film's Poisson's ratio. Tien et al (2001) proposed a way associated

with an image processing technique to determine the mechanical properties of thin films atop a substrate, in which the change of the substrate deflection was obtained by a digital phase shifting interferometry. At present, the Young's modulus, Poisson's ratio and CTE can be determined using this method (Zhao et al 1999, Zhao et al 2000a).

Thermally induced bending method is based on the variation in curvature of bilayer structures upon temperature fluctuation, which can be easily measured by many conventional techniques. But most of the methods proposed in the literature are derived from simplified solutions and are more applicable in finding only some mechanical properties of elastic thin films.

On the other hand, residual stress, which normally includes two parts, namely the intrinsic stress and thermal stress, in multilayer structures is an important issue largely due to its possible strong influence on the performance and reliability of structures. Many approaches have been proposed in the past years in order to determine the residual stress. However, most of them are not applicable to multilayer structures and/or fail to quantitatively separate the intrinsic stress and thermal stress.

The purpose of this chapter is to propose simple approaches to determine thermo-mechanical properties of thin films on an elastic substrate. In Section 4.2, a simple approach, which is similar to the thermally induced bending method, is presented. For a bilinear material, by carrying out up to three experiments, this approach can cope with up to five thermo-mechanical properties of thin films, namely, the Young's modulus, CTE, Poisson's ratio, yield start stress, and strain hardening modulus. In Section 4.3, a

curvature-based approach, which can determine not only the residual stress but also the intrinsic stress and thermal stress in each layer in multilayer structures, is proposed.

4.2 Five Properties in a Bilinear Material

4.2.1 Simplified formula in the literature

In Chapter 3, we have shown that the average stress in the thin film can be expressed as

$$\sigma_f^{mean} = \frac{\Delta T E_s E_f t_s (E_s t_s^3 + E_f t_f^3)(\alpha_s - \alpha_f)}{E_f^2 t_f^4 + E_s^2 t_s^4 + 2E_f E_s t_f t_s (2t_f^2 + 3t_f t_s + 2t_s^2)} \tag{4.1}$$

The meanings of the symbols are the same as those in Chapter 3. In the case that $t_f << t_s$, i.e., very thin film, by ignoring terms with orders higher than t_f and replacing σ_f^{mean} by σ_f, Equation (4.1) can be reduced to

$$\sigma_f = E_f (\alpha_s - \alpha_f) \Delta T \tag{4.2}$$

From Equation (4.2), one can easily determine the stress vs. temperature variation curve. The slope of the stress vs. temperature variation curve can be expressed as

$$\frac{d\sigma_f}{dT} = E_f (\alpha_s - \alpha_f) \tag{4.3}$$

Note that in the case of biaxial stress, biaxial modulus, $\overline{E_f}$ [$= \frac{E_f}{1-\upsilon_f}$, where υ_f is Poisson's ratio], should be used instead of E_f. The simplified formula, i.e., Equation (4.3), has been used widely by many researchers.

4.2.2 Determine thermo-mechanical properties of a thin film

Consider a layer of thin film deposited atop a substrate. The properties of this thin film are unknown. For simplicity, assume the materials constants of the thin film and substrate are temperature independent (at least within the testing temperature range), the properties of the substrate are known, and the substrate is always in the elastic deformation range. The thickness, Young's modulus, and coefficient of thermal expansion of thin film are denoted as t_f, E_f, and α_f, and those of substrate are t_s, E_s and $\alpha_s \left(\neq \alpha_f\right)$, respectively, as defined in Chapter 3. Given a small temperature variation (ΔT), the bilayer structure tends to bend due to the difference in CTE. The stresses in the film and substrate are denoted by σ_f and σ_s, respectively.

Based on the equilibrium conditions, the curvature of the bilayer structure, K_e, can be expressed as (Hu and Huang 2004, Hsueh 2002)

$$K_e = \frac{6E_f E_s t_f t_s (t_f + t_s)(\alpha_f - \alpha_s)\Delta T}{E_f^2 t_f^4 + E_s^2 t_s^4 + 2E_f E_s t_f t_s (2t_f^2 + 3t_f t_s + 2t_s^2)} \qquad (4.4)$$

where the subscript '*e*' indicates that the thin film is in the elastic range. Upon heating or cooling, one can obtain the curvature vs. temperature relationship of the structure as illustrated in Figure 4.1.

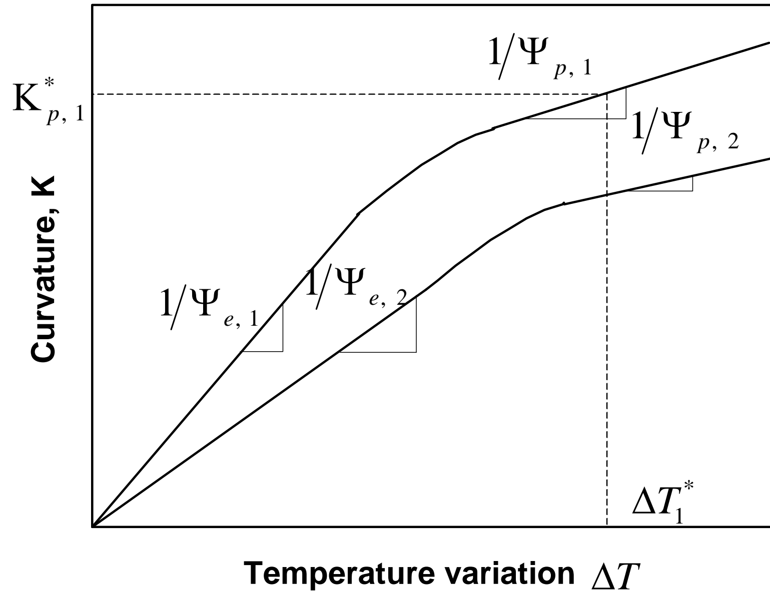

Figure 4. 1 Illustration of curvature as a function of temperature variation. Subscripts "1" and "2" stand for the results of two structures. (ΔT_1^*, $K^*_{p,1}$) is any point in the full plastic range (for the film).

The curvature has a linear relationship with temperature variation if the whole film is in the pure elastic deformation range (refer to Section 3.5). Let $dK_e/dT = 1/\Psi_e$. From Equation (4.4), one can obtain that

$$E_f^2 t_f^4 + 2E_f E_s t_f t_s [(2t_f^2 + 3t_f t_s + 2t_s^2) - 3\Psi_e (t_f + t_s)(\alpha_f - \alpha_s)] + E_s^2 t_s^4 = 0 \qquad (4.5)$$

If the temperature variation is significant, the film may be over its elastic deformation range partially or fully. However, for most cases, it might be reasonable to say that the plastic strain is well limited within a regime slightly over the yield start point.

The stress vs. strain relationship of most engineering materials in a range slightly over the elastic range may be estimated using a bilinear model as illustrated in Figure 3.7.

Hence, the curvature of the bilayer structure after the thin film is fully in the plastic range can be expressed as (refer to Section 3.5)

$$K_p = \frac{6E_s t_f t_s (t_f + t_s)(\Delta T H_f (\alpha_f - \alpha_s) - \sigma_Y + \frac{H_f}{E_f}\sigma_Y)}{H_f^2 t_f^4 + E_s^2 t_s^4 + 2H_f E_s t_f t_s (2t_f^2 + 3t_f t_s + 2t_s^2)} \tag{4.6}$$

where the subscript '*p*' indicates that the thin film is in the pure plastic range (Figure 4.1). Our previous investigation in Section 3.5 shows that the curvature has a linear relationship with temperature variation again if the whole film is in pure plastic deformation. If only part of the film is in plastic deformation, the relationship is non-linear. Let $dK_p / dT = 1/\Psi_p$ (Figure 4.1). From Equation (4.6), we can obtain that

$$H_f^2 t_f^4 + 2H_f E_s t_f t_s [(2t_f^2 + 3t_f t_s + 2t_s^2) - 3\Psi_p (t_f + t_s)(\alpha_f - \alpha_s)] + E_s^2 t_s^4 = 0 \tag{4.7}$$

One may carry out two tests on two structures (for instance, same thin film thickness but different substrate thickness, namely, $t_{s,1}$ and $t_{s,2}$), two curvature vs. temperature

variation curves can be obtained. Hence, two Ψ_e ($\Psi_{e,1}$ and $\Psi_{e,2}$) and two Ψ_p ($\Psi_{p,1}$ and $\Psi_{p,2}$) are resulted. Provided that E_s and α_s are known, E_f and α_f can be obtained by solving two equations in the form of Equation (4.5), which results in

$$E_f = \frac{-E_s t_f t_{s,1} t_{s,2}(\theta_1 - \theta_2) \pm \sqrt{E_s^2 t_f^2 t_{s,1}^2 t_{s,2}^2 (\theta_1 - \theta_2)^2 - E_s^2 t_f^4 t_{s,1} t_{s,2} (\theta_3 - \theta_4)(\theta_5 - \theta_6)}}{t_f^4 (\theta_3 - \theta_4)} \quad (4.8)$$

$$\alpha_f = \frac{E_f^2 t_f^4 + E_s^2 t_{s,1}^4 + 2E_f E_s t_f t_{s,1}(2t_f^2 + 3t_f t_{s,1} + 2t_{s,1}^2)}{6E_f E_s t_f t_{s,1}(t_f + t_{s,1})\Psi_{e,1}} + \alpha_s \quad (4.9)$$

where

$$\theta_1 = \Psi_{e,1}(t_f + t_{s,1})(2t_f^2 + 3t_f t_{s,2} + 2t_{s,2}^2);$$

$$\theta_2 = \Psi_{e,2}(t_f + t_{s,2})(2t_f^2 + 3t_f t_{s,1} + 2t_{s,1}^2);$$

$$\theta_3 = \Psi_{e,1} t_{s,1}(t_f + t_{s,1});$$

$$\theta_4 = \Psi_{e,2} t_{s,2}(t_f + t_{s,2});$$

$$\theta_5 = \Psi_{e,1} t_{s,2}^3 (t_f + t_{s,1});$$

$$\theta_6 = \Psi_{e,2} t_{s,1}^3 (t_f + t_{s,2}).$$

Note that in the case of $t_{s,1} > t_{s,2}$, the sign of square root in Equation (4.8) should be plus, otherwise, minus. The expression of α_f [i.e., Equation (4.9)] can also be expressed in terms of $t_{s,2}$ and $\Psi_{e,2}$.

After E_f and α_f are obtained, H_f and σ_Y can be resulted by solving Equations (4.6) and (4.7), which results in that

$$H_f = -\frac{E_s t_s \theta_7}{t_f^3} - \frac{E_s t_s \sqrt{\theta_7^2 - t_f^2 t_s^2}}{t_f^3} \tag{4.10}$$

$$\sigma_Y = E_f \frac{6\Delta T_1^* E_s t_s H_f t_f (t_s + t_f)(\alpha_f - \alpha_s) - K_{p,1}^* \theta_8}{6E_s t_s t_f (t_s + t_f)(E_f - H_f)} \tag{4.11}$$

where

$$\theta_7 = 2t_f^2 + 3t_f t_s + 2t_s^2 - 3\Psi_{p,1}(t_f + t_s)(\alpha_f - \alpha_s)$$

$$\theta_8 = H_f^2 t_f^4 + E_s^2 t_s^4 + 2H_f E_s t_f t_s (2t_f^2 + 3t_f t_s + 2t_s^2)$$

and ΔT_1^* and $K_{p,1}^*$ are defined in Figure 4.1.

In the case of $t_f << t_s$, i.e., very thin film, after deleting terms about t_f with an order higher than 1, Equation (4.5) can be reduced to,

$$2E_f t_f [2t_s - 3\Psi_e(\alpha_f - \alpha_s)] + E_s t_s^2 = 0 \tag{4.12}$$

Subsequently, E_f and α_f can be solved as (first-order approximation)

$$E_f = \frac{E_s(\Psi_{e,1}t_{s,2}^2 - \Psi_{e,2}t_{s,1}^2)}{4t_f(\Psi_{e,2}t_{s,1} - \Psi_{e1}t_{s,2})} \tag{4.13}$$

$$\alpha_f = \frac{2t_{s,1}t_{s,2}(t_{s,1} - t_{s,2})}{3(\Psi_{e,2}t_{s,1}^2 - \Psi_{e,1}t_{s,2}^2)} + \alpha_s \tag{4.14}$$

For the zero-order approximation, any term about t_f is removed in Equation (4.5) except the one multiplying with Ψ_e. Thus, Equation (4.5) can be reduced to,

$$\frac{dK_e}{dT} = \frac{6E_f t_f(\alpha_f - \alpha_s)}{E_s t_s^2} \tag{4.15}$$

Obviously, one cannot determine both E_f and α_f from Equation (4.15). Note that combining Equation (4.15) with the well-known Stoney equation (Stoney 1909), which is

$$\sigma = \frac{E_s t_s^2 K_e}{6t_f} \tag{4.16}$$

one can obtain that

$$\frac{d\sigma}{dT} = E_f(\alpha_f - \alpha_s) \tag{4.17}$$

which is identical to that in, for instance, Zhao et al (1999), Lima et al (1999).

Similarly, for a first-order approximation, Equation (4.7) can be reduced to,

$$2H_f t_f [2t_s - 3\Psi_p(\alpha_f - \alpha_s)] + E_s t_s^2 = 0 \tag{4.18}$$

Subsequently, H_f and σ_Y can be obtained as

$$H_f = \frac{E_s t_{s,1}^2}{6\Psi_{p,1} t_f (\alpha_f - \alpha_s) - 4 t_f t_{s,1}} \tag{4.19}$$

$$\sigma_Y = E_f \frac{6\Delta T_1^* H_f t_f (\alpha_f - \alpha_s) - K_{p,1}^* (E_s t_{s,1}^2 + 4 H_f t_f t_{s,1})}{6 t_f (E_f - H_f)} \tag{4.20}$$

For a zero-order approximation,

$$H_f = \frac{E_s t_{s,1}^2}{6\Psi_{p,1} t_f (\alpha_f - \alpha_s)} \tag{4.21}$$

$$\sigma_Y = E_f \frac{6\Delta T_1^* H_f t_f (\alpha_f - \alpha_s) - K_{p,1}^* E_s t_{s,1}^2}{6 t_f (E_f - H_f)} \tag{4.22}$$

At this point, the Young's modulus, CTE, yield start stress, and strain hardening modulus are obtained based on the curvature vs. temperature variation curves measured in two tests. One more curvature vs. temperature variation curve is required to determine Poisson's ratio. Assume that in the above mentioned two tests the structures are under uniaxial stress state. As such, the additional curve should be obtained from a

biaxial stress state test. Otherwise, the additional test should be under uniaxial stress state instead.

In the case of biaxial stress, biaxial modulus, $\overline{E}$ (where '-' stands for the case of biaxial stress), should be used instead of uniaxial modulus. Then, we have

$$\overline{E_f}^2 t_f^4 + 2\overline{E_f}\,\overline{E_s} t_f t_s [(2t_f^2 + 3t_f t_s + 2t_s^2) - 3\overline{\Psi_e}(t_f + t_s)(\alpha_f - \alpha_s)] + \overline{E_s}^2 t_s^4 = 0 \quad (4.23)$$

where $\overline{E_f} = E_f/(1-\upsilon_f)$ and $\overline{E_s} = E_s/(1-\upsilon_s)$. υ_f and υ_s are Poisson's ratios of the film and substrate, respectively. If E_f and α_f are available, we can obtain υ_f from Equation (4.23) as

$$\upsilon_f = \frac{\overline{E_s} t_s^3 + 2E_f t_f [2t_f^2 + 3t_f t_s + 2t_s^2 - 3\overline{\Psi_e}(t_f + t_s)(\alpha_f - \alpha_s)]}{\overline{E_s} t_s^3} \quad (4.24)$$

In the case of $t_f << t_s$, υ_f can be solved as

$$\upsilon_f = 1 - \frac{2t_s - 3\overline{\Psi_e}(\alpha_f - \alpha_s)}{2t_s - 3\Psi_e(\alpha_f - \alpha_s)}(1-\upsilon_s) \quad (4.25)$$

as a first-order approximation.

For a zero-order approximation, υ_f can be solved as

$$\upsilon_f = 1 - \frac{\overline{\Psi_e}}{\Psi_e}(1 - \upsilon_s) \tag{4.26}$$

The derivation presented above is mainly for the case that the substrates are of the same material but in different thickness. In real engineering practice, there are many alternatives. For instance, one may consider using substrates made of different materials (same as that in Retajczyk et al 1980), or different film thickness instead of different substrate thickness (provided that the properties of a thin film is independent on the thickness).

The comments by Malzbender (2005) on our above approach (Huang et al 2004) present a few remarks to further extend our approach as an effective tool to simplify the analysis of the mechanical properties of materials. The use of differentiates was suggested by Malzbender (2005) for assessing the properties of thin films at a particular temperature and applied strain. It was also mentioned that the strain-load ($\partial\varepsilon / \partial P$) or load-deflection differentiation ($\partial P / \partial d$) curve in a uniaxial or biaxial bending test can be utilized to determine the entire nonlinear stress–strain relationship of a thin film. Further extension of this idea into multilayer composites is, at least in theory, possible.

In the next chapter, we will show that the nonlinear stress-strain relationship of a thin film, which is coated atop a linear elastic substrate, can be determined by one single test, either a thermally induced curvature test or a four-point bending test. The closed-form solutions for the case of ultra-thin films are derived. That is to say, the stress-strain curvature of a thin film can be derived from the temperature-curvature curve measured in a thermally induced curvature test or the load-deflection curve measured in

a bending test (if the coefficient of thermal expansion is not approximately a constant within the concerned temperature range).

4.3 Determination of Intrinsic Stress and Thermal Stress

4.3.1 Introduction

Residual stress is almost unavoidable in multilayer structures. Residual stress may cause cracking and/or other damage to the structures. For instance, if the residual stress is over a certain limit, catastrophic or long-term failure may occur. Contact peel-off due to a higher tensile stress, and de-adherence and/or buckling due to a high compressive stress are two typical examples (Ohring 2002). On the other hand, the presence of residual stress may sometimes enhance the strength of structures. For example, a high compressive stress can prevent the initiation of surface cracks. Therefore, in order to obtain reliable multilayer structures, it is necessary to determine the residual stress. Our literature review reveals that this issue has attracted a lot of attention for some years (Janda and Stefan 1984, Janda 1986, Nie et al 2006).

It is well known that in the absence of external loads, there are two major contributors to residual stress in multilayer structures: intrinsic stress and thermal stress. The former is largely due to the lattice mismatch between two adjacent layers and growth of strains (in the literature some researchers define the stress due to the difference in structural properties between two adjacent layers as interfacial stress), while the latter is due to temperature change, which most likely refers to the fluctuation of environmental temperature and/or a high film deposition temperature. In the past decades, many

dedicated methods have been developed in order to determine the residual stresses, but without separating the intrinsic stress and thermal stress (Nie et al 2006). Recently, some researchers proposed some methods to separate the thermal stress and intrinsic stress in bilayer structures (Yu et al 2000, Jeong et al 2001, Choi et al 2005), but none of them is for multilayer structures. Most of these methods require the thermo-mechanical properties of thin films to be known first (Janda and Stefan 1984). Using the equivalent reference temperature (ERT) technique, Nejhad et al (2003) managed to model the intrinsic strain in a trial and error fashion.

The residual stress can be determined using many advanced technologies. Among them, curvature-based method, in which Stoney equation is utilized (Stoney 1909), might be the most popular one (Gunnars and Wiklund 2002, Mezin 2006). In this section, a curvature-based approach, which can determine not only the residual stresses but also the intrinsic stress and thermal stress in each layer, is presented. In addition, it only requires the thermo-mechanical properties of substrate to be known, but nothing about the thin film.

4.3.2 Determination of residual stress

Assume that a multilayer structure is long enough as compared with its thickness, and its curvature is much larger than the thickness. Consider the case of a *n*-layer thin film on the top of a substrate as illustrated in Figure 4.2. The thickness, Young's modulus and coefficient of thermal expansion of layer *i* are denoted as t_i, E_i, and α_i, and those of substrate are t_s, E_s, and α_s, respectively. Note that in the case of biaxial stress,

biaxial modulus $\bar{E}_i$ $[=E_i/(1-\upsilon_i)$, where υ_i is Poisson's ratio] should be used instead of E_i.

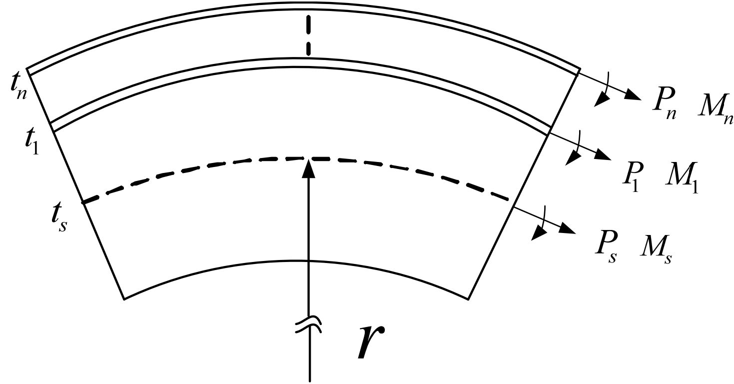

Figure 4.2 Schematic sketch of a multilayer structure (*n* layers atop a thick substrate).

In Figure 4.2, each layer suffers force and moment, which can be replaced by a statically equivalent combination of an average force and a moment (Ohring 2002) as illustrated in Figure 4.2, in which P_i and M_i are in the *i*th layer, and P_s and M_s in the substrate. Force P_i can be imagined to be uniformly applied over the whole cross-sectional area ($t_i w$, where w is the width of the structure). Hence, the total stress σ_i (including intrinsic stress and thermal stress) in the *i*th layer can be expressed as $P_i/(t_i w)$. The equilibrium conditions for force and moment are (Feng and Liu 1983),

$$\sigma_s t_s w + \sum_{i=1}^{n} \sigma_i t_i w = 0 \tag{4.27}$$

$$M_s + \sigma_s t_s w(t_s/2) + \sum_{i=1}^{n} M_i + \sum_{i=1}^{n} \sigma_i t_i w[t_s + (t_i/2) + \sum_{j \le i-1} t_j] = 0 \tag{4.28}$$

where $M_i = E_i t_i^3 w/(12r)$, $M_s = E_s t_s^3 w/(12r)$, and r is the radius of curvature. In the case of thin films, i.e., $t_s >> \sum_{i=1}^{n} t_i$ and $E_s t_s >> \sum_{i=1}^{n} E_i t_i$ (Klein 2000a), Equation (4.28) can be simplified as

$$E_s t_s^3 w/(12r) + \sigma_s t_s w(t_s/2) + \sum_{i=1}^{n} \sigma_i t_i w t_s = 0 \qquad (4.29)$$

With Equations (4.27) and (4.29), one has,

$$1/r = -6\sum_{i=1}^{n} \sigma_i t_i / (E_s t_s^2) \qquad (4.30)$$

In the above equation, the minus sign is duo to the sign convention in defining the curvature. The residual stress in the *n*th layer σ_n can be determined from the curvatures measured before and after the removal of the *n*th layer, i.e.,

$$\sigma_n = -\frac{E_s t_s^2}{6t_n}\left(\frac{1}{r_n} - \frac{1}{r_{n-1}}\right) \qquad (4.31)$$

where r_n is the measured curvature of the multilayer structure before the *n*th layer is removed, while r_{n-1} is the curvature after the *n*th layer is removed, i.e., *n-1* layers are still on the substrate. If the thin films are etched away layer by layer from the top layer and the corresponding curvatures are measured, the residual stress in each layer can be determined. This sounds conventional (Nie et al 2006). However, a quantitative determination of the intrinsic and thermal stresses is still a challenge.

4.3.3 Determination of intrinsic stress and thermal stress

As described above, after film processing (including deposition and post-deposition treatment, e.g. annealing), the residual stress has two components, namely, thermal stress σ^{th} which is temperature dependent and intrinsic stress σ^{in} which is temperature independent (i.e., $\sigma_i = \sigma_i^{in} + \sigma_i^{th}$) (Choi et al 2005).

In the case of thin layers, the thermal stress in the *i*th layer can be expressed as (Hsueh 2002, Townsend et al 1987)

$$\sigma_i^{th1} = E_i(\alpha_s - \alpha_i)(T_i^1 - T_i^0) \tag{4.32}$$

where T_i^0 is the deposition temperature of the *i*th layer, T_i^1 is the temperature at which the curvature and residual stress are measured and σ_i^{th1} is the thermal stress in the *i*th layer at T_i^1.

If we prepare two identical multilayer structures (i.e., produced simultaneously in batch or following the same process under the same conditions), and subsequently, measure the curvature of both structures before and after the removal of the *i*th layer at two different (but constant) temperatures T_i^1 and T_i^2. Consequently, one has the following two equations,

$$\sigma_i^1 = \sigma_i^{in} + E_i(\alpha_s - \alpha_i)(T_i^1 - T_i^0) \tag{4.33}$$

$$\sigma_i^2 = \sigma_i^{in} + E_i(\alpha_s - \alpha_i)(T_i^2 - T_i^0) \tag{4.34}$$

Note that both residual stresses σ_i^1 and σ_i^2 in the above equations can be determined by Equations (4.30) and (4.31). Referring to Equations (4.33) and (4.34), we can determine the intrinsic stress in the *i*th layer as,

$$\sigma_i^{in} = \frac{\sigma_i^2(T_i^0 - T_i^1) - \sigma_i^1(T_i^0 - T_i^2)}{T_i^2 - T_i^1} \tag{4.35}$$

After the intrinsic stress is determined, thermal stress at a given temperature can be obtained subsequently as $\sigma_i = \sigma_i^{in} + \sigma_i^{th}$. Repeat the above procedure layer by layer, the intrinsic stress and thermal stress in each layer can be determined. Practically, we may need a few identical samples tested at some different temperatures for data-fitting, so that more accurate result of intrinsic stress can be obtained.

4.4 Conclusions

In this chapter, first a simple approach to determine five thermo-mechanical properties of thin films, namely, the Young's modulus, coefficient of thermal expansion (CTE), yield start stress, strain hardening modulus and Poisson's ratio, is proposed. The approach is based on the conventional curvature test on bilayer structures upon temperature variation and can be easily implemented using many conventional techniques. Three tests, which result in three curvature vs. temperature curves, are enough to determine the values of these properties.

Apart from that, a curvature-based approach, which can determine not only the residual stress but also the intrinsic stress and thermal stress in each layer of a multilayer structure, is proposed. This approach is simple and convenient to follow, as the curvature can be easily measured by many current techniques.

CHAPTER 5 DETERMINATION OF STRESS VERSUS STRAIN RELATIONSHIP AND OTHER THERMO-MECHANICAL PROPERTIES OF THIN FILMS

5.1 Introduction

In recent years, many dedicated techniques have been developed for characterizing thin films, as discussed briefly in Chapter 2, such as X-ray diffraction technique (Badawi et al 2002), membrane deflection methodology (Espinosa et al 2003), nanoindentation (Malzbender and Steinbrech 2003), etc. In general, these proposed techniques either require dedicated equipments or are very tedious in sample preparation. Therefore, simple approaches for characterizing the thermo-mechanical properties of thin films, including stress versus strain relationship, coefficient of thermal expansion (CTE), Young's modulus and Poisson's ratio, etc., are still highly in demand.

In Chapter 4, a simple technique to determine five thermo-mechanical properties of thin ductile linear strain hardening films has been proposed. Since it is based on the thermally induced curvature approach, it is only applicable to films with temperature independent material properties (at least within the temperature range of interest). In this Chapter, our study will be extended and some more generic approaches, which can

deal with films with nonlinear stress versus strain relationship and/or temperature dependent material properties, will be presented.

Thermally induced curvature test and bending test (e.g., four-point bending, three-point bending, and bending a cantilever beam, etc) are standard techniques for testing thin films atop an elastic substrate for various purposes (Florando and Nix 2005). The approaches purposed here involve no other tests but only these conventional ones.

In Section 5.2, a thermally induced curvature approach, which can capture the nonlinear stress versus strain relationship in thin films, is presented. In the case of very thin films, closed-form solutions for nonlinear stress versus strain relationship are also developed. In addition, the analytical solutions are compared with Stoney equation. In Section 5.3, a bending approach is proposed as an alternative in the case that the mechanical properties of a film are temperature dependent. Similarly, a closed-form solution is also developed. A case study of determination of nonlinear stress versus strain relationship of film using thermally induced curvature method is presented in Section 5.4. Section 5.5 is conclusions.

5.2 Thermally Induced Curvature Approach

Before determining the nonlinear stress vs. strain relationship of a thin film, the CTE of the thin film is assumed to be a constant. If it is an unknown, it can be determined either from the thermally induced curvature test following the approach described in Chapter 4 or by the method mentioned later.

5.2.1 Nonlinear stress versus strain relationship of thin films by thermal tests

Consider a thin film deposited atop an elastic substrate (its material properties are well-known) as illustrated in Figure 5. 1(a). Hereinafter, the symbols and nomenclature (thickness, Young's modulus, and CTE) are the same as those defined in Chapter 3. Subscripts *f* and *s* stand for the film and substrate, respectively. Note that here α_f is assumed to be a constant.

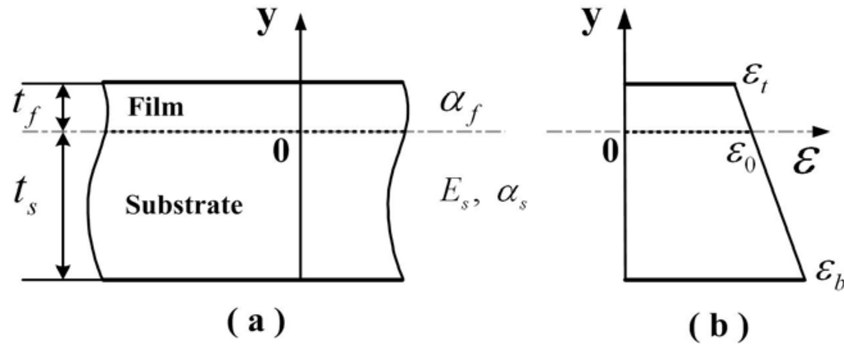

Figure 5. 1 Film and substrate. (a) Coordinate system; (b) illustration of strain distribution.

Upon temperature fluctuation (ΔT), a bilayer structure tends to bend due to the difference in CTE between the film and substrate. The strain (ε) at a point *y* away from the interface can be expressed in terms of the strain at the interface (ε_0) [Figure 5. 1 (b)] and curvature of the bilayer structure (ΔK) by

$$\varepsilon = \Delta K y + \varepsilon_0 \tag{5.1}$$

Here, ε has two components, namely, thermal strain ($\varepsilon_T = \alpha \Delta T$) and mechanical strain (ε_m), i.e., $\varepsilon = \varepsilon_m + \alpha \Delta T$. ΔK can be expressed in terms of the strains at the top and bottom surfaces (ε_t and ε_b) by

$$\Delta K = (\varepsilon_t - \varepsilon_b) / (t_f + t_s) \tag{5.2}$$

At a particular temperature, ΔK can be measured by many conventional techniques. Therefore, one can obtain a curvature variation versus temperature variation relationship as illustrated in Figure 5. 2.

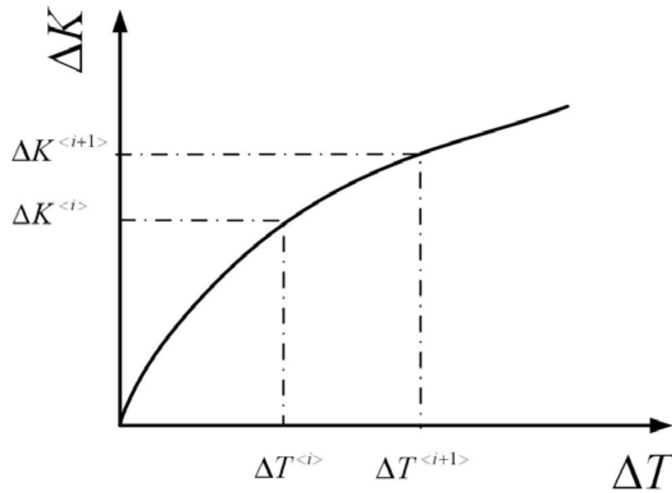

Figure 5. 2 Curvature variation versus temperature variation.

In the first step (<1>), given a very small temperature variation ($\Delta T^{<1>}$), so that a linear stress versus strain relationship can be assumed for the film in the very early stage. Thus, $\varepsilon_0^{<1>}$ (strain at the interface) and H_1 (slope of the stress vs. strain relationship of film, refer to Figure 5. 3) are two unknowns to be determined from $\Delta K^{<1>}$ and $\Delta T^{<1>}$.

The equilibrium conditions require that both the total force and total moment are zero, i.e.,

$$\int_{\varepsilon_0^{<1>}-\Delta K^{<1>}t_s}^{\varepsilon_0^{<1>}} E_s(\varepsilon-\alpha_s\Delta T^{<1>})d\varepsilon+\int_{\varepsilon_0^{<1>}}^{\varepsilon_0^{<1>}+\Delta K^{<1>}t_f} H^{<1>}(\varepsilon-\alpha_f\Delta T^{<1>})d\varepsilon=0 \tag{5.3}$$

$$\int_{\varepsilon_0^{<1>}-\Delta K^{<1>}t_s}^{\varepsilon_0^{<1>}} E_s(\varepsilon-\alpha_s\Delta T^{<1>})\frac{\varepsilon-\varepsilon_0^{<1>}}{\Delta K^{<1>}}d\varepsilon+\int_{\varepsilon_0^{<1>}}^{\varepsilon_0^{<1>}+\Delta K^{<1>}t_f} H^{<1>}(\varepsilon-\alpha_f\Delta T^{<1>})\frac{\varepsilon-\varepsilon_0^{<1>}}{\Delta K^{<1>}}d\varepsilon=0 \tag{5.4}$$

Figure 5. 3 Stress versus strain relationship.

Equations (5.3) and (5.4) can be solved for $\varepsilon_0^{<1>}$ and $H^{<1>}$. Subsequently, the maximum mechanical strain $\varepsilon_{0,m}^{<1>}$ can be obtained as

$$\varepsilon_{0,m}^{<1>}=\varepsilon_0^{<1>}-\alpha_f\Delta T^{<1>} \tag{5.5}$$

Provided that the stress versus strain relationship of film ($f^{<i>}\left(\varepsilon_m\right)$) has been obtained from the previous i steps (Figure 5. 3). In the next step ($<i+1>$), we determine $\varepsilon_{0,m}^{<i+1>}$ (through $\varepsilon_0^{<i+1>}$) and $H^{<i+1>}$. The equilibrium conditions are

$$
\begin{aligned}
&\int_{\varepsilon_0^{<i+1>}-\Delta K^{<i+1>}t_s}^{\varepsilon_0^{<i+1>}} E_s(\varepsilon-\alpha_s\Delta T^{<i+1>})d\varepsilon \\
&+\int_{\varepsilon_0^{<i+1>}}^{\varepsilon_{0,m}^{<i>}+\alpha_f\Delta T^{<i+1>}} (\sigma^{<i>}+H^{<i+1>}(\varepsilon-\alpha_f\Delta T^{<i+1>}-\varepsilon_{0,m}^{<i>}))d\varepsilon \\
&+\int_{\varepsilon_{0,m}^{<i>}+\alpha_f\Delta T^{<i+1>}}^{\varepsilon_0^{<i+1>}+\Delta K^{<i+1>}t_f} f^{<i>}(\varepsilon-\alpha_f\Delta T^{<i+1>})d\varepsilon=0
\end{aligned}
\tag{5.6}
$$

$$
\begin{aligned}
&\int_{\varepsilon_0^{<i+1>}-\Delta K^{<i+1>}t_s}^{\varepsilon_0^{<i+1>}} E_s(\varepsilon-\alpha_s\Delta T^{<i+1>})\frac{\varepsilon-\varepsilon_0^{<i+1>}}{\Delta K^{<i+1>}}d\varepsilon \\
&+\int_{\varepsilon_0^{<i+1>}}^{\varepsilon_{0,m}^{<i>}+\alpha_f\Delta T^{<i+1>}} (\sigma^{<i>}+H^{<i+1>}(\varepsilon-\alpha_f\Delta T^{<i+1>}-\varepsilon_{0,m}^{<i>}))\frac{\varepsilon-\varepsilon_0^{<i+1>}}{\Delta K^{<i+1>}}d\varepsilon \\
&+\int_{\varepsilon_{0,m}^{<i>}+\alpha_f\Delta T^{<i+1>}}^{\varepsilon_0^{<i+1>}+\Delta K^{<i+1>}t_f} f^{<i>}(\varepsilon-\alpha_f\Delta T^{<i+1>})\frac{\varepsilon-\varepsilon_0^{<i+1>}}{\Delta K^{<i+1>}}d\varepsilon=0
\end{aligned}
\tag{5.7}
$$

$\varepsilon_0^{<i+1>}$ (then $\varepsilon_{0,m}^{<i+1>}$) and $H^{<i+1>}$ can be solved from Equations (5.6) and (5.7). Step by step, one can get the whole stress versus strain relationship of the film based on the measured points in the curvature variation versus temperature variation curve (Figure 5. 2).

5.2.2 Closed-form solutions for very thin films

As technologies are moving continuously towards smaller, thinner and lighter devices, the thickness of films has reduced dramatically, towards micron and even nanometer regime (Stafford et al 2004). In this sub-section the study is extended to obtain closed-

form solutions for very thin films with a nonlinear stress vs. strain relationship.

In the case of very thin film, the film stress σ_f can be considered as a constant (refer to Figure 3.4). Similarly, the strain in the film is also approximately a constant (ε_t) and can be estimated to be the same as the strain atop the substrate. In other words, the stress and strain in the film are approximately uniform in the thickness direction (Hsueh 2002, Hu and Huang 2004). As such, $\varepsilon_t \approx \varepsilon_0$ in Figure 5.1 (b).

Given a (ΔK , ΔT) point in Figure 5. 2, based on that the equilibrium conditions are the total resultant in-plane force must be zero and the total moment must be null, one has

$$\int_{-t_s}^{0} E_s(\varepsilon - \alpha_s \Delta T)dy + \int_0^{t_f} \sigma_f \; dy = 0 \tag{5.8}$$

$$\int_{-t_s}^{0} E_s(\varepsilon - \alpha_s \Delta T)ydy + \int_0^{t_f} \sigma_f \, ydy = 0 \tag{5.9}$$

where

$$\varepsilon = \Delta K y + \frac{\varepsilon_t t_s + \varepsilon_b t_f}{t_f + t_s}$$

Solving Equations (5.8) and (5.9), one has,

$$\sigma_f = -\frac{\Delta K E_s t_s^3}{6 t_f (t_f + t_s)} \tag{5.10}$$

$$\varepsilon_t = \frac{1}{6}\Delta K[4t_s + t_f(5 + \frac{t_f}{t_f + t_s})] + \alpha_s \Delta T \tag{5.11}$$

$$\varepsilon_b = -\frac{\Delta K t_s(3t_f + 2t_s)}{6(t_f + t_s)} + \alpha_s \Delta T \tag{5.12}$$

The total strain, ε, has two parts, namely, thermal strain ε_T $(= \alpha\Delta T)$, and mechanical strain ε_m, i.e., $\varepsilon = \varepsilon_T + \varepsilon_m$. Consequently, the mechanical strain in the thin film ε_m can be expressed as

$$\varepsilon_m = \varepsilon_t - \alpha_f \Delta T = \frac{1}{6}\Delta K[4t_s + t_f(5 + \frac{t_f}{t_f + t_s})] + (\alpha_s - \alpha_f)\Delta T \tag{5.13}$$

Corresponding to each (ΔT , ΔK) point in the curvature vs. temperature variation relationship, which can be measured experimentally, ε_m and σ_f obtained from Equations (5.13) and (5.10) form a point in the stress vs. strain relationship of the film. Thus, given a series of (ΔT , ΔK) point, a series of ε_m and σ_f are resulted from Equations (5.13) and (5.10). As such, the stress and strain relationship of the thin film is obtained.

The second term of the right side of Equation (5.13) is the total thermally induced mismatch. The film accommodates most of the mismatch strain, but not all. The first term is normally smaller as compared with the second term and is often ignored in many previous papers (Baker et al 2003). However, a closer look shows that, under normal conditions, the first term is about 1/4 of the second term at $t_f / t_s = 1/10$. On the

other hand, given a thickness ratio t_f / t_s up to 1/10, the variation in film stress is less than about 5% against the average.

For simplicity, take the linear elastic case as an example for analysis. With Equation (3.11c), Equation (5.13) can be rewritten as,

$$\varepsilon_m = \frac{\Delta T[E_f^2 t_f^4 + E_s^2 t_s^4 - E_f E_s t_f t_s (2t_f^2 + 3t_f t_s)](\alpha_s - \alpha_f)}{E_f^2 t_f^4 + E_s^2 t_s^4 + 2E_f E_s t_f t_s (2t_f^2 + 3t_f t_s + 2t_s^2)} \tag{5.14}$$

The second term of the right side of Equation (5.13) is denoted by $\varepsilon_{\sec}$, i.e.,

$$\varepsilon_{\sec} = (\alpha_s - \alpha_f)\Delta T \tag{5.15}$$

In order to compare the difference between ε_m and $\varepsilon_{\sec}$, we may define $\eta_\varepsilon = (\varepsilon_{\sec} - \varepsilon_m) / \varepsilon_{\sec}$ as a parameter for measurement. Hence,

$$\eta_\varepsilon = \frac{6\gamma\lambda^3 + 9\gamma\lambda^2 + 4\gamma\lambda}{1 + 4\gamma\lambda^3 + 6\gamma\lambda^2 + 4\gamma\lambda + \gamma^2\lambda^4} \tag{5.16}$$

where γ is E_f / E_s and λ is t_f / t_s. η_ε is plotted against γ and λ in Figure 5. 4.

It reveals that η_ε may be significant for relatively thick films and in particular for hard films. Depending on the precision required and the thickness ratio, one may refer to Figure 5. 4 to determine which set of equations are more suitable in the determination

of stress versus strain relationship of a film (Equations (5.13) and (5.10), or Stoney equation and Equation (5.15)).

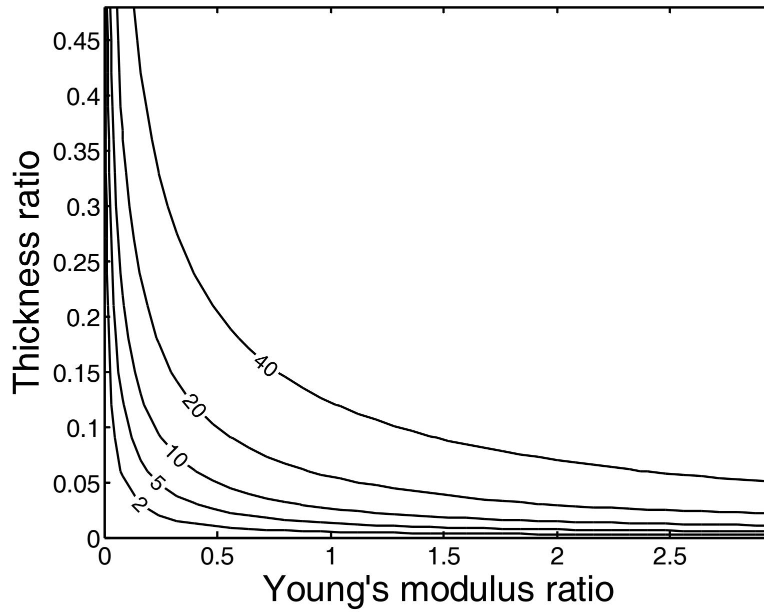

Figure 5. 4 Contour of η_{ε} (%) against thickness ratio (t_f / t_s) and modulus ratio (E_f / E_s).

The thermo-mechanical properties of film and substrate listed in Table 3.1 are used to reveal the difference. However, the thicknesses of film and substrate are now $5\ \mu\text{m}$ and $40\ \mu\text{m}$, respectively. Utilizing Equation (3.11c), a "virtual" curvature versus temperature variation curve can be obtained. Then we use Equations (5.13) and (5.10) to determine the stress versus strain relationship of the film. For comparison, Stoney equation and Equation (5.15) are also used to determine the stress versus strain relationship of film based on the curvature versus temperature curve.

Figure 5. 5 shows that there might be some cases in which the approximation (Stoney equation) is not precise enough, but it is still valid to assume that the stress and strain in the film are uniform. In these cases, Equations (5.10) and (5.13) are required.

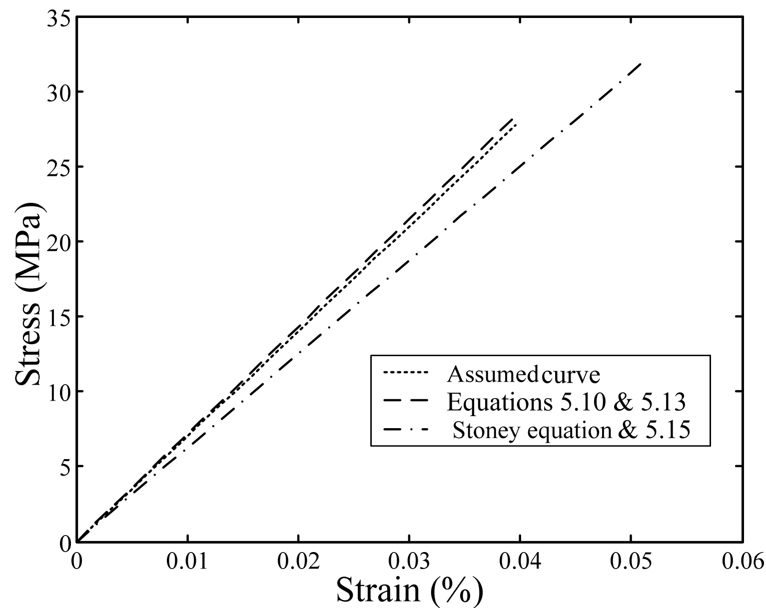

Figure 5. 5 Comparison of stress versus strain relationships.

5.3 Four-Point Bending Approach

Thermally induced curvature approach is only applicable to films with temperature independent material properties. In the case that the mechanical properties of a film are temperature dependent, bending test at a fixed temperature can be applied as an alternative.

5.3.1 Nonlinear stress versus strain relationship of thin films by bending test

Take the four-point bending test illustrated in Figure 5. 6 as an example. Upon loading (P), the bending moment in the middle span M $(= Pa)$ versus displacement (δ) curve can be measured. Since M in the middle span is a constant, the central region has a constant curvature (Gere and Timoshenko 1991), which can be expressed as

$$\Delta K = -2\delta / (\delta^2 + l^2 / 4) = (\varepsilon_t - \varepsilon_b) / (t_f + t_s) \tag{5.17}$$

Here, for convenience, ΔK has a minus sign, which is opposite to the conventional definition. In a bending test, the stress versus strain relationship of the film can be derived from the measured moment versus displacement curve in a similar manner as that described previously in the thermally induced curvature test. Note that here, we can delete thermal strain since temperature is a constant. Hence, $\varepsilon = \varepsilon_m$. Apart from that, in the thermally induced curvature test, the maximum mechanical strain in the film is located in the interface. In contrast, in the four-point bending test, it is located at the top surface of the film.

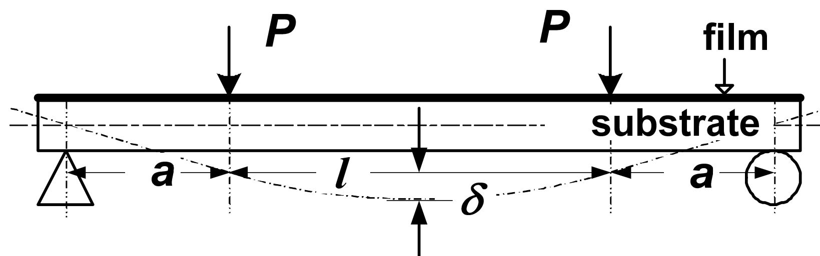

Figure 5. 6 Four-point bending of bilayer structure.

5.3.2 Closed-form solutions for very thin films

Similarly, closed-form solutions can be obtained for very thin film cases in four-point bending test. In the case of very thin films, the equilibrium conditions are (refer to Figure 5. 6)

$$\int_{-t_s}^{0} E_s \varepsilon dy + \int_{0}^{t_f} \sigma_f dy = 0 \tag{5.18}$$

$$\int_{-t_s}^{0} E_s \varepsilon y dy + \int_{0}^{t_f} \sigma_f y dy = M = Pa \tag{5.19}$$

Hence, σ_f and ε_t can be solved as

$$\sigma_f = \frac{6Pa(4\delta^2 + l^2) + 4\delta E_s t_s^3}{3t_f(t_f + t_s)(4\delta^2 + l^2)} \tag{5.20}$$

$$\varepsilon_t = \frac{-6Pa(4\delta^2 + l^2) + 4\delta E_s t_s (6t_f^2 + 9t_f t_s + 4t_s^2)}{3E_s t_s (t_f + t_s)(4\delta^2 + l^2)} \tag{5.21}$$

Thus, from the δ versus $M(= Pa)$ curve, through Equations (5.20) and (5.21), the stress versus strain relationship of the film can be resulted.

Similar to above-mentioned four-point bending test, the stress versus strain relationship of a film can also been determined by the three-point bending test or cantilever test. If the beam is in a particular type of triangular shape, so that the bending moment per unit width of the bilayer beam is a constant (Florando and Nix 2005), after ignoring the

biaxial effect, the curvature of the beam is uniform throughout the beam. Practically, it is reduced to that of the four-point bending test.

In addition to above stress versus strain relationship of thin films, using the slope in the early unloading part of a bending test, one can obtain the Young's modulus of the film. With it, α_f (if it is a constant) can be derived from the slope in the early thermally unloading part of a thermally induced curvature test. Measuring the elastic constants in uniaxial and biaxial stress states, one can estimate Poisson's ratio.

5.4 A Case Study

This section will show a case study of determination of nonlinear stress versus strain relationship of films using thermally induced curvature method. First, a nonlinear stress versus strain relationship is assumed. Second, based on the assumed relationship, two methods are utilized to obtain the curvature versus temperature variation curve, namely, analytical method and numerical method (finite element analysis). Finally, based on the "calculated" curvature versus temperature variation curve, the method developed in the above section is utilized to determine the nonlinear stress versus stress relationship and then the determined nonlinear stress versus stress relationship is compared with the assumed one.

As a demonstration, consider a layer of thin film with a nonlinear stress vs. strain relationship as (Exadaktylos et al 2001)

$$\sigma(\varepsilon) = E\varepsilon + F\varepsilon^2 \qquad (5.22)$$

It is deposited atop a silicon substrate. Here, E is 70 GPa and F is -112000 GPa ($=-1600\ E$). Refer to Figure 5. 7 for the stress versus strain curve. Other parameters are listed in Table 5.1. The length of bilayer strip is assumed to be 800 μm in the finite element analysis.

Parameter	Young's modulus	CTE	Thickness
Thin film		$23\times10^{-6}\,/\,^{o}C$	1 μm
Silicon	162 GPa	$2.6\times10^{-6}\,/\,^{o}C$	40 μm

Table 5. 1 Parameters.

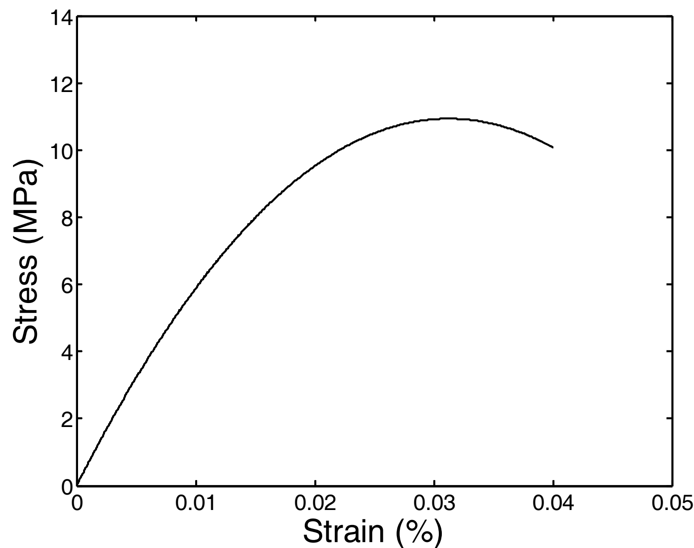

Figure 5. 7 Nonlinear stress vs. strain relationship.

The curvature vs. temperature variation curve can be calculated by the method described in Chapter 3. For a nonlinear stress versus strain relationship of a film here, it needs some minor modifications. The equilibrium equations are,

$$\int_{-t_s}^{0} E_s(\varepsilon-\alpha_s\Delta T)dy+\int_{0}^{t_f} E(\varepsilon-\alpha_f\Delta T)+F(\varepsilon-\alpha_f\Delta T)^2 dy=0 \tag{5.23}$$

$$\int_{-t_s}^{0} E_s(\varepsilon-\alpha_s\Delta T)ydy+\int_{0}^{t_f} [E(\varepsilon-\alpha_f\Delta T)+F(\varepsilon-\alpha_f\Delta T)^2]ydy=0 \tag{5.24}$$

Then, the curvature can be obtained by Equation (5.2) after solving Equations (5.23) and (5.24) as shown in Figure 5. 8.

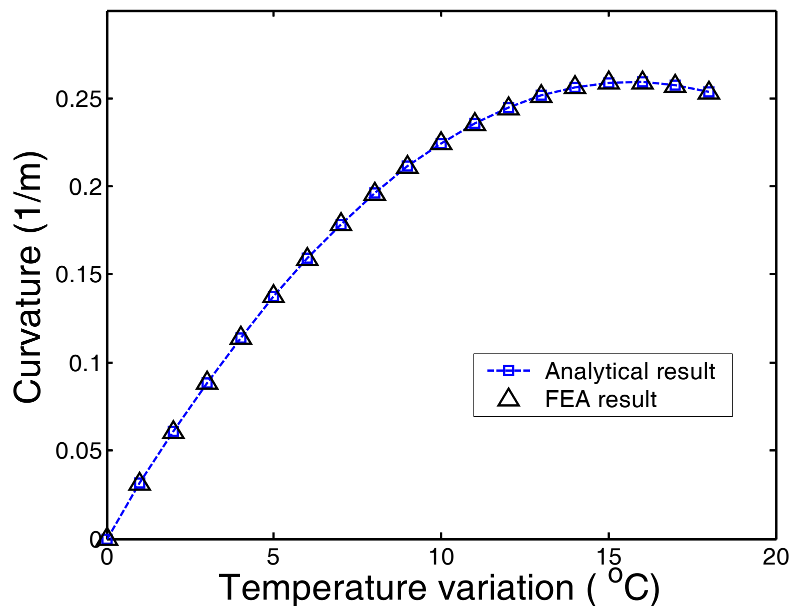

Figure 5. 8 Curvature vs. temperature variation.

In the numerical simulation, commercial finite element analysis package ANSYS 8.0 is utilized. The substrate is modeled as isotropic and perfectly elastic. The nonlinear stress versus strain relationship of the film is modeled using multilinear isotropic hardening principle by von Mises plasticity (MISO). The nonlinear stress versus strain

relationship of the film in the numerical simulation is represented by twenty linear segments, which is about accurate enough.

The bilayer strip is simplified as a two dimensional model using eight-node quadrilateral plane-stress elements PLANE82 with two degrees of freedom at each node. Due to the symmetry of bilayer strip, only half of it needs to be calculated. When the radius of curvature r is much greater than the length, the curvature of the bilayer strip can be estimated as

$$K = \frac{1}{r} = \frac{2\delta}{L^2} \tag{5.25}$$

where L is the length and δ is the bow of the bilayer at position L as shown in Figure 5. 9. In the simulation, the bilayer strip changes its curvature upon temperature fluctuation. The displacement of the node located at the bottom of substrate in Y direction in the simulation is defined as the bow (δ). Then through Equation (5.25), the curvature versus temperature variation curve can be obtained.

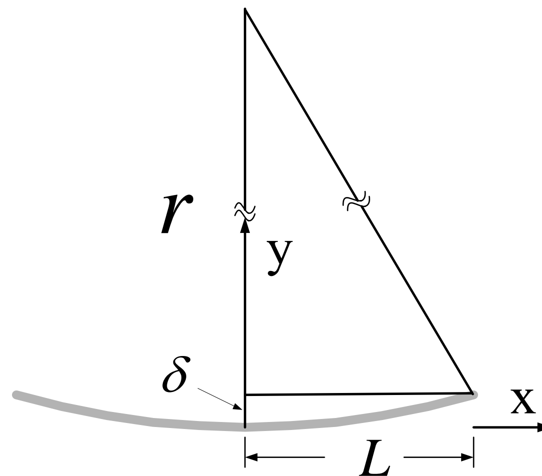

Figure 5. 9 Schematic illustration of the bow of the bilayer.

The curvature obtained by numerical simulation is plotted in Figure 5. 8. Using the values at the points with symbols in the curvature vs. temperature variation curve, the stress vs. strain relationship of the thin film is obtained from Equations (5.10) and (5.13). As shown in Figure 5. 10, it is identical to the initially assumed one.

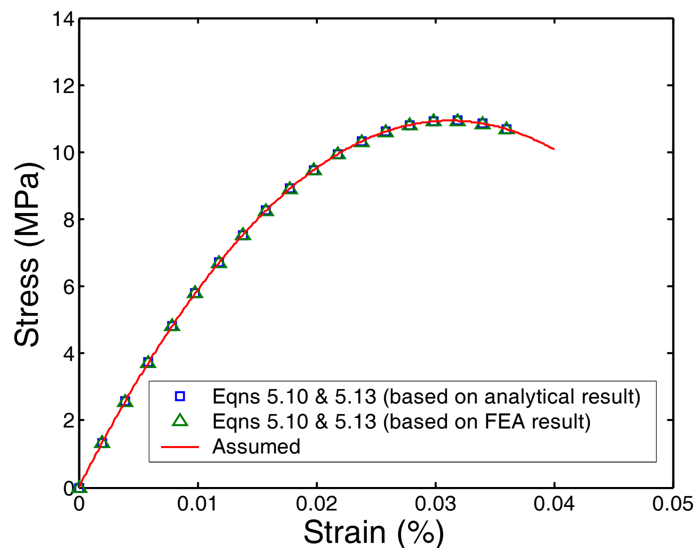

Figure 5. 10 Comparison of the stress vs. strain curves.

5.5 Conclusions

In this chapter, some simple and generic approaches for characterization of thin films with nonlinear stress versus strain relationship and/or temperature dependent material properties are proposed. Only standard testing techniques are required. The analytical solutions of very thin films are presented. For thermally induced curvature approach, a comparison between the results of commonly used Stoney equation and those of the analytical solutions reveals that the difference between them may be significant for relatively thick films and in particular for hard films.

Apart from that, a case study of determination of nonlinear stress versus strain relationship of films using thermally induced bending method is demonstrated.

CHAPTER 6 APPLICATIONS

6.1 Introduction

In this Chapter, first, we apply the thermally induced curvature method for on-wafer determination of the Young's moduli of three types of metallic thin films (copper, aluminum, and silver films deposited atop a (100)-type silicon wafer).

Next, the approaches and formulas developed in Chapter 5 are applied to investigate the underlying mechanism of the reversible trenches atop NiTi shape memory thin films.

6.2 Characterization of Metallic Thin Films

Thermally induced curvature method is applied to determine the Young's moduli of three types of metallic thin films, namely copper (Cu), aluminum (Al) and silver (Ag), deposited on a (100)-type silicon wafer. The thicknesses of both Cu and Al films are 1 μm, while Ag films have four different thicknesses, ranging from 0.4, 0.8, 1.2 to 1.6 μm.

6.2.1 Experimental procedure

All metallic thin films were prepared by sputtering at room temperature (Coxial Magnetron Sputter) with the help from Mr. Pek Soo Siong, in Micro Machines Centre. Commercially obtained 4-in. (100)-type silicon wafers were used as the substrate for all metallic thin films. Before deposition, the Si substrates were ultrasonically cleaned in acetone, methanol and then de-ionized water, successively. The base pressure of the main chamber was 2.0×10^{-5} Pa (1.5×10^{-4} m Torr) before deposition. The substrate-to-target distance was 100 mm, and argon gas flow rate was 20 sccm and the working pressure was 0.5 Pa (4 mTorr). The substrate holder was rotated during deposition for good uniformity of thin films. The deposition duration varied for Ag films. Thus, Ag films with different thicknesses, as listed in Table 6. 1, were obtained.

Films	Cu	Al	Ag			
Thickness (μm)	1	1	0.4	0.8	1.2	1.6

Table 6. 1 Thicknesses of metallic films.

Since the deposited thin film and silicon substrate are firmly bonded together, the mismatch due to their different CTE will result in the deflection of the bilayer structure upon temperature fluctuation. A Tencor FLX-2908 laser system was used to measure the curvature of the bilayer structure in situ at different temperatures at a heating/cooling rate of 1°C/min for all metallic films.

For Cu films, the temperature was first increased from 24 ^{o}C to 100 ^{o}C, and then decreased down to 24 ^{o}C, followed by heating again from 24 ^{o}C to 250 ^{o}C. For Al films,

a thermal cycle was from 24 ^{o}C to 100 ^{o}C then to 24 ^{o}C. For all Ag films, a thermal cycle was conducted from 24 ^{o}C to 100 ^{o}C then to 24 ^{o}C and repeated one more time.

Based on the curvature variation versus temperature (or temperature variation) curve and Equation (5.10), one can work out the relationship between the film stress and temperature. In the same way, film strain can also be derived using Equation (5.13).

Note that curvature variation (ΔK) should refer to the initial curvature of wafer before deposition, and the deposition temperature (room temperature) is taken as the reference point for temperature variation (ΔT).

Taking film stress and film strain at the deposition temperature as the starting point, the relationship between the relative stress and relative strain of the film can be established. The Young's modulus and Poisson's ratio of silicon wafer used in our calculation are 130.2 GPa and 0.28, respectively (Fu et al 2006). The CTEs used in calculation are listed in Table 6. 2. CTE of Si is from Fu et al (2006). All others are taken from Freund and Suresh (2003). It is noteworthy to point out that CTEs of metallic films are slightly temperature dependent. So the average values within the testing temperature range are used.

Materials	Si	Cu	Al	Ag
CTE($10^{-6} / {}^{o}C$**)**	2.6	17.23	23.98	19.17

Table 6. 2 CTEs of materials used in calculation.

6.2.2 Experimental results and comparison

The measured curvature variation versus temperature relationships of Cu and Al films are plotted in Figure 6.1 and Figure 6.2, respectively. Those of Ag films are plotted in Figure 6.3.

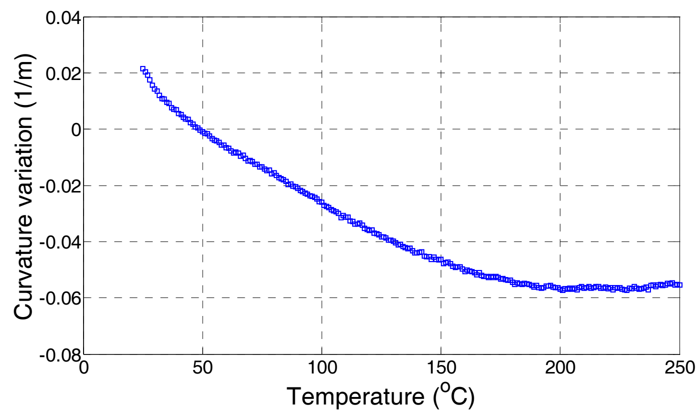

Figure 6.1 Curvature variation vs. temperature relationship of Cu film deposited on Si substrate during heating.

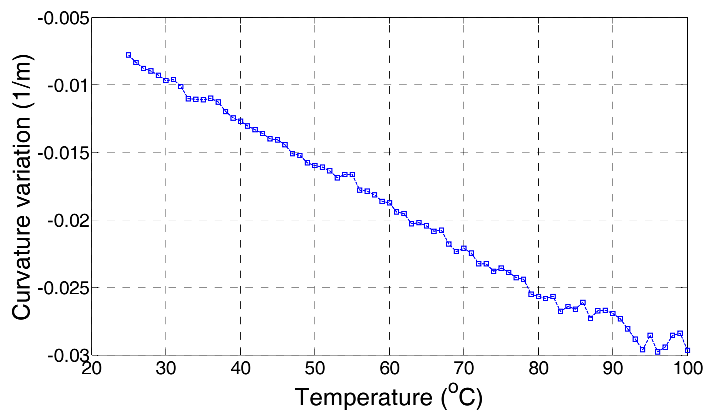

Figure 6.2 Curvature variation vs. temperature relationship of Al film deposited on Si substrate during cooling.

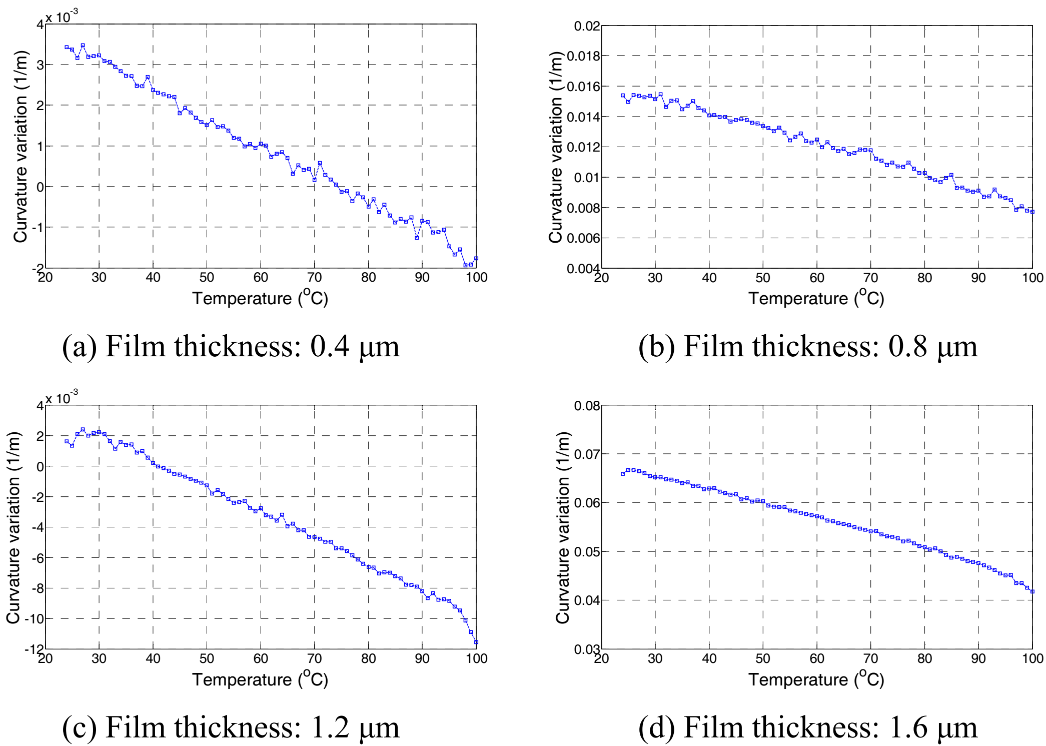

(a) Film thickness: 0.4 μm (b) Film thickness: 0.8 μm

(c) Film thickness: 1.2 μm (d) Film thickness: 1.6 μm

Figure 6.3 Curvature variation vs. temperature relationship of Ag film deposited on Si substrate during second cooling (the curves obtained in the first cooling process follow almost the same curve).

Based on these curvature variation vs. temperature relationships, using Equations (5.10) and (5.13), we can work out both the stress vs. temperature relationship and strain vs. temperature relationship.

The stress evolution and strain evolution in Cu film are plotted in Figure 6. 4. Upon heating, both Cu film and Si substrate trend to expand. Cu film would expand more than Si substrate if they were not bonded together since the CTE of Cu is larger than that of Si. Now Cu film is unable to expand freely and subjected to the constraint from Si substrate because of the bond between them. As such, Cu film is in compressive stress state and the compressive stress will increase as the temperature increases. As we

can see in Figure 6.4, the initial part of the stress-temperature curve of Cu film is almost linear from about 24°C till to 150°C.

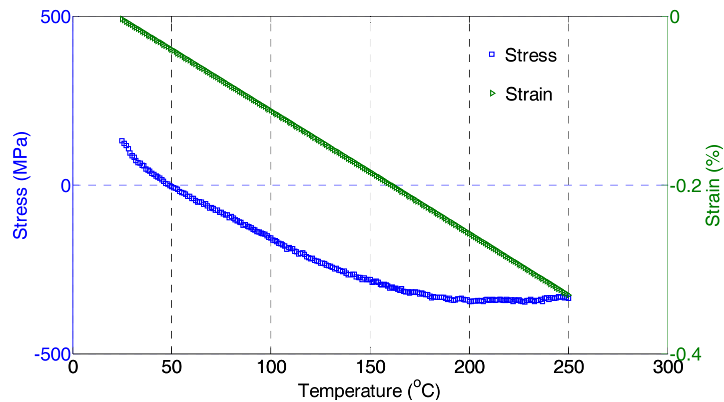

Figure 6. 4 Stress evolution and strain evolution in Cu film.

The stress evolution and strain evolution in Al film are plotted in Figure 6. 5. The stress-temperature curve of Al film is almost linear within the temperature range from 24 °C to 100°C. The stress in Al film is also compressive.

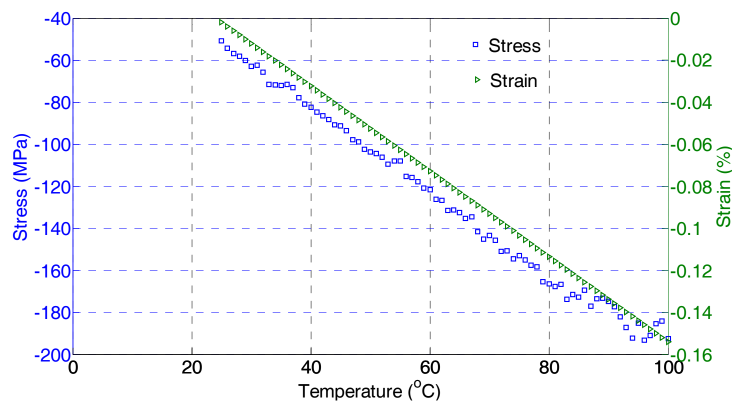

Figure 6. 5 Stress evolution and strain evolution in Al film.

The stress evolution and strain evolution in Ag films are plotted in Figure 6. 6. Figure 6. 7 to Figure 6. 9 plot the relative stress vs. relative strain relationships of Cu, Al, and Ag films, respectively.

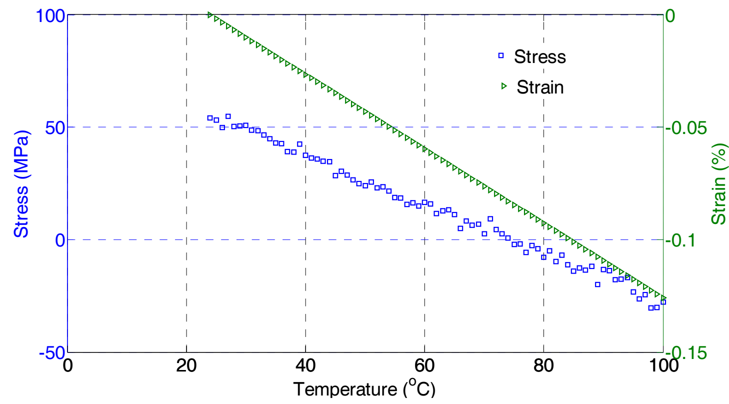

(a) Film thickness: 0.4 μm

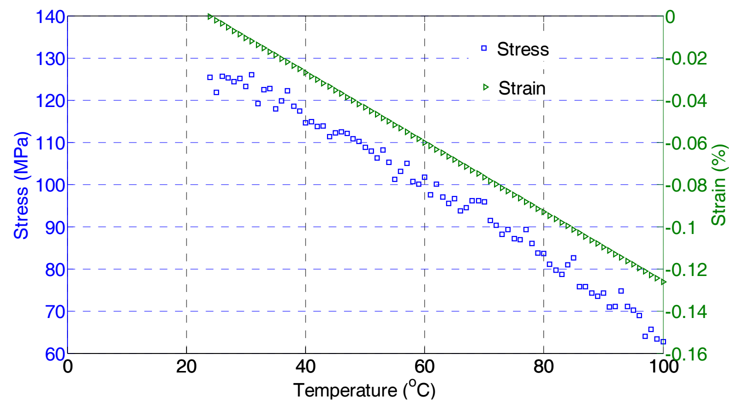

(b) Film thickness: 0.8 μm

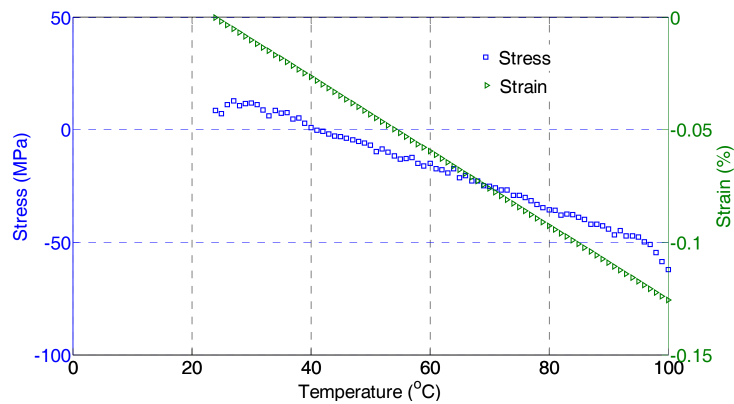

(c) Film thickness: 1.2 μm

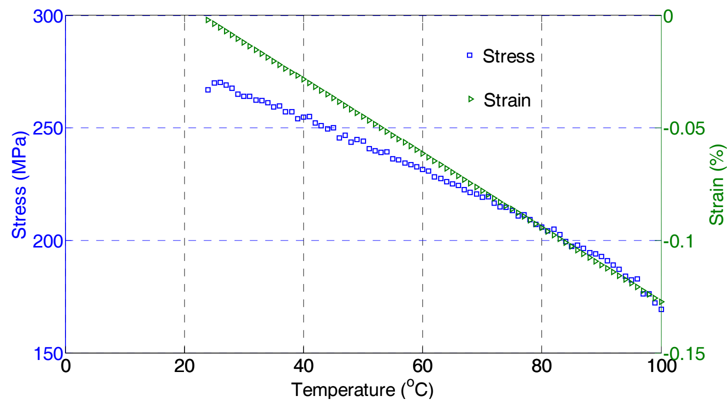

(d) Film thickness: 1.6 μm

Figure 6. 6 Stress evolution and strain evolution in Ag films.

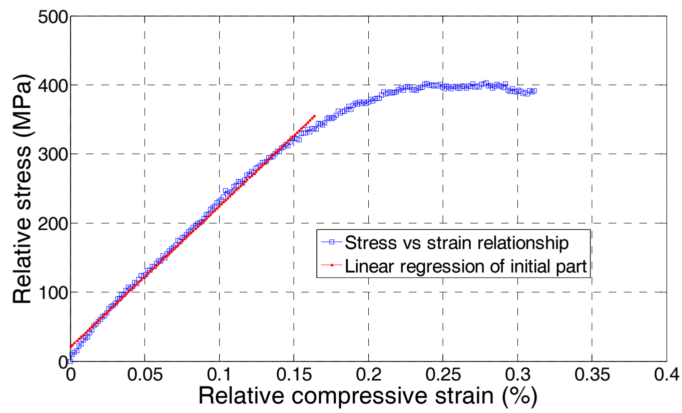

Figure 6. 7 Relative stress vs. relative strain relationship of Cu film.

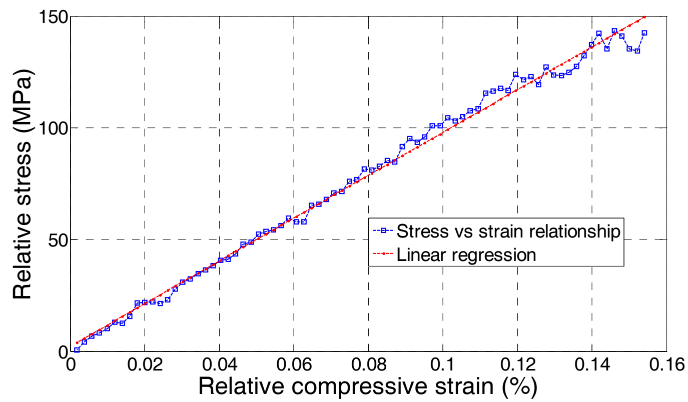

Figure 6. 8 Relative stress vs. relative strain relationship of Al film.

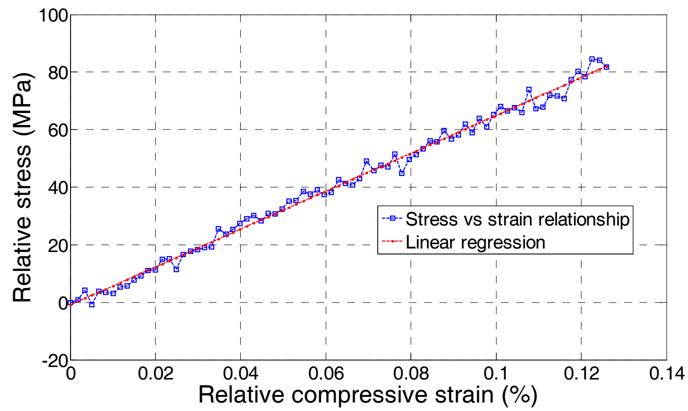

(a) Film thickness: 0.4 μm

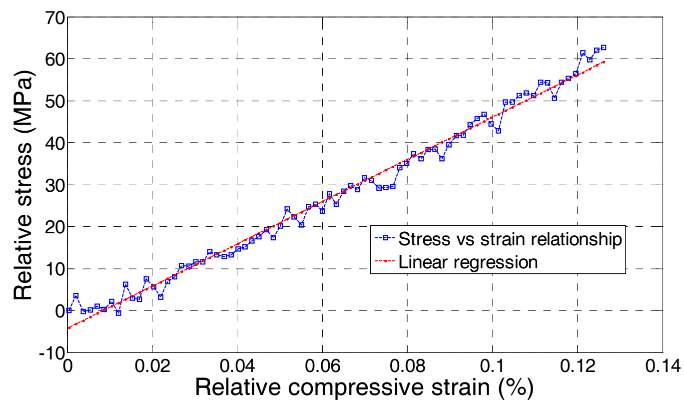

(b) Film thickness: 0.8 μm

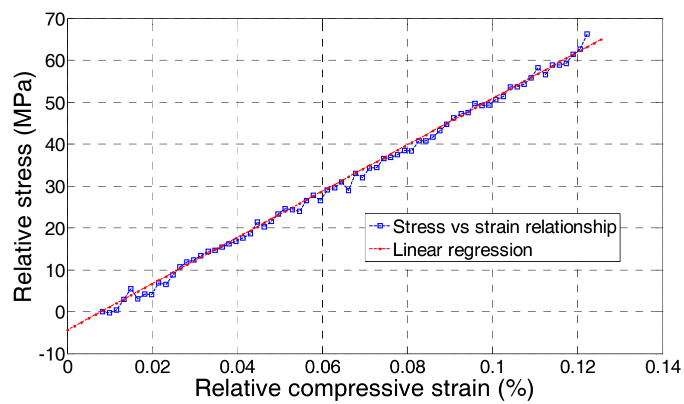

(c) Film thickness: 1.2 μm

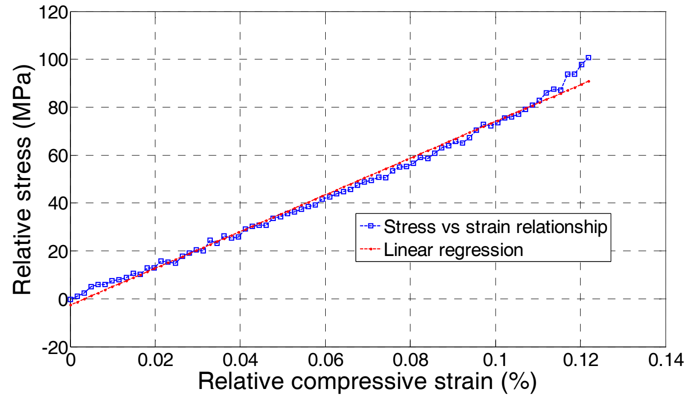

(d) Film thickness: 1.6 µm

Figure 6. 9 Relative stress vs. relative strain relationship of Ag films.

Based on the slope in these stress vs. strain relationships, we can obtain the moduli of films which are listed in Table 6. 3. The results of this work are compared with others from references.

Films		Cu	Al	Ag			
				0.4 µm	0.8 µm	1.2 µm	1.6 µm
Modulus (GPa) (this work)		212.3	91.3	65.8	50.3	55.2	75.9
Reference (GPa)	Film	160.8[a] (1.6 µm)	62±10[b] (0.4 µm)	50±10[b] (4.8 µm)			
	Bulk	178.1[a]	105.3[b]	76[c]			

Table 6. 3 Moduli of films obtained by stress vs. strain relationship slope. a: Zhao (2000), b: Lima et al (1999) c: Zoo et al (2006).

As we can see in Table 6. 3, the moduli of both Cu film and Al film determined here are comparable to those reported in the literature. For Ag films, the modulus of 0.4 µm Ag film is 65.8 GPa. At a thickness of 0.8 µm, the modulus decreases to 50.3 GPa. However in the case of 1.2 µm thick Ag film, the modulus increases slightly to 55.2 GPa. For 1.6 µm Ag film, the modulus increases further to 75.9 GPa, which is about the

same as the value reported in Zoo et al (2006). The moduli of different thickness Ag films are plotted in Figure 6. 10.

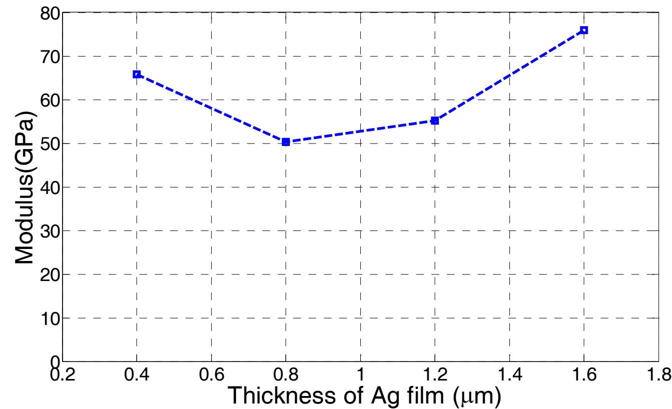

Figure 6. 10 Moduli of different thickness Ag films.

In the case of 0.4 μm Ag film, there might be strong nano effect on the modulus, which results in an increase in modulus. As the thickness of Ag film increases, the nano effect becomes weaker. As such, the modulus decreases in 0.8 μm Ag film. However, with further increase in thickness, the modulus increases from 50.3 GPa to 55.2 GPa, and to 75.9 GPa, which is comparable to the value reported in the literature. More experiments and investigations are needed to find out the underlying mechanism.

6.3 Reversible Trenches atop NiTi Thin Films

6.3.1 Reversible trenches atop shape memory alloy thin films

NiTi based shape-memory thin films (NiTiCu) of about 4 μm thick were prepared at 350°C by co-sputtering of a 3-in. TiNi target (RF, 400W) and a 3-in. pure Cu target (DC, 2W) on a standard commercial 4-in. (100) silicon wafer of 450 μm thickness. The

films were then left in air for several days before postannealed at 450°C for one hour inside a vacuum chamber (Wu MJ *et al* 2009).

Observation using a temperature controlled Atom Force Microscope (AFM) reveals that there are reversible trenches atop the surface of thin films upon thermal cycling. This phenomenon is repeatable even after many thermal cycles. Some subsequent tests reveal that a thin oxide layer (TiO_2), tens of nanometers thick, is formed on the surface of NiTi based thin films. This TiO_2 layer is indeed one of requirements for the trenching phenomenon confirmed by further investigation (Wu MJ et al 2009).

6.3.2 Determination of curvature and stress in TiO_2

In order to investigate the stress evolution in the TiO_2 layer, curvature test on NiTiCu thin film was conducted to measure curvature evolution upon thermal cycling using a Tencor FLX-2908 laser system. A typical result is shown in Figure 6. 11.

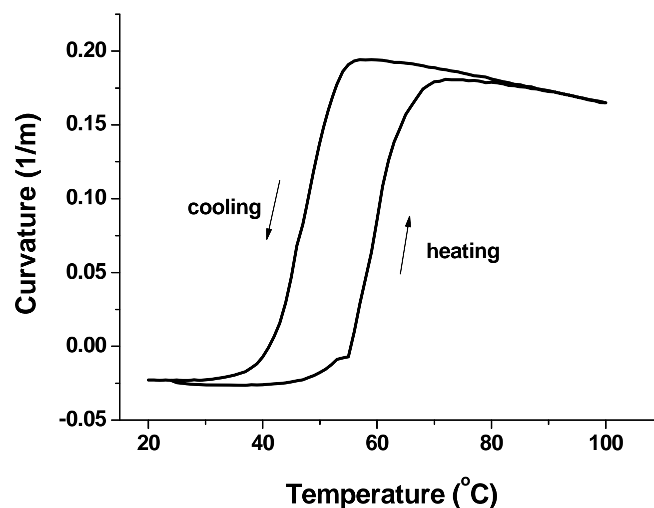

Figure 6. 11 Curvature evolution upon thermal cycling in a NiTiCu film (From Wu 2009 with permission).

Based on the curvature vs. temperature relationship and Equations (5.10) and (5.11), we can find the stress and strain in the NiTiCu film (denoted by σ_f and ε_f , respectively). The annealing temperature should be taken as the initial temperature. The material properties and other parameters used in the analysis are listed in Table 6. 4.

The contribution of TiO_2 layer on the stiffness of the whole structure is neglectable, since its thickness is much thinner as compared with those of both NiTiCu film and Si substrate. Another point, which needs to be noted, is that the CTE of NiTiCu film changes during the phase transformation. The CTE must be estimated based on the phase fraction experimentally (Fu et al 2006, Wu MJ et al 2009).

<table>
<tr><th colspan="2"></th><th>CTE</th><th>E (GPa)</th><th>ν</th><th>Thickness</th></tr>
<tr><td colspan="2">TiO2</td><td>9×10^{-6} /^{o}C</td><td>282.76</td><td>0.28</td><td>10~20 nm</td></tr>
<tr><td rowspan="2">NiTi</td><td>Austenite</td><td>11×10^{-6} /^{o}C</td><td>83</td><td rowspan="2">0.33</td><td rowspan="2">4.2 μm</td></tr>
<tr><td>Martensite</td><td>6.6×10^{-6} /^{o}C</td><td>20</td></tr>
<tr><td colspan="2">Silicon (100)</td><td>2.6×10^{-6} /^{o}C</td><td>130.2</td><td>0.28</td><td>450 μm</td></tr>
</table>

Table 6. 4 Material properties and thickness of each layer used in the analysis (Wu MJ et al 2009).

After the determination of stress and strain in NiTiCu film, the stress in TiO_2 layer (σ_o) can be worked out based on the following relationship (Wu MJ et al 2009),

$$\sigma_o = \overline{E}_o[(\delta - 1)(1 + \varepsilon_f) - (\alpha_o - \alpha_f)\Delta T] \tag{6.1}$$

where α_o and α_f are CTEs of TiO_2 layer and NiTiCu film, respectively. δ is the length ratio of TiO_2 line over NiTiCu line, which is found experimentally. $\overline{E}_o$ is biaxial modulus of TiO_2 layer.

The stress evolution in TiO_2 layer is plotted in Figure 6. 12 together with stress evolution in NiTiCu film.

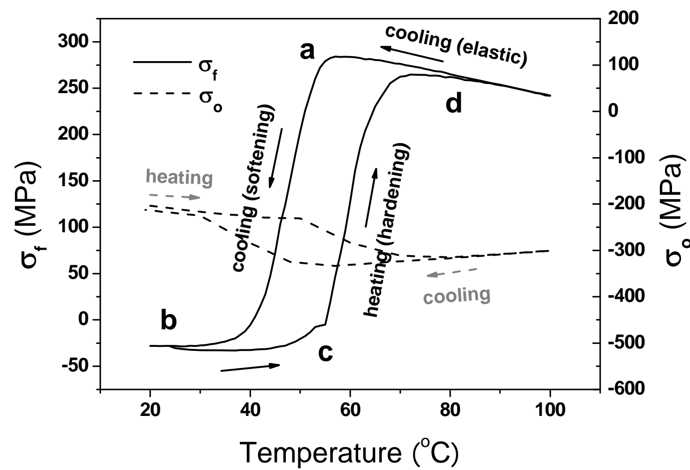

Figure 6. 12 Stresses in NiTiCu thin film and TiO_2 layer upon thermal cycling (Wu MJ et al 2009).

It is found that the TiO_2 layer is always under compression during thermal cycle and the reversible trenches in NiTiCu film are indeed the result of buckling of TiO_2 layer due to large compressive stress.

6.4 Conclusions

Thermally induced curvature method has been applied to investigate moduli of Cu, Al, and Ag films based on the equations developed in Chapter 5. The moduli of Cu and Al

films are determined to be 212.3 GPa and 91.3 GPa, respectively, which are comparable to those reported in the literature. The moduli of Ag films are 65.8 GPa, 50.3 GPa, 55.2 GPa, and 75.9 GPa, for film thickness of 0.4 µm, 0.8 µm, 1.2 µm and 1.6 µm, respectively. Thickness effect on the modulus of Ag films is observed. For 0.4 µm Ag film, there might be a kind of nano effect so that the modulus increases instead of decreasing as following the trend from 1.6 µm to 0.8 µm.

The critical role of a compressive stress in thin oxide layer (TiO_2) atop NiTiCu film in the reversible trench phenomenon is identified.

CHAPTER 7 CONCLUSIONS AND FUTURE WORKS

7.1 Conclusions

This dissertation presents a systematic and detailed study of the thermally induced stress in multilayer thin films within both the elastic and elastic-plastic deformation ranges, and several approaches to determine thermo-mechanical properties of thin films.

The elastic analysis based on the linear strain assumption results in the identical closed-form solutions and approximations (for very thin films) as those reported in the literature.

Closed-form solutions are obtained for fully plastically deformed films. It is found that the difference between pure elastic solution and pure plastic solution is that the Young's modulus (E_f) is replaced by the strain hardening modulus (H_f) if both solutions are expressed in terms of the radius of curvature (r).

It is also found that in most of cases, the film stress within one layer should be of the same sign upon heating or cooling. The location of neutral axes can be determined by the Young's modulus and the thickness of the film and substrate.

The difference among the maximum stress, average stress and Stoney stress in films against the thickness ratio and Young's modulus ratio of film and substrate is investigated systematically. It is concluded that taken Stoney stress as reference, for an error within $\pm 10\%$, it is required that the thickness ratio should be about 0.1 or less for whatever elastic or elastic-plastic analysis.

The result of a case study reveals that the yield start point may be estimated as a linear function of temperature in the elastic-plastic deformation range.

Although above investigations are more focused on bilayer structures, the approach presented in Chapter 3 can be easily applied into multilayer thin films.

A simple approach to determine the values of five thermo-mechanical properties of thin films, namely, the Young's modulus, coefficient of thermal expansion (CTE), yield start stress, strain hardening modulus and Poisson's ratio, is proposed. The approach is based on the conventional curvature test on bilayer structures upon temperature variation and can be easily implemented using many conventional techniques. Three tests are enough to determine the values of these properties. Apart from that, a curvature-based approach, which can determine not only the residual stress but also the intrinsic stress and thermal stress in each layer of a multilayer structure, is presented.

Some simple and generic approaches for the characterization of thin films with nonlinear stress versus strain relationship and/or temperature dependent material properties are proposed. In the case of very thin films, analytical solutions are obtained.

Solutions developed here are applied to investigate the moduli of Cu, Al and Ag films. The moduli of Cu and Al films obtained here are comparable to those reported in the literature. The film thickness effect on the moduli of Ag films has been observed.

The approach developed here is also utilized to identify the critical role of a compressive stress in thin TiO_2 layer atop NiTiCu films in the reversible trench phenomenon.

7.2 Future Works

In terms of future works, there are a few directions to pursue. Several most important ones are listed as follows,

1. To extend the approach described in Chapter 4 into multilayer films. It should be very useful in practice as the deposited films are often with gradient properties, which can be treated as multilayer thin films. It also can be used in the study of very thin films, e.g. nano films, as at such a thickness level, many new phenomena have been observed, which at present are regarded as the results of the size effect and strain gradient.

2. Nonlinear deformation of multilayer structures subjected to thermal loading together with the effects of geometrical nonlinearity and property gradient can be further explored. Our current investigation is based on the linear beam theory. In some cases, large deformation may occur and cause a remarkable change in

the wafer curvature. Subsequently, some new phenomena may happen, such as bifurcation (Zhang et al 2004). This is an interesting area for further study.

3. To investigate the thickness effects on the mechanical properties of thin films on substrates.

References

[1] Aviles F, Oliva AI, and May PA (2008), Determination of elastic modulus in a biomaterial through a one-dimensional laminated model. *Journal of Materials Engineering and Performance*, 17 (482-488).

[2] Badawi KF, Villain P, Goudeau PH, and Renault PO (2002), Measuring thin film and multilayer elastic constants by coupling in situ tensile testing with x-ray diffraction. *Applied Physics Letters*, 80 (4705-4707).

[3] Baker SP, Keller-Flaig RM and Shu JB (2003), Bauschinger effect and anomalous thermomechanical deformation induced by oxygen in passivated thin Cu films on substrates. *Acta Materialia* 51(3019-3036).

[4] Benard WL, Kahn H, Heuer AH and Huff MA (1998), Thin-film shape-memory alloy actuated micropumps. *Journal of Microelectromechanical Systems*, 7 (245-251).

[5] Bradby JE, Kucheyev SO, Williams JS, Wong L, Swain MV, Munroe P, Li G, and Phillips MR (2002), Indentation-induced damage in GaN epilayers. *Applied Physics Letters*, 80 (383-385).

[6] Brenner A and Senderoff S (1949), Calculation of stress in electrodeposits from the curvature of a plated strip. *Journal of research of the National Bureau of Standards*, 42 (105-123).

[7] Caceres D, Vergara I, Gonzalez, Monroy E Calle F, Munoz and Omnes F (1999), Nanoindentation on AlGaN thin films. *Journal of Applied Physics*, 86 (6773-6778).

[8] Carlotti G, Colpani P, Piccolo D, Santucci, Senez V, Socino G and Verdini L (2002), Measurement of elastic and viscoelastic properties of dielectrie films used in microelectronics. *Thin Solid Films*, 414 (99-104).

[9] Carmen MH, Murray TW and Krishnaswamy S (2002), Photoacoustic characterization of the mechanical properties of thin films. *Applied Physics Letters*, 80 (691-693).

[10] Chae JH, Lee JY, and Kang SW (1999), Measurement of thermal expansion coefficient of poly-Si using microgauge sensors. *Sensors and actuators A: physical*, 75 (222-229).

[11] Chang WJ, Fang TH, and Weng CI (2007), Thermoviscoelastic stresses in thin films/substrate system. *Thin Solid Films*, 515 (3693-3697).

[12] Chen KS, and Ou KS (2002), Modification of curvature-based thin-film residual stress measurement for MEMS applications. *Journal of Micromechanics and Microengineering*, 12 (917-924).

[13] Chiu CC (1990), Determination of the elastic modulus and residual stresses in ceramic coating using a strain gage. *Journal of the American Ceramic Society*, 73 (1999-2005).

[14] Choi D, Shinavski RJ, Steffier WS, and Spearing SM (2005), Residual stress in thick low-pressure chemical-vapor deposited polycrystalline SiC coatings on Si substrates. *Journal of Applied Physics*, 97 (074904).

[15] Cornella G, Lee SH, Nix WD and Bravman JC (1997), An analysis technique for extraction of thin film stresses from x-ray data. *Applied Physics Letters*, 71 (2949-2951).

[16] Courtney TH (2000), Mechanical behavior of materials, McGraw Hill, Boston.

[17] Elshabini-Riad, Aicha A, and Fred D (1998), *Thin film technology handbook*, McGraw-Hill.

[18] Espinosa HD, Prorok BC, and Fischer M (2003), A methodology for determining mechanical properties of freestanding thin films and MEMS materials. *Journal of the Mechanics and Physics of Solids*, 51 (47-67).

[19] Exadaktylos GE, Vardoulakis I, and Kourkoulis SK (2001), Influence of nonlinearity and double elasticity on flexure of rock beams –I. Technical theory. *International Journal of Solids and Structures*, 38 (4091-4117).

[20] Fang W and Wickert JA (1995), Comments on measuring thin-film stress using bi-layer micromachined beams. *Journal of Micromechanics and Microengineering*, 5 (276-281).

[21] Fang W and Wickert JA (1996), Determining mean and gradient residual stresses in thin films using micromachined cantilevers. *Journal of Micromechanics and Microengineering*, 6 (301-309).

[22] Fang W, Tsai HC and Lo CY (1999), Determining thermal expansion coefficients of thin films using micromachined cantilevers. *Sensors and Actuators A: Physical*. 77 (21-27).

[23] Fang W and Lo CY (2000), On the thermal expansion coefficients of thin films. *Sensors and Actuators A: Physical*, 84 (310-314).

[24] Fartash A, Grimsditch M, Fullerton EE and Schuller IK (1993), Breakdown of Poisson's effect in Nb/Cu superlattices. *Physical Review B*, 47 (12813-12919).

[25] Feng ZC and Liu HD (1983), Generalized formula for curvature radius and layer stresses caused by thermal strain in semiconductor multilayer structures. *Journal of Applied Physics,* 54 (83-85).

[26] Florando JN and Nix WD (2005), A microbema bending method for studying stress-strain relations for metal thin films on silicon substrates. *Journal of the Mechanics and Physics of Solids*, 53 (619-638).

[27] Freund LB, Floro JA and Chason E (1999), Extensions of the Stoney formula for substrate curvature to configurations with thin substrate or large deformations. *Applied Physics Letters,* 74 (1987-1989).

[28] Freund LB and Suresh (2003), Thin Film Materials: Stress; Defect Foemation, and Surface Evolution. Cambridge University Press, Cambridge, UK.

[29] Fu YQ, Zhang S, Wu MJ, Huang WM, Du HJ, Luo JK, Flewitt AJ, and Milne WI (2006), On the lower thickness boundary of sputtered TiNi films for shape memory application. *Thin Solid Films*, 515 (80-86).

[30] Fullerton EE, Kumar S, Grimsditch M, Kelly DM, and Schuller IK (1993), X-ray-diffraction characterization and sound-velocity measurements of W/Ni multilayers. *Physical Review B*, 48 (2560-2567).

[31] Gere JM and Timoshenko SP (1991), *Mechanics of materials*, 3rd edition, Chapman & Hall.

[32] Godin M, Tabard-Cossa V and Grütter P (2001), Quantitive surface stress measurement using a microcantilever. *Applied Physics Letters*, 79 (551-553).

[33] Guckel H, Randazzo T, and Burns DW (1985), A simple technique for the

determination of mechanical strain in thin films with application to polusilicon. *Journal of Applied Physics*, 57 (1671-1675).

[34] Gunnars J and Wiklund U (2002), Determination of growth-induced strain and thermo-elastic properties of coatings by curvature measurements. *Materials Science and Engineering A*, 336 (7-21).

[35] Haque and Saif (2003), A review of MEMS-based microscale and nanoscale tensile and bending testing. *Experimental Mechanics*, 43 (248-255).

[36] Harms U, Gäertner M, Schütze A, Bewilogua and Neuhäuser H (2001), Elastic and anelastic properties, internal stress and thermal expansion coefficient of cubic boron nitride films on silicon. *Thin Solid Films*, 385 (275-280).

[37] Hoffman RW (1966), in Physics of Thin Films, Vol. 3, eds. Hass G and Thun RE. Academic Press, New York.

[38] Hommel M and Kraft O (2001), Deformation behavior of thin copper films on deformable substrates. *Acta Materialia,* 49 (3935-3947).

[39] Hsueh CH (2002), Modeling of elastic deformation of multilayers due to residual stresses and external bending. *Journal of Applied Physics*, 91 (9652-9656).

[40] Hsueh CH, Lee S and Chuang TJ (2003), An alternative method of solving multilayer bending problems. *Transactions of ASME: Journal of Applied mechanics*, 70 (151-154).

[41] Hsueh CH and Paranthaman M (2008), Analytical modeling of residual stresses in multilayered superconductor systems. *Journal of Materials Science*, 43 (6223-6232).

[42] Hu YY and Huang WM (2004), Elastic and Elastic-Plastic Analysis of Multilayer Thin Films: Closed-Form Solutions. *Journal of Applied Physics*, 96 (4154-4160).

[43] Huang WM, Gao XY and Tan JP (2001), Design of Thin Film Based Micro Grippers. *SPIE: Micromachining and Microfabrication Process Technology and Devices*, Nanjing, China, 4601 (123-130).

[44] Huang WM, Tan JP, Gao XY and Yeo JH (2003), Design, Testing and Simulation of NiTi Shape Memory Alloy Thin Film Based Micro-Grippers. *Journal of Microlithography, Microfabrication, and Microsystems*, 2 (185-190).

[45] Huang WM, Liu QY, He Lm and Yeo JH (2004), Micro NiTi-Si cantilever with three stable positions. *Sensors and Actuators A: Physical*, 114 (118-122).

[46] Huang WM, Hu YY, and An L (2004), A simple approach to determine five thermo mechanical properties of thin ductile films on an elastic substrate. *Applied Physics Letters,* 85 (6173-6175).

[47] Huang WM, Hu YY, and An L (2005), Response to 'Comment on "A simple approach to determine five thermomechanical properties of thin ductile films on an elastic substrate" [Appl. Phys. Lett. 87, 116101]. *Applied Physics Letters,* 85 (116102).

[48] Huang WM, Hu YY, and An L (2005), Determination of stress versus strain relationship and other thermomechanical properties of thin films. *Applied Physics Letters,* 87 (201904-1-3).

[49] Jacobs SF, Bradford JN and Berthold JW(1970), Ultraprecise measurement of thermal expansion coefficient. *Applied Optics*, 9 (2477-2480).

[50] Jain A, Rogojevic S, Gill WN, Plawsky JL, Matthew I, Tomozawa M and Simonyi E (2001), Effects of processing history on the modulus of silica xerogel films. *Journal of Applied Physics*, 90 (5832-5834).

[51] Janda M and Stefan (1984), Intrinsic stress in chromium thin films measured by a Novel method. *Thin Solid Films*, 112 (127-137).

[52] Janda M (1986), On the intrinsic stress in thin chromium films. *Thin Solid Films*, 142 (37-45).

[53] Jeong J, Kwon D, Lee WS, and Baik YJ (2001), Intrinsic stress in chemical vapor deposited diamond films: An analytical model for the plastic deformation of the Si substrate. *Journal of Applied Physics*, 90 (1227-1236).

[54] Jin XS, Kim CO, Lee YP, Zhou Y and Xu HB (2001), Simultaneous measurements of the magnetostrictive coefficient, Young's modulus, and Poisson ratio thin films. *Applied Physics Letters*, 79 (650-652).

[55] Kalkman AJ, Verbruggen AH and Janssen GCAM (2001), Young's modulus measurements and grain boundary sliding in free-standing thin metal films. *Applied Physics Letters*, 78 (2673-2675).

[56] Kinzly RE (1967), A new interferometer capable of measuring small optical path difference. *Applied Optics*, 6 (137-140).

[57] Kim JS, Paik KW and Oh SH (1999), The multilayer-modified Stoney's formula for laminated polymer composites on a silicon substrate. *Journal of Applied Physics*, 86 (5474-5479).

[58] Kim SH, Boyd JG and Mani S (2007), Mechanical behavior of mismatch strain-

driven microcantilever. *Microelectronics Journal*, 38 (371-380).

[59] Klein CA (2000a), Strains and stresses in multilayered elastic structures: The case of chemically vapor-deposited ZnS/ZnSe laminates. *Journal of Applied Physics*, 87 (2265-2272).

[60] Klein CA (2000b), How accurate are Stoney's equation and recent modifications. *Journal of Applied Physics*, 88 (5487-5489).

[61] Klein CA (2000c), Comment on "The multilayer-modified Stoney's formula for laminated polymer composites on a silicon substrate"[J. Appl. Phys. 86. 5474 (1999)]. *Journal of Applied Physics*, 88 (5499-5500).

[62] Krulevitch P, Lee AP, Ramsey PB, Trevino JC, Hamilton J and Northrup MA (1996), Thin film shape memory alloy microactuators. *Journal of Microelectromechanical Systems*, 5 (270-282).

[63] Kucheyev SO, Bradby JE, JS Williams, Jagadish C, Toth M, Phillips MR and Swain MV (2000), Nanoindentation of epitaxial GaN films. *Applied Physics Letters*, 77 (3373-3375).

[64] Lima MM, Lacerda RG, Vilcarromero J and Marques FC (1999), Coefficient of thermal expansion and elastic modulus of thin films. *Journal of Applied Physics*, 86 (4936-4942).

[65] Liu HC and Murarka SP (1992), Elastic and viscoelastic analysis of stress in thin films. *Journal of Applied Physics,* 72 (3458-3463).

[66] Maissel L and Glang R (1970), *Handbook of Thin Film Technology*, McGraw-Hill.

[67] Malzbender J and Steinbrech RW (2003), Determination of the stress-dependent

stiffness of plasma-sprayed thermal barrier coatings using depth-sensitive indentation. *Journal of Materials Research*, 18 (1975-1983).

[68] Malzbender J and Steinbrech RW (2004), Mechanical properties of coated materials and multi-layered composites determined using bending methods. *Surface and Coatings Technology*, 176 (165-172).

[69] Malzbender J (2005), Comment on "A simple approach to determine five thermomechanical properties on thin ductile films on an elastic substrate [Appl. Phys. Lett. 85, 6173 (2004)]". *Applied Physics Letters*, 87 (116101).

[70] Mezin A (2006), Coating internal stress measurement through the curvature method: A geometry-based criterion delimiting the relevance of Stoney's formula. *Surface and Coatings Technology*, 200 (5259-5267).

[71] Murarka SP and Retajczyk TF (1983), Effect of phosphorus doping on stress in silicon and polycrystalline silicon. *Journal of Applied Physics*, 54 (2069-2072).

[72] Nejhad MNG, Pan CL, and Feng HW (2003), Intrinsic Strain Modeling and Residual Stress Analysis for Thin-Film Processing of Layered Structures. *Journal of Electronic Packaging*, 125 (4-17).

[73] Nie M, Huang QA, and Li WH (2006), Measurement of residual stress in multilayered thin films by a full-field optical method. *Sensors and Actuators A: Physical*, 126 (93-97).

[74] Nikishkov GP (2003), Curvature estimation for multilayer hinged structures with initial strains. *Journal of Applied Physics,* 94 (5333-5336).

[75] Nix WD (1989), Mechanical-properties of thin-films. *Metallurgical Transactions.*

A, 20 (2217-2245).

[76] Nowak R, Pessa M, Suganma M, Leszczynski M, Grzegory I, Porowski S and Yoshida F (1999), Elastic and plastic properties of GaN determined by nano-indentation of bulk crystal. *Applied Physics Letters*, 75 (2070-2072).

[77] Ohring M (2002), *The materials science of thin films: deposition and structure (Second Edition),* Academic Press.

[78] Oliver, W. C. and G. M. Pharr (1992), An improved technique for determining hardness and elastic modulus using load and displacement sensing indentation experiments. *Journal of Materials Research,* 7 (1564-1583).

[79] Olsen GH and Ettenberg M (1977), Calculated stresses in mutilayered heteroepitaxial structures. *Journal of Applied Physics,* 48 (2543-2547).

[80] Osterberg PM and Senturia SD (1997), M-test: a test chip for MEMS material property measurement using electrostatically actuated test structures. *Journal of Microelectromechanical Systems*, 6 (107-118).

[81] Petern KE (1978), Dynamic micromechanics on silicon: techniques and devices, *IEEE Trans. Electron Devices*, ED-25 (1241-1250).

[82] Rats D, Bimbault L, Vandenbulcke L, Herbin R and Badawi KF (1995), Crystalline quality and residual stresses in diamond layers by Raman and x‐ray diffraction analyses. *Journal of Applied Physics,* 78 (4994-5001).

[83] Reinhart FK and Logan (1973), Interface stress of $Al_xGa_{1-x}As$-GaAs layer structures. *Journal of Applied Physics,* 44 (3171-3175).

[84] Renault PO, Badawi KF, Bimbault L, Goudeau PH, Elkaïm E and Lauriat JP

(1998), Poisson's ratio measurement in tungsten thin films combining an x-ray diffractometer with in situ tensile tester. *Applied Physics Letters*, 73 (1952-1954).

[85] Retajczyk TF and Sinha AK (1980), Elastic stiffness and thermal expansion coefficient of BN films. *Applied Physics Letters*, 36 (161-163).

[86] Röll K (1976), Analysis of stress and strain distribution in thin films and substrates. *Journal of Applied Physics*, 47 (3224-3229).

[87] Saul RH (1969), Effect of a $GaAs_xP_{1-x}$ transition zone on the perfection of GaP crystals grown by deposition onto GaAs substrates. *Journal of Applied Physics,* 40 (3273-3279)

[88] Schäfer JD, Näfe H and Aldinger F (1999), Macro- and microstress analysis in sol-gel derived Pb (Zr_xTi_{1-x}) O3 thin films, *Journal of Applied Physics*, 85 (8023-8031)

[89] Shames H (1989), *Introduction to solid mechanics*, 2nd edition, Prentice-Hall.

[90] Singh J (1993), *Physics of semiconductors and their heterostructures*, McGraw-Hill, New York.

[91] Srikar VT and Spearing SM (2003), A critical review of microscale mechanical testing methods used in the design of microelectromechanical systems. *Experimental Mechanics*, 43 (238-247).

[92] Stafford1 CM, Harrison C, Beers KL, Karim A, Amis EJ, VanLandingham MR, Kim HC, Volksen W, Miller RD, and Simonyi EE (2004), A buckling-based metrology for measuring the elastic moduli of polymeric thin films. *Nature Materials*, 3 (545-550).

[93] Stoney GG (1909), The tension of metallic films deposited by electrolysis. *Proceedings of the Royal Society of London Series A*, 82 (172-175).

[94] Su JF (2004), Indentation and laser annealing of NiTi shape memory alloys, Thesis, Nanyang Technological University, Singapore.

[95] Suo Z, Ma EY, Gleskova H and Wagner S (1999), Mechanics of rollable and foldable film-on-foil electronics. *Applied Physics Letters*, 74 (1177-1179).

[96] Su YJ, Qian CF, and Zhao MH (2000), Microbridge testing of silicon oxide/silicon nitride bilayer films deposited on silicon wafers. *Acta Materialia*, 48 (4901-4915).

[97] Tada H, Kumpel AE, Lathrop RE, Slanina JB, Nieva P, Zavracky, Miaoulis IN and Wong PY (2000), Thermal expansion coefficient of polycrystalline silicon and silicon dioxide thin films at high temperatures. *Journal of Applied Physics*, 87 (4189-4193).

[98] Taylor Ca, Wayne MF and Chiu KS (2003), Heat treatment of thin carbon films and the effect on residual stress, modulus thermal expansion and microstructure. *Carbon*, 41 (1867-1875).

[99] Teixeira V (2001), Mechanical integrity in PVD coatings due to the presence of residual stresses. *Thin Solid Films*, 392 (276-281).

[100] Thurn J and Hughey MP (2004), Evaluation of film biaxial modulus and coefficient of thermal expansion from thermoelastic film stress measurements. *Journal of Applied Physics*, 95 (7892-7897).

[101] Tien CL, Lee CC, Tsai TL and Sun WS (2001), Determination of the mechanical properties of thin films by digital phase shifting interferometry. *Optics*

Communications, 198 (325-331).

[102] Timoshenko S (1925), Analysis of bi-metal thermostats. *Journal of the Optical Society of America*, 11 (233-255).

[103] Townsend PH, Barnett DM and Brunner TA (1987), Elastic relationship in layered composite media with approximation for the case of thin films on a thick substrate. *Journal of Applied Physics,* 62 (4438-4444).

[104] Trochu F and Qian YY (1997), Nonlinear finite element simulation of superelastic shape memory alloy parts. *Computers & Structures*, 62 (799-810).

[105] Tsai SH, Wang YT and Kan HC (2009), Analysis on the uniformly loaded rectangular cross-section cantilever by a modified load-deflection model. *Journal of Physics D: Applied Physics*, 42 (045505).

[106] Tsui TY and Pharr GM (1999), Substrate effects on nanoindentation mechanical property measurement of soft films on hard substrates. *Journal of Materials Research*, 14 (292-301).

[107] Varguez P, Aviles F, and Oliva AI (2008), Mechanical properties of gold nanometric films onto a polymeric substrate. *Surface & Coatings Technology*, 202 (1556-1563).

[108] Vilms J and Kerps D (1982), Simple stress formula for multilayered thin films on a thick substrate. *Journal of Materials Research*, 3 (1536-1537).

[109] Widjaja S, Limarga AM, and Yip TH (2003), Modeling of residual stresses in a plasma-sprayed zirconia/alumina functionally graded-thermal barrier coating. *Thin Solid Films,* 434 (216-227).

[110] Wu MJ, Huang WM, Fu YQ, Chollet F, Hu YY, and Cai M (2009), Reversible surface morphology in shape-memory alloy thin films. *Journal of Applied Physics*, 105 (033517-1-5).

[111] Wu MJ (2009), Surface metrology and optical properties of thin film shape memory alloys. PhD Dissertation, Nanyang Technological University, Singapore.

[112] Xu WH, Lu DX and Zhang TY (2001), Determination of residual stresses in $Pb(Zr_{0.53}Ti_{0.47})O_3$ thin films with Raman spectroscopy. *Applied Physics Letters*, 79 (4112-4114).

[113] Yu J, Kim JG, Chung JO, and Cho DH (2000), An elastic/plastic analysis of the intrinsic stresses in chemical vapor deposited diamond films on silicon substrates. *Journal of Applied Physics*, 88 (1688-1694).

[114] Yuan HR, Hichwa BP and Allen TH (1998), Noncontact method for measuring coefficient of linear thermal expansion of thin films. *Journal of Vacuum Science & Technology A-Vacuum Surfaces and Films*, 16 (3119-3122).

[115] Zhang TY, Su YJ, and Qian CF (2000), Microbridge testing of silicon nitride thin films deposited on silicon wafers. *Acta Materialia*, 48 (2843-2857).

[116] Zhang XC, Xu BS, Wang HD, and Wu YX (2005), Error analyses on some typically approximate solutions of residual stress within a thin film on a substrate. *Journal of Applied Physics*, 98 (053516-1-5).

[117] Zhang YH, Dunn ML, Gall K, and Elam JW (2004), Suppression of inelastic deformation of nanocoated thin film microstructures. *Journal of Applied Physics*, 95 (8216-8225).

[118] Zhao JH, Ryan T, Ho PS, McKerrow AJ and Shih WY (1999), Measurement of elastic modulus, Poisson ratio, and coefficient of thermal expansion of on-wafer submicroron films. *Journal of Applied Physics*, 85 (6421-6424).

[119] Zhao JH, Du Y, Morgen M and Ho PS (2000a), Simultaneous measurement of Young's modulus, Poisson ratio, and coefficient of thermal expansion of thin films on substrates. *Journal of Applied Physics*, 87 (1575-1577).

[120] Zhao JH, Kiene M, Hu C and Ho PS (2000b), Thermal stress and glass transition of ultrathin polystyrene films. *Applied Physics Letter*, 77 (2843-2845).

[121] Zhao JH (2000), Thermomechanical properties and phase transition of thin and ultra-thin films. Phd Dissertation, The University of Texas at Austin.

[122] Zheng DW, Xu YH, Tsai YP, Tu KN, Patterson, Zhao B, Liu QZ and Brongo M (2000), Mechanical property measurement of thin polymeric-low dielectric-constant films using bulge testing method. *Applied Physics Letters*, 76 (2008-2010).

[123] Zhou JB, Wu JS and Yang YX (1999), Research on the thermal expansion behavior of anodic films on aluminum. *Thin solid films*, 346(280-283).

[124] Ziebart V (1999), *Mechanical properties of CMOS thin films*, Phd Dissertation, Swiss Federal Institute of Technology Zurich.

[125] Zoo Y, Adams D, Mayer JW, and Alford (2006), Investigation of coefficient of thermal expansion of silver thin film on different substrates using X-ray diffraction. *Thin Solid Films*, 513 (170-174).

Appendix A

Derivation of the Stoney Formula

A.1 Derivation Based on Force and Moment Equilibrium (from Ohring 2002)

The Stoney formula and its variants have been used in the study of film stress. This formula can be derived based on force and moment equilibrium with reference to Figure A.1, which illustrates a film/substrate composite with a unit width w. The film thickness and Young's modulus are t_f and E_f , respectively, while those corresponding to the substrate are t_s and E_s. Because of lattice mismatch, difference in thermal expansion, film growth effects, etc., mismatch forces arise at the film/substrate interface.

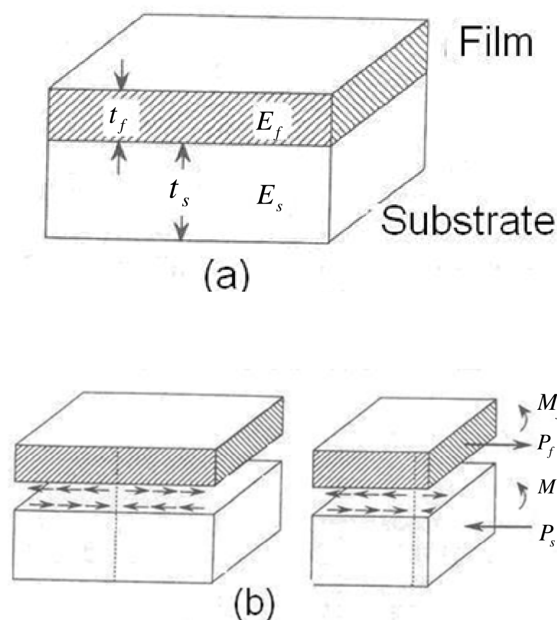

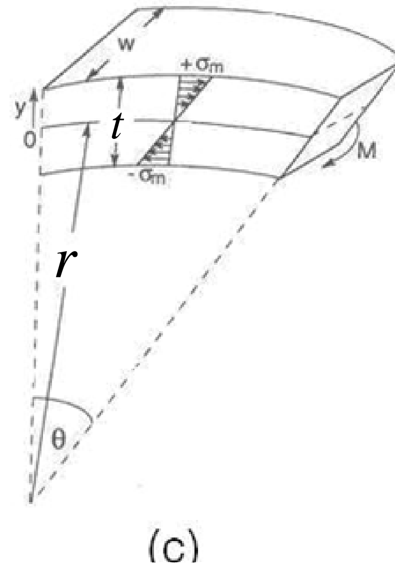

Figure A.1 Stress analysis of film/substrate composite: (a) composite structure; (b) free-body diagrams of film and substrate with indicated interfacial forces and end moments; (c) elastic bending of beam under applied end moment (Ohring 2002).

In the free-body diagrams of Figure A.1 (b) each interfacial set of forces can be replaced by the statically equivalent combination of a force and moment; P_f and M_f in the film, P_s and M_s in the substrate, where $P_f = P_s$. Force P_f can be imagined to act uniformly over the cross-sectional area ($t_f w$) giving rise to the film stress. The moments are responsible for the bowing of the film/substrate composite. The equilibrium condition is,

$$\frac{(t_f + t_s)P_f}{2} = M_f + M_s \tag{A.1}$$

Consider now an isolated beam bent by moment M as indicated in Figure A.1(c). The deformation is assumed to consist entirely of the extension or contraction of longitudinal beam fibers by an amount proportional to their distance from central or neutral axis, which remains unstrained in the process. The stress distribution reflects

this by varying linearly across the section from the maximum tension ($+\sigma_m$) to the maximum compression ($-\sigma_m$) at the beam fibers. In terms of the beam radius of curvature r, and angle θ subtended, Hooke's law yields,

$$\sigma_m = \frac{E[(r+t/2)\theta - r\theta]}{r\theta} = \pm\frac{Et}{2r} \tag{A.2}$$

Corresponding to this stress distribution is the bending moment across the beam section,

$$M = 2\int_0^{t/2} \sigma_m w(\frac{y}{t/2}) y dy = \sigma_m t^2 w/6 = Et^3 w/12r \tag{A.3}$$

By extension of this result, we have,

$$M_f = \frac{E_f t_f^3 w}{12r} \quad \text{and} \quad M_s = \frac{E_s t_s^3 w}{12r}$$

Lastly, in order to account for actual biaxial-stress distribution in films, rather than the uniaxial stresses assumed for ease of derivation, it is necessary to replace E_f by $\frac{E_f}{1-\upsilon_f}$, and similarly for E_s. Substitution of these terms in Equation (A.1) yields,

$$\frac{(t_f + t_s)P_f}{2} = \frac{wE_f t_f^3}{12r(1-\upsilon_f)} + \frac{wE_s t_s^3}{12r(1-\upsilon_s)} \tag{A.4}$$

Since t_s is normally much larger than t_f, the film stress σ_f is, for a reasonable approximation, given by,

$$\sigma_f = \frac{P_f}{t_f w} = \frac{E_s t_s^2}{6r(1-\upsilon_s)t_f} \tag{A.5}$$

This is the Stoney formula.

A.2 The flaw of Stoney Formula's derivation

Strictly speaking, Stoney did not clearly express the theoretical derivation of the equation for evaluating the residual in coatings (Chiu 1990). Brenner et al. also pointed out "…the theoretical side is not so satisfactory. There exists a lack of clarity in his definition of what is meant by the stress in deposit, and a lack of recognition that…" (Chiu 1990).

In this case, several approaches to derive Stoney formula have been developed. Freund et al proposed an approach, which is based on minimization of potential energy, to derive Stoney formula. Interested readers may refer to Freund et al (1999) for details.

Appendix B

Expressions for ε_t and ε_b

By substituting Equations (3.1)-(3.3) into Equations (3.4a) and (3.4d), we have,

$$\int_0^{t_s} E_s((\frac{\varepsilon_t-\varepsilon_b}{h_n+t_s}y+\varepsilon_b)-\alpha_s\Delta T)dy+\sum_{i=1}^{n}(\int_{t_s+h_{i-1}}^{t_s+h_i} E_i((\frac{\varepsilon_t-\varepsilon_b}{h_n+t_s}y+\varepsilon_b)-\alpha_i\Delta T)dy)=0 \quad \text{(B.1)}$$

$$\int_0^{t_s} E_s((\frac{\varepsilon_t-\varepsilon_b}{h_n+t_s}y+\varepsilon_b)-\alpha_s\Delta T)ydy+\sum_{i=1}^{n}(\int_{t_s+h_{i-1}}^{t_s+h_i} E_i((\frac{\varepsilon_t-\varepsilon_b}{h_n+t_s}y+\varepsilon_b)-\alpha_i\Delta T)ydy)=0 \quad \text{(B.2)}$$

The explicit expressions for ε_t and ε_b can be obtained by solving Equations (B.1) and (B.2). Commercial software Mathematica is applied to solve these two equations as follows,

```
eqn11 = ∫_0^(t_s) E_s * (((ϵ_t - ϵ_b)/(h_n + t_s) * z + ϵ_s) - α_s * T) ⅆz + Sum_(i=1)^n (∫_(t_s+h_(i-1))^(t_s+h_i) E_i * (((ϵ_t - ϵ_b)/(h_n + t_s) * z + ϵ_s) - α_i * T) ⅆz);
eqn12 = ∫_0^(t_s) E_s * (((ϵ_t - ϵ_b)/(h_n + t_s) * z + ϵ_s) - α_s * T) z ⅆz + Sum_(i=1)^n (∫_(t_s+h_(i-1))^(t_s+h_i) E_i * (((ϵ_t - ϵ_b)/(h_n + t_s) * z + ϵ_s) - α_i * T) z ⅆz);
equations = {eqn11 == 0, eqn12 == 0};
Results = FullSimplify[Solve[equations, {ϵ_t, ϵ_b}]]
```

The expression of ε_t is,

$$\varepsilon_t = (\Delta T(E_s^2 t_s^4 \alpha_s + 4(\sum_{i=1}^{n} E_i h_{i-1}^3 - \sum_{i=1}^{n} E_i h_i^3)(\sum_{i=1}^{n} E_i h_{i-1}\alpha_i - \sum_{i=1}^{n} E_i h_i \alpha_i) +$$

$$6h_n(\sum_{i=1}^{n} E_i h_i^2 - \sum_{i=1}^{n} E_i h_{i-1}^2)(\sum_{i=1}^{n} E_i h_{i-1}\alpha_i - \sum_{i=1}^{n} E_i h_i \alpha_i) +$$

$$(\sum_{i=1}^{n} E_i h_{i-1} - \sum_{i=1}^{n} E_i h_i)(\sum_{i=1}^{n} E_i h_{i-1}^2 \alpha_i - \sum_{i=1}^{n} E_i h_i^2 \alpha_i)) -$$

$$3(\sum_{i=1}^{n} E_i h_{i-1}^2 - \sum_{i=1}^{n} E_i h_i^2)(\sum_{i=1}^{n} E_i h_{i-1}^2 \alpha_i - \sum_{i=1}^{n} E_i h_i^2 \alpha_i) +$$

$$E_s t_s (4\alpha_s(\sum_{i=1}^{n} E_i h_i^3 - \sum_{i=1}^{n} E_i h_{i-1}^3) - 4t_s^2(\sum_{i=1}^{n} E_i h_{i-1}\alpha_i - \sum_{i=1}^{n} E_i h_i \alpha_i) -$$

$$3t_s(\alpha_s(\sum_{i=1}^{n} E_i h_{i-1}^2 - \sum_{i=1}^{n} E_i h_i^2) + \sum_{i=1}^{n} E_i h_{i-1}^2 \alpha_i - \sum_{i=1}^{n} E_i h_i^2 \alpha_i) +$$

$$6h_n(\alpha_s(\sum_{i=1}^{n} E_i h_{i-1}^2 - \sum_{i=1}^{n} E_i h_i^2) - \sum_{i=1}^{n} E_i h_{i-1}^2 \alpha_i +$$

$$t_s(\alpha_s(\sum_{i=1}^{n} E_i h_{i-1} - \sum_{i=1}^{n} E_i h_i) - \sum_{i=1}^{n} E_i h_{i-1}\alpha_i + \sum_{i=1}^{n} E_i h_i \alpha_i) + \sum_{i=1}^{n} E_i h_i^2 \alpha_i)))) /$$

$$(E_s^2 t_s^4 - 3(\sum_{i=1}^{n} E_i h_{i-1}^2 - \sum_{i=1}^{n} E_i h_i^2)^2 + 4(\sum_{i=1}^{n} E_i h_{i-1} - \sum_{i=1}^{n} E_i h_i)(\sum_{i=1}^{n} E_i h_{i-1}^3 - \sum_{i=1}^{n} E_i h_i^3) +$$

$$2E_s t_s(-2\sum_{i=1}^{n} E_i h_{i-1}^3 +$$

$$t_s(-3\sum_{i=1}^{n} E_i h_{i-1}^2 + 2t_s(\sum_{i=1}^{n} E_i h_i - \sum_{i=1}^{n} E_i h_{i-1}) + 3\sum_{i=1}^{n} E_i h_i^2) + 2\sum_{i=1}^{n} E_i h_i^3))$$

(B.3)

The expression of ε_b is,

$$
\begin{aligned}
\varepsilon_b = (&\Delta T(E_s^2 t_s^4 \alpha_s + 4(\sum_{i=1}^{n} E_i h_{i-1}^3 - \sum_{i=1}^{n} E_i h_i^3)(\sum_{i=1}^{n} E_i h_{i-1}\alpha_i - \sum_{i=1}^{n} E_i h_i \alpha_i) + \\
&6h_n(\sum_{i=1}^{n} E_i h_{i-1}^2 - \sum_{i=1}^{n} E_i h_i^2)(\sum_{i=1}^{n} E_i h_{i-1}\alpha_i - \sum_{i=1}^{n} E_i h_i \alpha_i) - \\
&(\sum_{i=1}^{n} E_i h_{i-1} - \sum_{i=1}^{n} E_i h_i)(\sum_{i=1}^{n} E_i h_{i-1}^2 \alpha_i - \sum_{i=1}^{n} E_i h_i^2 \alpha_i)) - \\
&3(\sum_{i=1}^{n} E_i h_{i-1}^2 - \sum_{i=1}^{n} E_i h_i^2)(\sum_{i=1}^{n} E_i h_{i-1}^2 \alpha_i - \sum_{i=1}^{n} E_i h_i^2 \alpha_i) + \\
&E_s t_s (4\alpha_s (\sum_{i=1}^{n} E_i h_i^3 - \sum_{i=1}^{n} E_i h_{i-1}^3) - 2t_s^2 (3\alpha_s (\sum_{i=1}^{n} E_i h_{i-1} - \sum_{i=1}^{n} E_i h_i) - \sum_{i=1}^{n} E_i h_{i-1}\alpha_i + \\
&\sum_{i=1}^{n} E_i h_i \alpha_i) - 3t_s (3\alpha_s (\sum_{i=1}^{n} E_i h_{i-1}^2 - \sum_{i=1}^{n} E_i h_i^2) - \sum_{i=1}^{n} E_i h_{i-1}^2 \alpha_i + \sum_{i=1}^{n} E_i h_i^2 \alpha_i)))) / \\
&(E_s^2 t_s^4 - 3(\sum_{i=1}^{n} E_i h_{i-1}^2 - \sum_{i=1}^{n} E_i h_i^2)^2 + 4(\sum_{i=1}^{n} E_i h_{i-1} - \sum_{i=1}^{n} E_i h_i)(\sum_{i=1}^{n} E_i h_{i-1}^3 - \sum_{i=1}^{n} E_i h_i^3) + \\
&2E_s t_s (-2\sum_{i=1}^{n} E_i h_{i-1}^3 + \\
&t_s (-3\sum_{i=1}^{n} E_i h_{i-1}^2 + 2t_s (\sum_{i=1}^{n} E_i h_i - \sum_{i=1}^{n} E_i h_{i-1}) + 3\sum_{i=1}^{n} E_i h_i^2) + 2\sum_{i=1}^{n} E_i h_i^3))
\end{aligned}
\tag{B.4}
$$

Appendix C

FEA Model for Section 3.7 Numerical Simulation

Commercial finite element analysis package ANSYS was utilized to simulate the thermal mismatch induced stress in a steady-state analysis for the case that an aluminum film is deposited atop a silicon substrate as assumed in Section 3.6. The thickness of substrate is $15\,\mu\text{m}$, while that of film is 5 μm except the cases that the effect of film thickness is studied in which film thickness varies from 1 μm to 5 μm. The length of the bilayer structure is $240\,\mu\text{m}$.

The substrate is modeled as isotropic and perfectly elastic. The plastic behavior of film is assumed to be isotropic. Hence, its stress versus strain relationship is modeled using bilinear (or multilinear) isotropic hardening (BISO or MISO). The interface between the film and substrate is assumed to be perfectly bonded at all times during simulation. The simulation is simplified as a two dimensional model using eight-node quadrilateral elements (PLANE82 with plane stress option) with two degrees of freedom at each node: translations in the nodal X and Y directions. The element size of the film is minimized gradually from top to interface, as interface is most likely to be with high stress concentration since both the maximum stress in the film and maximum stress in the substrate could appear at the interface as found in the previous studies. Due to the fact that film stress is more of our interest, coarser mesh is used for the substrate except in the area near the edge where stress concentration may also happen. The bilayer strip is symmetrical about its mid-point in the length direction and hence only half of it

needs to be modeled. Finally, a two-dimensional rectangular mesh for the right half of the bilayer strip consists of 576 elements and 1849 nodes (in the case of 5 μm film).

The boundary and initial conditions are as follow: a) the middle line in X direction (left boundary of the model) is treated as symmetrical axis and hence all nodes on it are constrained from moving in X direction (X direction is along length of the bilayer structure); b) the node at the lower left corner is fixed to prevent from moving in both X and Y directions in a rigid body fashion (Y direction is along thickness of the bilayer structure); c) all other nodes are free to move; d) the bilayer strip is in free stress state during deposition. The simulation assumes a uniform temperature distribution in the strip and the temperature variation (ΔT) starts from cooling from the deposition temperature. The FEA model for the case of 5 μm thick film is shown in Figure C.1.

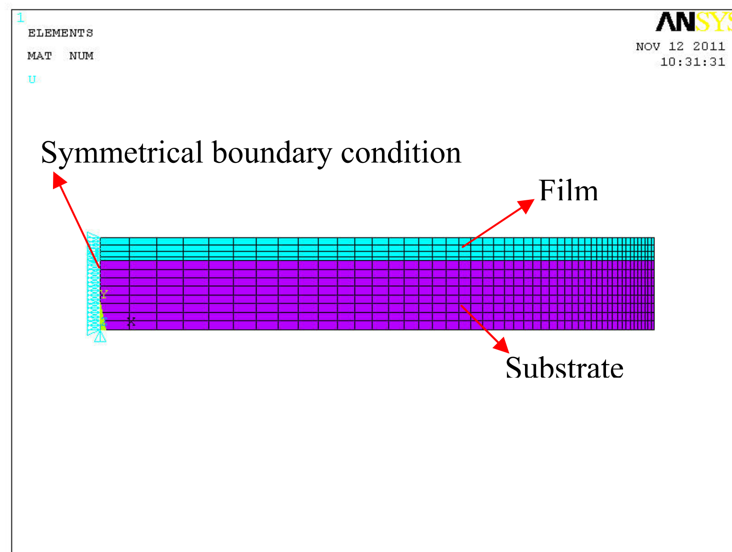

Figure C.1 FEA model for the case that the thickness of film is 5 μm.

The ANSYS Parametric Design Language (APDL) for this model is attached below.

```
/prep7
antype,static
et,1,plane82,,,0,,,3
mp,ex,1,70e9            !define film property
mp,nuxy,1,0.33
tb,miso,1
tbpt,defi,2e-3/7,20e6
tbpt,defi,16e-3/7,50e6
mp,ex,2,162e9           !define substrate property
mp,nuxy,2,0.3
mp,alpx,1,23e-6
mp,alpx,2,2.6e-6
k,1
k,2,0,15e-6
k,3,0,20e-6
kgen,2,1,3,1,120e-6
a,2,3,6,5
a,1,2,5,4
aglue,all
asel,s,area,,1
aatt,1
asel,all
asel,s,area,,2
aatt,2
asel,all

lesize,2,,,48,0.1       !define mesh size
lesize,4,,,48,10
lesize,1,,,4,2
lesize,3,,,4,0.5
lesize,7,,,48,10
lesize,5,,,8
lesize,6,,,8

mshkey,1
amesh,2
amesh,1

nsel,s,loc,x,0
dsym,symm,x
nsel,r,loc,y,-1e-7,1e-7
d,all,all
nsel,all
tref,0
bfunif,temp,-15         !temperature variation is 15 degree Celsius
finish
/solu
solve
finish
/post1
nsel,s,,,node(0,15e-6,0),node(0,20e-6,0),node(0,20e-6,0)-node(0,15e-
6,0)
set,last
prnsol,s,comp
```

Publications

[1] **Hu, Y.Y.** and Huang, W.M. (2004), Elastic and elastic-plastic analysis of multilayer thin films: closed-form solutions, *Journal of Applied Physics*, Vol. 96, pp4154-4160.

[2] Huang, W.M., **Hu, Y.Y.** and An, L. (2004), A simple approach to determine five thermomechanical properties of thin ductile films on an elastic substrate, *Applied Physics Letters*, Vol. 85, pp6173-6175.

[3] Huang, W.M., **Hu, Y.Y.** and An, L. (2005), Response to 'Comment on "A simple approach to determine five thermomechanical properties of thin ductile films on an elastic substrate"' , *Applied Physics Letters*, Vol. 87, pp116102-1.

[4] Huang, W.M., **Hu, Y.Y.** and An, L. (2005), Determination of stress versus strain relationship and other thermomechanical properties of thin films, *Applied Physics Letters,* Vol. 87, pp201904-1-3.

[5] **Hu, Y.Y.**, Oh, K.C., Huang, W.M. (2005), Determination of stress-strain relationships of a NiTi shape memory alloy in tension and compression by four-point bending test, *International Conference on Mechanical Engineering and Mechanics*, October 26-28, 2005, Nanjing, China, pp937-940.

[6] Wu, M.J., Huang, W.M., Fu, Y.Q., Chollet, F., **Hu Y.Y.** and Cai M. (2009), Reversible surface morphology in shape-memory alloy thin films, *Journal of Applied Physics*, Vol. 105, pp033517.